NUREG/CR–5794

Ground-Water Flow and Transport Modeling of the NRC-Licensed Waste Disposal Facility, West Valley, New York

Prepared by
J. B. Kool, Y. S. Wu

HydroGeoLogic, Inc.

Prepared for
U.S. Nuclear Regulatory Commission

AVAILABILITY NOTICE

Availability of Reference Materials Cited in NRC Publications

Most documents cited in NRC publications will be available from one of the following sources:

1. The NRC Public Document Room, 2120 L Street, NW., Lower Level, Washington, DC 20555

2. The Superintendent of Documents, U.S. Government Printing Office, P.O. Box 37082, Washington, DC 20013-7082

3. The National Technical Information Service, Springfield, VA 22161

Although the listing that follows represents the majority of documents cited in NRC publications, it is not intended to be exhaustive.

Referenced documents available for inspection and copying for a fee from the NRC Public Document Room include NRC correspondence and internal NRC memoranda; NRC bulletins, circulars, information notices, inspection and investigation notices; licensee event reports; vendor reports and correspondence; Commission papers; and applicant and licensee documents and correspondence.

The following documents in the NUREG series are available for purchase from the GPO Sales Program: formal NRC staff and contractor reports, NRC-sponsored conference proceedings, international agreement reports, grant publications, and NRC booklets and brochures. Also available are regulatory guides, NRC regulations in the *Code of Federal Regulations*, and *Nuclear Regulatory Commission Issuances*.

Documents available from the National Technical Information Service include NUREG-series reports and technical reports prepared by other Federal agencies and reports prepared by the Atomic Energy Commission, forerunner agency to the Nuclear Regulatory Commission.

Documents available from public and special technical libraries include all open literature items, such as books, journal articles, and transactions. *Federal Register* notices, Federal and State legislation, and congressional reports can usually be obtained from these libraries.

Documents such as theses, dissertations, foreign reports and translations, and non-NRC conference proceedings are available for purchase from the organization sponsoring the publication cited.

Single copies of NRC draft reports are available free, to the extent of supply, upon written request to the Office of Administration, Distribution and Mail Services Section, U.S. Nuclear Regulatory Commission, Washington, DC 20555.

Copies of industry codes and standards used in a substantive manner in the NRC regulatory process are maintained at the NRC Library, 7920 Norfolk Avenue, Bethesda, Maryland, for use by the public. Codes and standards are usually copyrighted and may be purchased from the originating organization or, if they are American National Standards, from the American National Standards Institute, 1430 Broadway, New York, NY 10018.

NUREG/CR--5794

TI92 003257

Ground-Water Flow and Transport Modeling of the NRC-Licensed Waste Disposal Facility, West Valley, New York

Manuscript Completed: September 1991
Date Published: October 1991

Prepared by
J. B. Kool, Y. S. Wu

T. J. Nicholson, NRC Project Manager

HydroGeoLogic, Inc.
1165 Herndon Parkway
Suite 900
Herndon, VA 22070

Prepared for
Division of Regulatory Applications
Office of Nuclear Regulatory Research
U.S. Nuclear Regulatory Commission
Washington, DC 20555
NRC FIN L1273

ABSTRACT

This report describes a simulation study of groundwater flow and radionuclide transport from disposal pits at the NRC licensed waste disposal facility in West Valley, New York. A transient, precipitation driven, flow model of the near-surface fractured till layer and underlying unweathered till was developed and calibrated against observed inflow data into a recently constructed interceptor trench for the period March - May, 1990. The results suggest that lateral flow through the upper, fractured till layer may be more significant than indicated by previous, steady state flow modeling studies. A conclusive assessment of the actual magnitude of lateral flow through the fractured till could however not be made. A primary factor contributing to this uncertainty is the unknown contribution of vertical infiltration through the interceptor trench cap to the total trench inflow. The second part of the investigation involved simulation of the migration of Sr-90, Cs-137 and Pu-239 from the one of the fuel hull disposal pits. A first-order radionuclide leach rate with rate coefficient of 10^{-6}/day was assumed to describe radionuclide release into the disposal pit. The simulations indicated that for wastes buried below the fractured till zone, no significant migration would occur. However, under the assumed conditions, significant lateral migration could occur for radionuclides present in the upper, fractured till zone.

TABLE OF CONTENTS

Section — Page

ABSTRACT iii

EXECUTIVE SUMMARY xiii

ACKNOWLEDGEMENT xv

1 INTRODUCTION 1-1
1.1 BACKGROUND 1-1
1.2 OBJECTIVES 1-5

2 SITE DESCRIPTION 2-1
2.1 LOCATION 2-1
2.2 CLIMATE AND PRECIPITATION 2-1
2.3 GEOHYDROLOGY 2-1
2.4 WASTE DISPOSAL HISTORY AND RADIONUCLIDE INVENTORY 2-7
2.5 GROUNDWATER MONITORING DATA 2-14

3 GROUNDWATER FLOW MODEL 3-1
3.1 MODELED CROSS-SECTIONS 3-1
3.2 GOVERNING EQUATIONS 3-1
3.3 SOIL HYDRAULIC CONSTITUTIVE 3-6
3.4 INITIAL AND BOUNDARY CONDITIONS 3-10
3.5 FINITE ELEMENT GRID DESIGN 3-11
3.6 TIME STEPPING SCHEME AND SIMULATION INTERVAL 3-15

4 GROUNDWATER FLOW MODELING RESULTS 4-1
4.1 CROSS-SECTION 1 4-1
4.1.1 Steady-State Flow Simulation 4-1
4.1.2 Transient Simulations 4-3
4.2 CROSS-SECTION 2 SIMULATIONS 4-11
4.2.1 Assignment of Initial Conditions 4-11
4.2.2 Transient Simulation 1 4-11
4.2.3 Transient Simulation 2 4-15
4.2.4 Transient Simulation 3 4-19
4.3 EFFECTS OF ANISOTROPY 4-26

5 RADIONUCLIDE TRANSPORT MODELING 5-1

5.1 MODELING APPROACH 5-1
5.2 TRANSPORT PARAMETER ESTIMATION 5-2
5.3 RESULTS 5-9

6 DISCUSSION 6-1
6.1 FLOW MODELING 6-1
6.2 RADIONUCLIDE TRANSPORT 6-3

REFERENCES R-1

APPENDIX A MEASURED RELATIVE PERMEABILITYAND SOIL MOISTURETENSION DATA A-1

APPENDIX B OBSERVED PRECIPITATION DATA B-1

APPENDIX C OBSERVED TRENCH INFLOW DATA C-1

APPENDIX D DIGITIZED WATER TABLE LEVELS IN SELECTED WELLS D-1

LIST OF FIGURES

Figure		Page
1.1	General Location Map of the Study Area.	1-2
2.1	Location of waste disposal facilities at the WNYNSC.	2-2
2.2	Monthly precipitation and potential evapotranspiration on the north plateau, October, 1982 through September, 1983 (From Yager, 1987).	2-3
2.3	Geological cross-section (from Bergeron et al., 1984).	2-5
2.4	Fracture patterns in the upper part of the Lavery till observed in a research trench excavated in the FDA (U.S. DOE, 1985).	2-6
2.5	Location map of disposal pits and trenches at the FDA	2-9
2.6	Position of the interceptor trench along the north-eastern and north-western boundary of the FDA.	2-11
2.7	Cross-sectional view showing typical design of the interceptor trench.	2-12
2.8	Observed inflows to interceptor trench for the period March to August, 1990.	2-13
2.9	Daily precipitation recorded at the FDA during the period March to August, 1990.	2-13
2.10	Observed water levels in Solvent Plume Exploratory wells during Spring, 1990	2-16
2.11	Observed water level variations for well no. 89-29-E.	2-17
2.12	Schematic diagram showing well installation in solvent disposal pits (from Blickwedehl et al., 1989).	2-18
2.13	Location of NDA RCRA monitoring wells	2-19
3.1	Locations of simulated cross-sections and interceptor trench at the Facility Disposal Area of the Western New York Nuclear Service Center.	3-2
3.2	Vertical cross-section through FDA and state-licensed disposal area used by Bergeron and Bugliosi (1988).	3-3

Figure Page

3.3 Section 1 (A-A′) of the FDA site showing position of fractured, weathered and unweathered till layers, assumed initial water table, and boundary conditions. (Location of section is shown in Figure 3.1.) 3-4

3.4 Section 2 (B-B′) of the FDA site position of fractured, weathered and unweathered till layers, assumed initial water table, and boundary conditions. (Location of section is shown in Figure 3.1) 3-5

3.5 Water content versus capillary pressure head relations used in VAM2D model. Observed data from U.S. DOE (1986). 3-8

3.6 Relative permeability versus water saturation curves used in VAM2D modeling. Observed data from U.S. DOE (1986). 3-9

3.7 VAM2D curvilinear finite element grid used in the simulation of groundwater flow along Section 1. 3-13

3.8 VAM2D curvilinear finite element grid used in the simulation of groundwater flow along Section 2. 3-14

4.1 Distribution of hydraulic head in Section 1 calculated from steady-state infiltration rate on ground surface. 4-3

4.2 Distribution of hydraulic head in Section 1 based on the best-fit steady-state simulation of March 1983 conditions (from Bergeron et al., 1988). 4-3

4.3 Comparison of simulated infiltration flux and observed precipitation rate along Section 1; Cross-Section 1, first transient simulation. 4-5

4.4 Comparison of simulated cumulative infiltration and observed cumulative precipitation along Section 1; Cross-Section 1, first transient simulation. 4-5

4.5 Comparison of simulated and observed daily inflow rates into interceptor trench; Cross-Section 1, first transient simulation. 4-6

4.6 Comparison of and observed simulated cumulative inflow into interceptor trench; Cross-Section 1, first transient simulation. 4-6

4.7 Simulated velocity distribution of groundwater flow in Cross-Section 1 at t = 11 d. 4-8

4.8 Comparison of simulated infiltration flux and observed precipitation rate; Cross-Section 1, second transient simulation. 4-9

Figure Page

4.9 Comparison of simulated cumulative infiltration and observed cumulative precipitation; Cross-Section 1, second transient simulation. 4-9

4.10 Comparison of simulated and observed daily inflow rates into interceptor trench; Cross-Section 1, second transient simulation. 4-10

4.11 Comparison of simulated and observed cumulative inflow into interceptor trench; Cross-Section 1, second transient simulation. 4-10

4.12 Comparison of simulated infiltration flux and observed precipitation rate; Cross-Section 2, first transient simulation 4-13

4.13 Comparison of simulated cumulative infiltration and observed cumulative precipitation; Cross-Section 2, first transient simulation. 4-13

4.14 Comparison of simulated and observed daily inflow rates into interceptor trench; Cross-Section 2, first transient simulation. 4-14

4.15 Comparison of simulated and observed cumulative inflow into interceptor trench; Cross-Section 2, first transient simulation. 4-14

4.16 Comparison of simulated infiltration flux and observed precipitation rate; Cross-Section 2, second transient simulation. 4-16

4.17 Comparison of simulated cumulative infiltration and observed cumulative precipitation; Cross-Section 2, second transient simulation. 4-16

4.18 Comparison of simulated and observed daily inflow rates into interceptor trench; Cross-Section 2, second transient simulation. 4-17

4.19 Comparison of simulated and observed cumulative inflow into interceptor trench; Cross-Section 2, second transient simulation. 4-17

4.20 Groundwater flow velocities at t = 9 d; Cross-Section 2, second transient simulation. 4-18

4.21 Groundwater flow velocities at t = 60 d; Cross-Section 2 second transient simulation. 4-18

4.22 Comparison of simulated infiltration flux and observed precipitation rate; Cross-Section 2, final transient simulation. 4-21

Figure Page

4.23 Comparison of simulated cumulative infiltration and observed cumulative precipitation; Cross-Section, final transient simulation. 4-21

4.24 Comparison of simulated and observed daily inflow rates into interceptor trench; Cross-Section 2, final transient simulation. Observed data for case in which 50% of total trench inflow is caused by subsurface seepage. 4-22

4.25 Comparison of simulated and observed cumulative inflow into interceptor trench; Cross-Section 2, final transient simulation. 4-22

4.26 Comparison of simulated and observed daily inflow rates into interceptor trench; Cross-Section 2, final transient simulation. Observed data for case in which 80% of total trench inflow is caused by subsurface seepage. 4-23

4.27 Comparison of simulated and observed cumulative inflow into interceptor trench; Cross-Section 2, final transient simulation. 4-23

4.28 Groundwater flow velocities at t = 9 d; Cross-Section 2, final transient simulation. 4-24

4.29 Groundwater flow velocities at t = 60 d; Cross-Section 2 final transient simulation. 4-24

4.30 Comparison of simulated water table with observation data from Well 85-I-11; Cross-Section 2, final transient simulation. 4-25

4.31 Comparison of simulated water table with observation data from Well 89-13-W; Cross-Section 2, final transient simulation. 4-25

5.1 Schematic cross-sectional view of the radionuclide source, representing a typical fuel hull burial bit 5-3

5.2 Finite element grid, consisting of 4370 elements, used in the transport simulations 5-4

5.3 Steady state groundwater flow field used in the radionuclide transport simulations 5-5

5.4 Sr-90 migration after 20 years; concentration contour represents 10^{-3} μCi/L level 5-9

5.5 Sr-90 migration after 200 years; concentration contour represents 10^{-3} μCi/L level 5-9

Figure Page

5.6 Cs-137 migration after 20 years; concentration contour represents 10^{-3} μCi/L level 5-10

5.7 Cs-137 migration after 200 years; concentration contour represents 10^{-3} μCi/L level 5-10

5.8 Pu-239 migration after 50 years; concentration contour represents 10^{-3} μg/L level 5-11

5.9 Pu-239 migration after 500 years; concentration contour represents 10^{-3} μg/L level 5-11

5.10 Sr-90 migration after 20 years for second transport scenario; concentration contour represents 10^{-3} μCi/L level 5-13

5.11 Sr-90 migration after 200 years for second transport scenario; concentration contour represents 10^{-3} μCi/L level 5-13

5.12 Cs-137 migration after 20 years for second transport scenario; concentration contour represents 10^{-3} μCi/L level 5-14

5.13 Cs-137 migration after 200 years for second transport scenario; concentration contour represents 10^{-3} μCi/L level 5-14

5.14 Pu-239 migration after 50 years for second transport scenario; concentration contour represents 10^{-3} μg/L level 5-15

5.15 Pu-239 migration after 500 years for second transport scenario; concentration contour represents 10^{-3} μg/L level 5-15

LIST OF TABLES

Table		Page
2.1	Estimated 1991 Radionuclide inventory of Fuel Hull pits	2-8
2.2	Shallow water level data for FDA RCRA monitoring wells	2-20
3.1	Completion Schedule of Interceptor Trench	3-15
4.1	Physical parameters used in the simulation of steady-state surface infiltration case for Cross-Section 1.	4-2
4.2	Physical parameters used in the simulation of initial head distributions in Section 2.	4-12
4.3	Physical parameters used in the final transient simulation of groundwater flow along Section 2.	4-20
5.1	Transport parameter values used in radionuclide migration simulations	5-7
A.1	Parameters of unsaturated flow constitutive relations used for fitting the functions of relative permeability and capillary pressure (U.S. DOE, 1988)	A-1
B.1	Precipitation data for West Valley FDA Site, March 1 to August 10, 1990.	B-1
C.1	Observed daily inflow rate and cumulative inflow into interceptor trench from March 1 to August 10, 1990	C-1
D.1	Observed Water levels in Well 89-13-W	D-1
D.2	Observed Water levels in Well 85-I-11	D-3

EXECUTIVE SUMMARY

A groundwater modeling study of the NRC licensed Facility Disposal Area at the Western New York Nuclear Service Center at West Valley, New York has been conducted. The present study was designed to investigate the significance of groundwater flow and radionuclide migration through the upper fractured layer in the glacial till burial medium. In the first part of the study, a transient, precipitation driven flow model of the surface fractured till layer and underlying unweathered till was developed and calibrated against observed inflow data into a recently constructed interceptor trench for the period March-May, 1990. The model was calibrated by adjusting the effective hydraulic conductivity of the fractured till layer. In the second part of the study, the migration of Sr-90, Cs-137 and Pu-239 from a representative fuel hull disposal pit at the site was simulated. The transport simulations were conducted for periods of up to 200 years for Sr-90 and Cs-137, and 500 years for Pu-239. Steady state flow was assumed during the long-term transport simulations, with steady state groundwater flow rates based on average annual flow rates estimated from the calibrated transient flow model.

Both the flow and transport simulations were conducted using the two-dimensional VAM2D computer code. Flow and transport were modelled along representative subsurface cross-sections through the site.

In the initial flow simulations, an effective hydraulic conductivity of $K = 2 \times 10^{-4}$ m/d (2.32×10^{-7} cm/sec) was assigned to the fractured till. Simulations based on this hydraulic conductivity values resulted in a much lower predicted than observed trench inflow. After calibration, the hydraulic conductivity of the fractured till was increased to a value of $k = 5 \times 10^{-3}$ m/d or $K = 5 \times 10^{-2}$ m/d. These two values represent two cases which were found to yield reasonably good agreement with observed trench inflow data. Using the lower of the two conductivity values, the rate of trench inflow was underpredicted during the first month of simulation, but good agreement was obtained for the second half of the 90-day simulation period. Using the higher conductivity value, the agreement between predicted and observed trench inflow during the initial part of the simulation period was better, but in this case the model overpredicted trench inflows during the second part of the simulation period. Different interpretations and explanations exist for these differences. The high initial rate of trench inflow may reflect the influence of infiltration of surface run-off through the trench cap, rather than subsurface seepage through the fractured till. In this interpretation the lower trench inflow rates observed during the second half of April and May reflect the influence of subsurface flow, since settling of the clay cap reduced the infiltration of surface run-off into the trench. This interpretation thus favors lower hydraulic conductivities in the fractured till. On the other hand, the reduction of observed trench inflows with time could be caused by increased evapotranspiration during April and May, compared to March. In this interpretation, more importance is given to the initially high trench inflow rates and thus favoring higher effective conductivities and lateral flow rates in the fractured till. These uncertainties preclude a conclusive assessment of the actual magnitude of lateral flow through the fractured till. However, simulations of the calibrated model with either the lower (5×10^{-3} m/d) or the higher (5×10^{-2} m/d) hydraulic conductivity of the fractured till layer through the fractured till is more

significant than previous, steady state modeling has indicated. Continuing collection of rainfall and trench inflow data should allow the uncertainty in how to interpret these data to be resolved, e.g., by performing additional model validation studies.

Based on the transient flow simulations, net annual infiltration at the site was estimated to be on the order of 3 cm/year. Of this infiltration, approximately 2 cm is expected to eventually flow downward through the unweathered till, with the remaining 1 cm/year moving laterally through the fractured till into the interceptor trench. Based on these estimated average flow rates, the migration of radionuclides from a single, representative fuel hull disposal pit was simulated. In the absence of data on the actual release of radionuclides from the buried fuel hulls into the surrounding soil environment, a first-order leach rate with rate coefficient of 10^{-6}/day was used to model the radionuclide source term. The disposal protocol for the fuel hulls prescribed the fuel hulls to be buried at depths of 4 feet or more below the disturbed zone. If the latter is taken to be the interface between the unweathered and fractured till, all waste materials should be buried well below the depths at which significant lateral flow is expected to occur. The model simulations confirmed that in this scenario no significant migration of radionuclides would occur. However, under the assumed groundwater flow conditions, significant lateral migration could occur for radionuclides that are present, either through shallow burial or moved upward by seasonally fluctuating water table levels, in the upper, fractured till zone.

ACKNOWLEDGEMENT

The work described herein was conducted for the U.S. Nuclear Regulatory Commission under contract no. NRC-04-89-090, entitled "Validation and Testing of the VAM2D Computer Code." The support and many helpful suggestions of Project Officer Tom Nicholson throughout the project is gratefully acknowledged. The work has alsc benefitted greatly from discussions with Davis Hurt and Jack Parrott of the NRC Office NMSS and many individuals at the West Valley Project Office.

1 INTRODUCTION

1.1 BACKGROUND

This report describes the results of a modeling study of subsurface groundwater flow and contaminant transport at the Facility Disposal Area (FDA), also known as the NRC-licensed disposal area, of the Western New York Nuclear Service Center (WNYNSC). The WNYNSC is located on the west side of the Buttermilk Creek Valley in Cattaraugus County in the western part of New York State (Figure 1.1), located approximately 48 km south of Buffalo. The WNYNSC comprises plant facilities associated with the West Valley Waste Solidification Demonstration Project, the FDA, and an inactive, state-licensed radioactive waste burial area.

The FDA received wastes from the spent fuel reprocessing from 1966 to the plant closure in 1972. Since 1972, mostly low-level wastes consisting of decontamination residues have been disposed in the FDA. Radioactive wastes were disposed by burial in a number of surface pits and trenches. The pits and trenches were then backfilled and capped with excavated soil material. The geologic disposal medium is a low permeability glacial till, known as the Lavery Till. While the upper most few meters of the till is weathered and fractured, the underlying unweathered till is characterized by a very low hydraulic conductivity with values on the order of 10^{-8} cm/s. The disposal pits and trenches were designed such that all waste materials would be buried at depths below the weathered-unweathered till transition (Nicholson and Hurt, 1985). The hydraulic gradient in the unweathered till is predominantly vertically downward, with an approximately unit hydraulic gradient. Downward water flow rates are thus on the same order as the hydraulic conductivity of the till. Under these low flow rates diffusion becomes the dominant transport mechanism for water dissolved radionuclides (Prudic, 1986). However, an alternative pathway may exist whereby contaminants migrate laterally through the fractured, upper layer of the till. As the disposal pits fill with water, contaminants could move upward into the upper fractured zone and from there travel laterally through this more permeable zone to nearby streams or other exposure points. A number of groundwater modeling studies of the FDA and adjacent state-licensed disposal areas have been conducted previously (Prudic, 1986; U.S. DOE, 1986; Bergeron and Bugliosi, 1988). In general, these studies have been designed to delineate groundwater flow paths and to provide quantitative estimates of radionuclide travel times.

Prudic (1986) modeled infiltration into the disposal trenches of the state licensed burial area using a two-dimensional finite element saturated-unsaturated flow model. This model predicted predominantly downward movement of infiltrating water through the till, with flow rates between 0.3 and 2.3 cm/yr. Prudic did however also conclude that "if the water level in the trenches were to rise into the reworked till covering them, the trench water could seep out through the cover to the land surface." The estimated recharge rates from the flow model were used as input to calculations of the rate of radionuclide migration from the disposal trenches. A one-dimensional analytical transport solution was used for these calculations. The results of these calculations suggested that molecular diffusion would be the dominant transport mechanism. The overall conclusion was that "radionuclides are far less likely to reach the

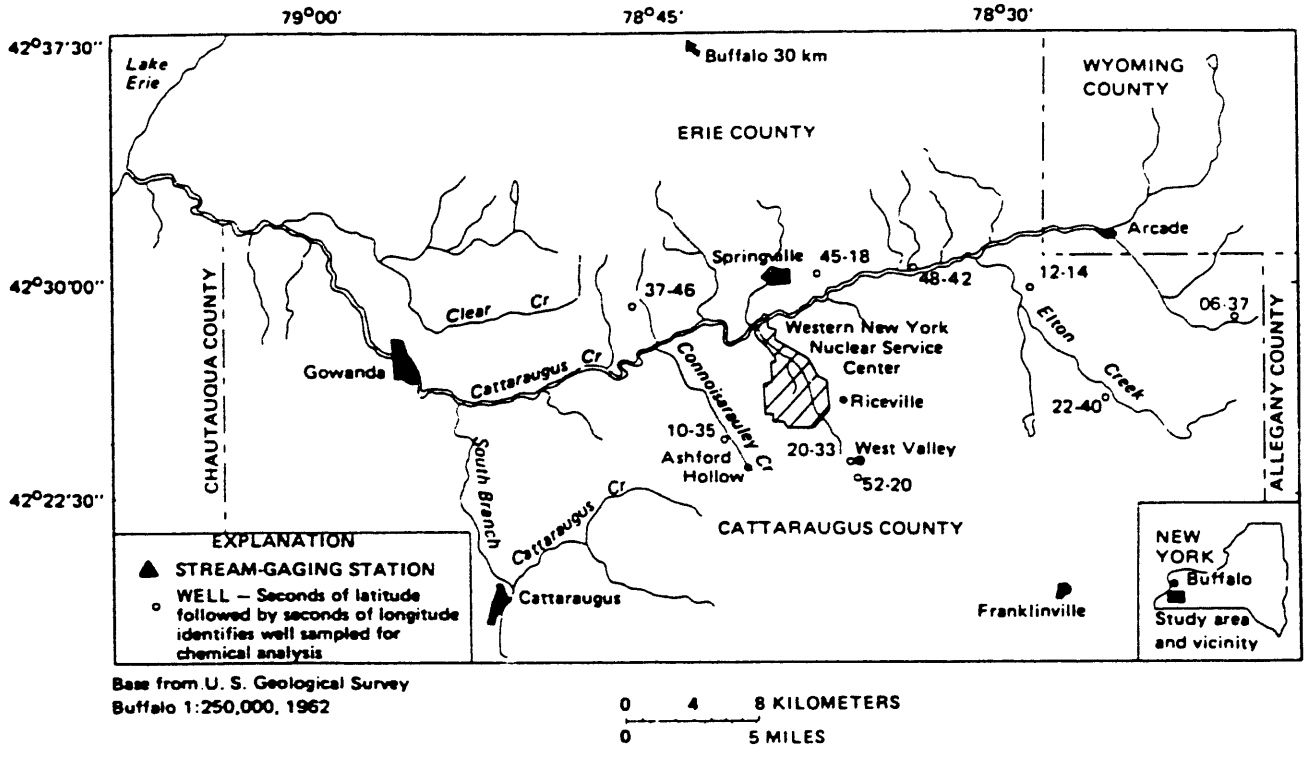

Figure 1.1 General Location Map of the Study Area.

environment through subsurface migration than by saturation and overflow of the trenches, which can occur when cracks break the cover and serve as avenues of rapid recharge."

U.S. DOE (1986) modeled saturated-unsaturated flow underneath the FDA using the two-dimensional FEMWATER code. Four vertical cross-sections were simulated. This modeling was performed as part of an environmental impact assessment for the disposal of wastes from the solidification demonstration project. Results of the FEMWATER flow modeling were fed into the PRESTO-EPA model for radionuclide migration analysis. Only steady-state simulations were performed. The long term average infiltration rate was adjusted to 2 cm/yr in order to match predicted to observed average piezometric head levels. A two-order of magnitude difference between hydraulic conductivity in the weathered, fractured and non-weathered till was assumed. Simulated flow in the unweathered till was predominantly vertically downward. The predicted steady state flow direction in the fracture surface zone was vertically downward in regions of level surface topography; significant lateral flow occurred only where the land surface had a noticeable slope such as near creek embankments.

Bergeron and Bugliosi (1988) modeled steady-state saturated-unsaturated groundwater flow underneath both the FDA and the state-licensed disposal area. The computer code used was the FEMWATER code used also by U.S. DOE (1986). Two vertical cross-sections were modeled; one extending northwest from underneath the FDA to the Lagoon Creek Ravine/Erdman's Brook, the other one ran northeast-southwest from underneath the FDA and state-licensed disposal area to Frank's Creek. The cross-sectional model accounted for the presence of an upper, weathered and fractured till layer, a transition layer, and underlying unweathered till. The fractured till layer was assigned a saturated hydraulic conductivity 10x higher than the unweathered till. A constant infiltration rate boundary condition was imposed along the soil surface. The magnitude of the infiltration rate was adjusted to match predicted and simulated piezometric heads. The resulting infiltration rate varied from 1.6 to 3.1 cm/year, which is quite similar to the value used by U.S. DOE (1986). The model of Bergeron and Bugliosi (1988) predicted predominantly vertically downward groundwater flow. Lateral flow through the fractured till was predicted to occur only over short distances. Such lateral flow was predicted to result from locally varying infiltration rates. The model predicted that lateral movement would occur over relatively short distances, less than 20 m, before changing to downward flow. It was concluded that "subsurface migration of radionuclides in groundwater to points of discharge at land surface would be unlikely, given that the water level in the pit does not rise into the reworked cover material capping the pit."

Hydrogeologic conditions and previous investigations of the state-licensed disposal area have recently been reviewed by Bergeron et al. (1991), from the perspective of a hydrogeologic performance assessment of this disposal facility. Bergeron et al. (1991) discussed previous investigations of the state-licensed area to identify radionuclides most likely to migrate appreciable distance from the disposal trenches and possible migration pathways. Two primary groundwater pathways were identified. The first pathway corresponded to the upper few meters of the burial medium where overflowing trench water could potentially migrate laterally through fractured and weathered till to nearby surface water drainages. The potential significance of this

pathway was inferred from the observed presence of a plume of solvent in the FDA, which is migrating laterally through the fractured till with an average velocity of several meters per year. The second pathway is deep vertical migration through the Lavery till and subsequent lateral groundwater migration through the more permeable lacustrine unit underlying the Lavery till, to offsite locations.

Since neither monitoring data, nor earlier hydrologic modeling provided direct information on the extent and magnitude of lateral flow through the fractured till, Bergeron et al. used the observed rate of migration of the solvent plume in the FDA to obtain a lateral flow rate through the fractured till for radionuclide transport analyses. A travel time for water and non-retarded radionuclides from the trenches to Franks Creek, of 100 years was calculated in this way. With exception of tritium and C-14, the effects of decay and adsorption during migration were estimated to eliminate the majority of radionuclides in the trench inventory. The combined effect of radioactive decay and dilution due to the annual average flow in Franks Creek would reduce calculated levels of tritium and C-14 to insignificant levels. Migration via the deep pathway was assessed using a one-dimensional stream tube transport model, with flow rates through the unweathered till obtained from earlier modeling work of Prudic (1986). Within the deep pathway, tritium and C-14 would be the only radionuclides released from the site in any significant concentrations. While predicted tritium levels all remained below regulatory levels, the predicted C-14 concentrations would exceed the limit for the full garden scenario. In this assessment it was assumed that the release rate of C-14 from the trench would be equal to the maximum measured trench water concentration times the estimated infiltration rate, and that all forms of C-14 (organic and inorganic) have the same geochemical behavior. Moreover, C-14 was assumed to migrate with minimal retardation (Retardation coefficient, $R=7$), which should result in a conservative transport assessment. In the performance assessment the analysis of Bergeron et al., the release rate of C-14 and geochemical behavior of different carbon species are the most uncertain and sensitive factors.

Relevant to the present investigation is also the groundwater modeling work of Yager (1987). Yager developed a two-dimensional, areal model of the groundwater system underneath the nuclear fuel reprocessing plant and related waste facilities, i.e., the area adjacent to the FDA and state-licensed disposal area. In the area modeled by Yager, the glacial till does not extend to the soil surface but is overlain by a several meter-thick deposit of silty sand and gravel, deposited as an alluvial fan. An unconfined water table is present in the permeable surface sand and gravel which overlies the much less permeable till. The sequence of sand and gravel overlying glacial till is somewhat analogous to the sequence of fractured till overlying unweathered till at the FDA. The hydraulic conductivity of the sand and gravel was given by Yager as varying from 7.10^{-4} to 10^{-2} cm/sec, whereas reported values for the fractured till at the FDA are much less, i.e., on the order of 10^{-6} cm/sec (U.S. DOE, 1986). A quite significant difference between the modeling of Yager and that summarized above for the FDA is the magnitude of infiltration into the surface soil. Rather than treating infiltration strictly as a calibration parameter, Yager developed independent estimates of infiltration based on precipitation, evapotranspiration and other climatic data. The resulting estimate of annual recharge was 50 cm/year, or more than an order of magnitude larger than the value used by

Prudic (1986), U.S. DOE (1986), and Bergeron and Bugliosi (1988). The compacted cover material at the FDA probably causes more surface runoff and less infiltration than the sand/gravel surface layer in the area modeled by Yager. On the other hand, there appears to be little or no actually measured data on runoff and infiltration at the FDA and the 25-fold difference between 2 and 50 cm/year suggests that there may be considerable uncertainty in the infiltration rate values used in the before mentioned modeling studies of the FDA. Since the estimated recharge flux through the unweathered till of 1 to 2 cm/year is probably relatively accurate, uncertainties or errors in the assumed infiltration rate into the fractured till will directly affect estimates of the significance of lateral flow through the fractured till.

These existing modeling studies have tended to confirm that radionuclides that are released from their buried containers will migrate downward through the unweathered till. With the exception of the performance assessment analysis of Bergeron et al. (1991), none of these studies have examined in detail the potential for movement into and through the high permeability, fractured surface zone. Since all these studies have assumed steady state flow conditions, the significance of transient flow in response to high infiltration events such as snowmelt has also not been assessed in a quantitative manner. The potential for contaminant migration along this pathway is illustrated by the mentioned presence of a solvent plume originating from tanks buried in the FDA. Solvent was first detected in a monitoring well located outside the north western corner of the FDA, in November 1983. The plume is estimated to travel northward through the fractured surface layer with an average velocity of 3m per year (Blickwedehl et al., 1989).

While the presence of the solvent plume provides some direct evidence for the potential of lateral contaminant migration through the fractured surface layer, the solvent moves as an immiscible fluid phase and its behavior is in a number of ways distinctly different from that of water dissolved substances. The migration of solvent in itself therefore does not imply that solutes will also migrate significantly through the near surface fractured zone.

1.2 OBJECTIVES

The study reported herein was designed to evaluate potential subsurface radionuclide migration at the FDA with particular emphasis on the potential for lateral radionuclide migration through the near-surface, fractured till zone. In order to provide a quantitative assessment of solute migration, it is first necessary to delineate groundwater flow paths. The report is therefore divided into two parts; the first part contains the results of a groundwater flow modeling investigation in which data on precipitation and inflow into a recently constructed interceptor trench are used to calibrate a transient flow model. Results from the flow modeling are then used in the second part to simulate transport of Cs-137, Sr-90, and Pu-239. Since there is essentially no information on actual source release rates this part of the study has been designed to evaluate the potential for radionuclide migration through the shallow subsurface pathway and to provide a very rough, order-of-magnitude assessment of transport rates and concentration values.

2 SITE DESCRIPTION

2.1 LOCATION

The location of waste disposal facilities at the WNYNSC is depicted in Figure 2.1. The present study involves the Facility Disposal Area (FDA) shown just below the center of the figure. The FDA is approximately 5½ acres in size.

2.2 CLIMATE AND PRECIPITATION

The West Valley area has a moist continental climate with annual temperatures ranging between -26°C and +32°C. Mean monthly temperatures are -6°C for January to February and 20°C in July (Smoot, 1989). The average annual precipitation in the West Valley area is about 100 cm. Precipitation is distributed relatively evenly throughout the year. Rates of 9 cm/month are common in the spring, early summer, and late fall and range to 7 cm/month during the winter. Winter precipitation commonly occurs as snow; accumulations of 30 cm or more may result from a single storm. Accumulations of 125 cm during two consecutive months during the winter are not uncommon, and continuous snow cover may be expected from at least mid-December to mid-March (Smoot, 1989).

The distribution of monthly precipitation and potential evapotranspiration during a one-year period of October, 1982 through September, 1983 is shown in Figure 2.2. This graph indicates an excess of precipitation over potential evapotranspiration during the months October through March. Total precipitation during the 1 year period shown in Figure 2.2 was 92 cm. Actual evapotranspiration from native grasses during the same period was estimated by Yager (1987) to be 68 cm, based on a consumptive use coefficient of 0.75. These values pertain to the North Plateau which has sandy surface soils. Actual evapotranspiration could be higher at the FDA based on the fact that the clayey soils of the FDA will be better able to supply water to the grass vegetation during dry periods than the sandy soils of the North Plateau. The ratio of actual to potential evapotranspiration could be on the order of 0.8 to 0.85 at the FDA (Saxton, 1982), corresponding to an evapotranspiration of $\approx$ 80 cm/year. The precipitation excess would either infiltrate into the soil or be removed by surface runoff. These are speculative estimates however as no directly measured data are available.

2.3 GEOHYDROLOGY

The West Valley area has a rolling topography, intersected by many small streams. A geological cross-section of the area underlying the FDA is shown in Figure 2.3.

The FDA itself consists of a number of trenches and disposal pits, excavated in an approximately 30m-thick deposit of glacial till. This till, known as Lavery till, consists mainly of silty clay material with discontinuous lenses of sand and clay. The upper few meters of the Lavery till is weathered and fractured. Visual observations of the fractured zone indicate that the major fractures are spaced several meters apart. Most of these fractures are vertical and may

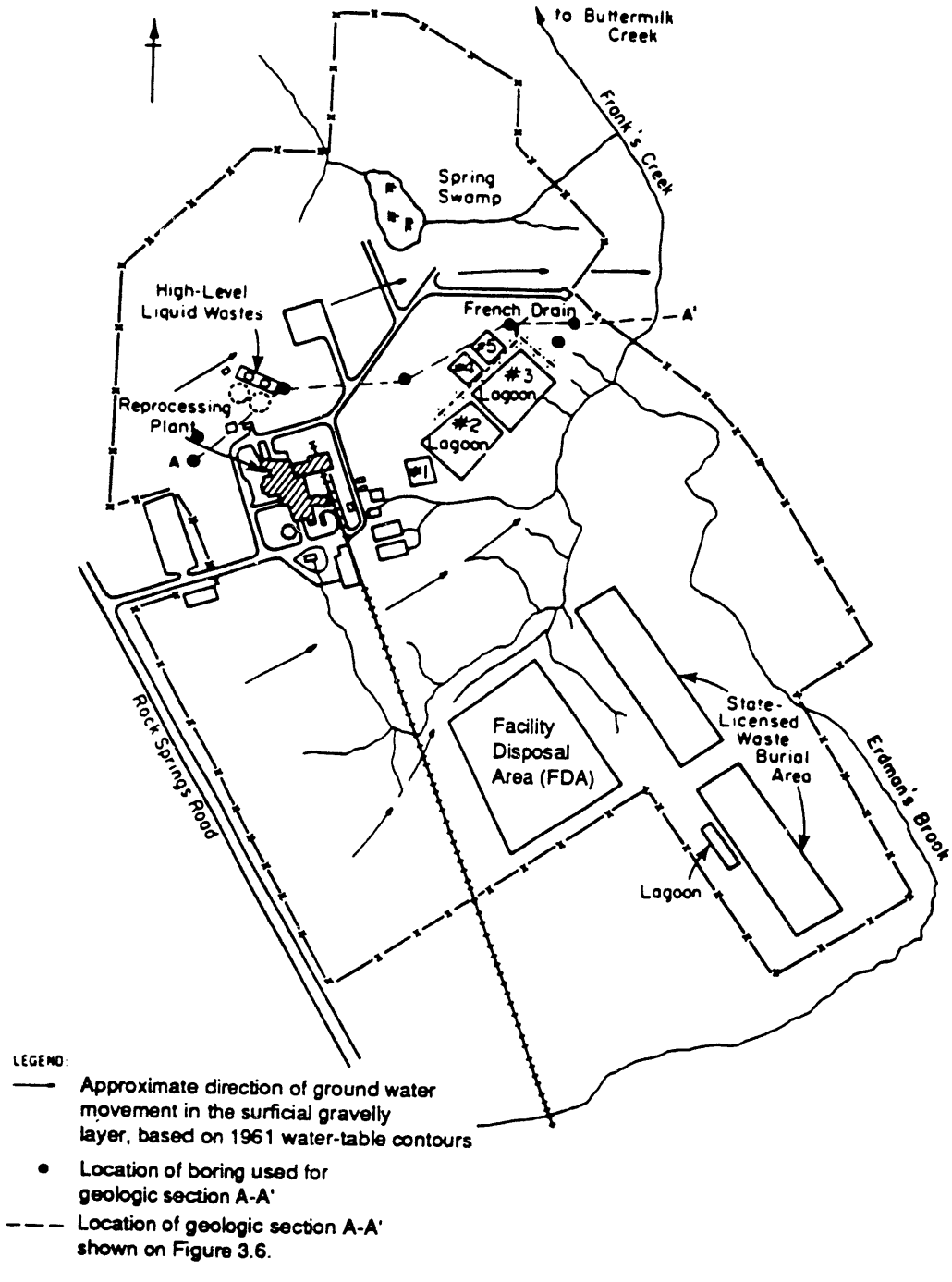

Figure 2.1 Location of waste disposal facilities at the WNYNSC.

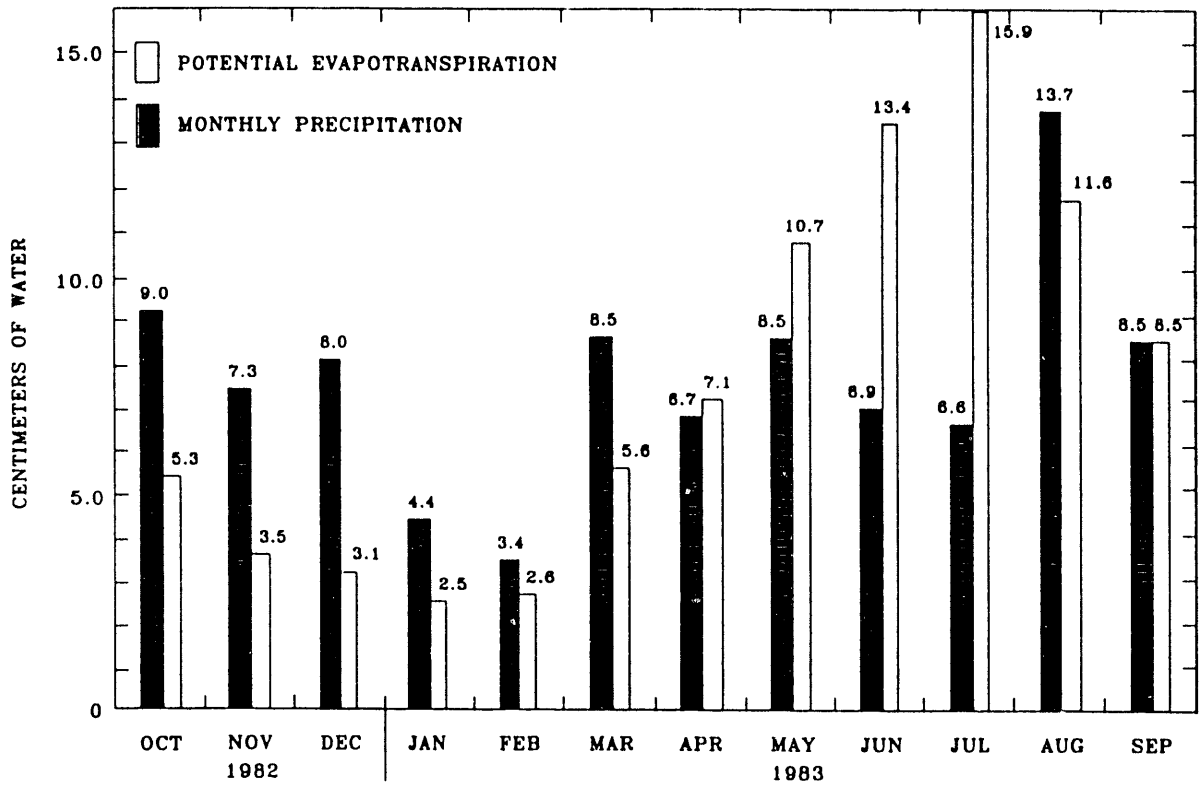

Figure 2.2 Monthly precipitation and potential evapotranspiration on the north plateau, October, 1982 through September, 1983 (From Yager, 1987).

extend to a depth of 5 m. The fracture density increases near the surface of the till. The underlying unweathered till is unoxidized and contains no visible fractures. Fracture characterization studies have been conducted by Dana et al. (1979) and by the U.S. DOE (1985). Dana et al. (1979) developed a visual characterization of near surface fractures from a research trench excavated in the state-licensed disposal area. U.S. DOE conducted a similar study at the FDA in 1985. A research trench was excavated and a mapping of fracture spacings, depth and orientation in the upper meters of the Lavery Till was made. Some results of this study are depicted graphically in Figure 2.4 and illustrate the characteristics of the dominantly vertical fracture pattern. Available data on fracture characteristics is mainly descriptive in nature. Estimates are available for fracture spacings and depths; however, no information has been encountered on fracture apertures and connectivity. The latter information would be required for direct estimates of the hydraulic conductivity of the fractured till.

The total thickness of the Lavery till is on the order of 30 m. Underlying the Lavery till is a 10 to 20 m thick sequence of lacustrine and deltaic deposits. The lacustrine unit is generally silty with some sand and clay lenses. Underlying the lacustrine unit is a clayey silty till referred to as Kent till (Smoot, 1989). Shale bedrock occurs at a depth of approximately 65 m underneath the center of the FDA. The bedrock surface dips downward toward the north-east.

The major hydrogeologic units in the vicinity of the FDA thus are the surface weathered and fractured till, the unweathered till and the underlying lacustrine unit. The unweathered till is characterized by a very low hydraulic permeability. Prudic (1982) has performed extensive testing of the unweathered Lavery till at the state-licensed burial site adjacent to the FDA. He conducted hydraulic conductivity tests on both laboratory samples as well as in-situ slug tests. The measurements were taken at depths varying from 4.5 to 15.4 m below the ground surface. The average hydraulic conductivity of the unweathered till ranged from 2×10^{-8} cm/s to 6×10^{-8} cm/s ($1.7 - 5.2 \times 10^{-5}$ m/d). Hydraulic conductivity of the unweathered till was found to be essentially isotropic (Prudic, 1982). The average porosity of 28 samples of till from all depths was 32.4 percent. The average dry bulk density was 1.82 g/cm^3. A number of infiltrometer tests have been conducted by the U.S. DOE (1986) as part of the research trench study mentioned above. These tests were conducted on the floor of the trench at different lifts. From the results of long-term infiltrometer tests conducted at a depth of 5 m, hydraulic conductivity was estimated to be 2×10^{-7} to 2×10^{-6} cm/s ($1.5 \times 10^{-2} - 1.8 \times 10^{-3}$ m/d). These values are substantially higher than those reported by Prudic. On the other hand, the infiltrometer data were obtained from a fairly shallow depth and may reflect the conductivity of the transition zone from weathered to unweathered till, rather than the unweathered till itself.

Little data is available on the permeability of the upper, fractured till. The conductivity of the fractured till has been estimated to be about an order of magnitude higher than the unweathered till (Prudic, 1986). The U.S. DOE (1986) used permeability values of the weathered till in a modeling study that were 100 times higher than the values for the unweathered till. In the U.S. DOE trench study referred to above, infiltrometer tests were also conducted at depths of 1.7 m and 3.4 m below ground surface. The 1.7 m tests did not yield

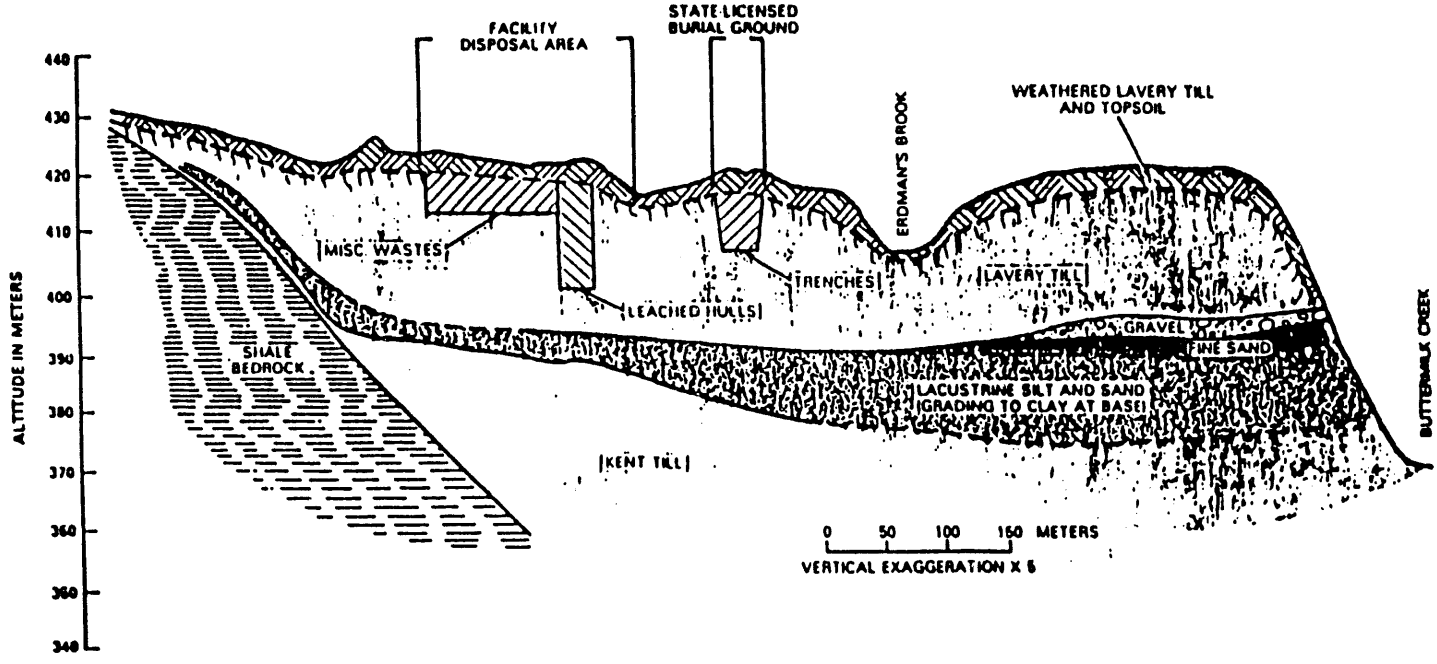

Figure 2.3 Geological cross-section (from Bergeron et al., 1984).

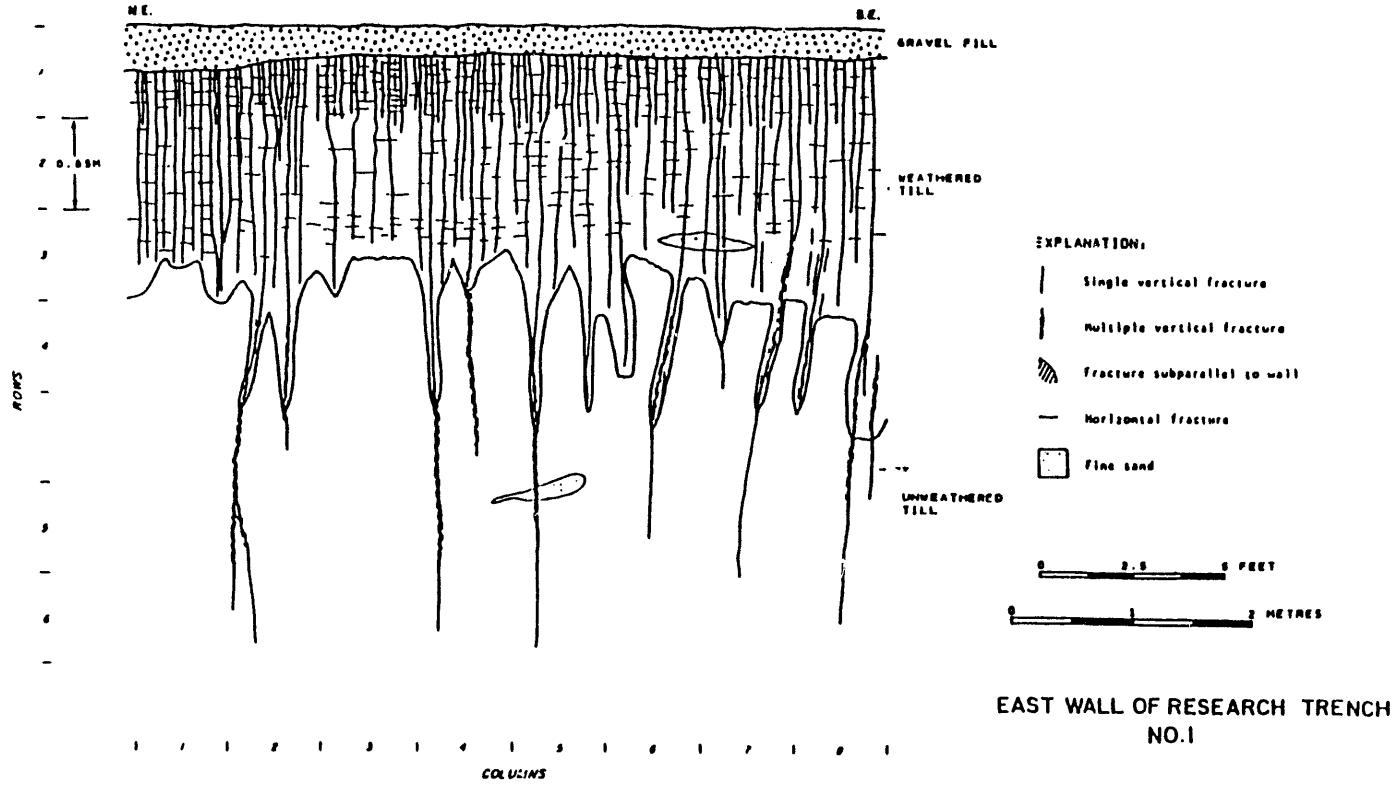

Figure 2.4 Fracture patterns in the upper part of the Lavery till observed in a research trench excavated in the FDA (U.S. DOE, 1985).

useable results. The 3.4 m tests yielded infiltration rates varying from 7.3×10^{-6} to 2.2×10^{-5} cm/s (6.3×10^{-3} - 1.8×10^{-2} m/d), with the highest value corresponding to an infiltrometer which was placed on a fracture. It should be noted however that these values were obtained from short duration (33 to 40 minutes) infiltration test and may yield values that are several times higher than the actual conductivity of the till.

No direct measurements of the hydraulic properties of the lacustrine units underlying the Lavery till are reported. However, the permeability of the lacustrine units is believed to be several orders of magnitude higher than that of the unweathered Lavery till, based on the coarser grained nature of the lacustrine sediments compared to the clay till (Smoot, 1989).

Piezometric data indicate that the hydraulic gradient in the Lavery till is mostly vertical downward. Saturated conditions prevail in the unweathered till. The position of the water table in the Lavery till fluctuates in response to seasonal variations in precipitation and evapotranspiration and may rise to close to the ground surface during Fall to Spring periods. A water table is also present in the Lacustrine units, with the hydraulic conductivity contrast between Lavery till and lacustrine deposits causing unsaturated conditions in the upper part of the Lacustrine unit.

2.4 WASTE DISPOSAL HISTORY AND RADIONUCLIDE INVENTORY

The FDA received wastes from the spent fuel reprocessing plant from 1966 to the plant closure in 1972. Since 1972, mostly low-level wastes consisting of decontamination residues have been disposed in the FDA. Project wastes associated with the West Valley Demonstration Project are currently being disposed in an area adjacent to the FDA. The wastes disposed in the FDA are described by Nicholson and Hurt (1985) as follows:

> "As of 1980, NFS has disposed of 4,300m^3 of waste in the facility disposal area. Approximately 4 percent (185m^3) of this waste was drums of leached hulls and spent fuel hardware. The remainder was composed of a wide variety of low activity solid wastes from the reprocessing plant, including failed equipment, used filters, laboratory wastes, sludge from the low-level waste treatment plant, and degraded organic solvent absorbed in vermiculite. Relatively little is known of the detailed chemical, physical, or radioisotopic characteristics of the wastes. Many of the buried containers were described in the records simply as "waste", with no further identification of contents.
>
> The miscellaneous wastes (i.e., those other than leached hulls or related spent fuel debris) were packaged in several types of containers, including steel drums, wooden crates, and cardboard boxes, and were placed in pits 20 to 30 feet deep. The horizontal dimensions of each pit varied according to the quantity of waste on hand and the dimensions of large waste items such as failed equipment. Most of the pits are about 12 (4m) feet wide and 20 to 30 (7 to 10m) feet long, although a few are much longer. The NRC imposed a technical specification that

the top of the waste had to be at least four feet below the top of the undisturbed till. The definition of undisturbed till was not provided but is presently regarded as the weathered/unweathered interface of the Lavery Till. Also the backfill was to be filled and compacted with the unweathered till.

The leached hulls and spent fuel hardware were disposed of somewhat differently than the miscellaneous wastes. They were loosely packaged in 30-gallon steel drums and stacked three abreast in narrow 50-foot shafts. As with the other wastes, the NRC imposed a requirement that the top of each stack of hull cans stop at least four feet below the top of the disturbed till. Three of the 30-gallon drums normally used for leached hulls contain irradiated, unreprocessed New Production Reactor (NPR) fuel. This fuel was emplaced in concrete at the bottom of one of the 50-foot deep leached hull shafts."

Although the leached hulls and NPR fuel represent a small portion of the total volume of wastes disposed in the FDA, most of the radioactivity (at least 95 percent) is contained in these two categories. The available information on total radioactivity disposed in the FDA and present in the different waste forms has been discussed by Nicholson and Hurt (1985).

Considering the half-lives of the various radio-isotopes present, the radionuclides of most concern are Sr^{90}, Cs^{137} an Pu^{239}/Pu^{240}. An estimate of the present (1991) inventory of the fuel hull pits is given in Table 2.1. A detailed map of the location of the waste disposal pits and trenches in the FDA is provided in Figure 2.5.

Table 2.1 Estimated 1991 Radionuclide inventory of Fuel Hull pits[1/]

Isotope	Half-life (yr)	Total Inventory	Average Pit Inventory[2/]
Sr^{90}	28.1	22,000 Ci	275 Ci
Cs^{137}	30.2	22,000 Ci	275 Ci
Pu^{239}	24,400	5 kg	60 gr
Pu^{240}	6,580	5 kg	60 gr

1/ T. Nicholson, U.S. NRC, Personal Communication, March, 1991.

2/ There are approximately 80 fuel hull burial pits.

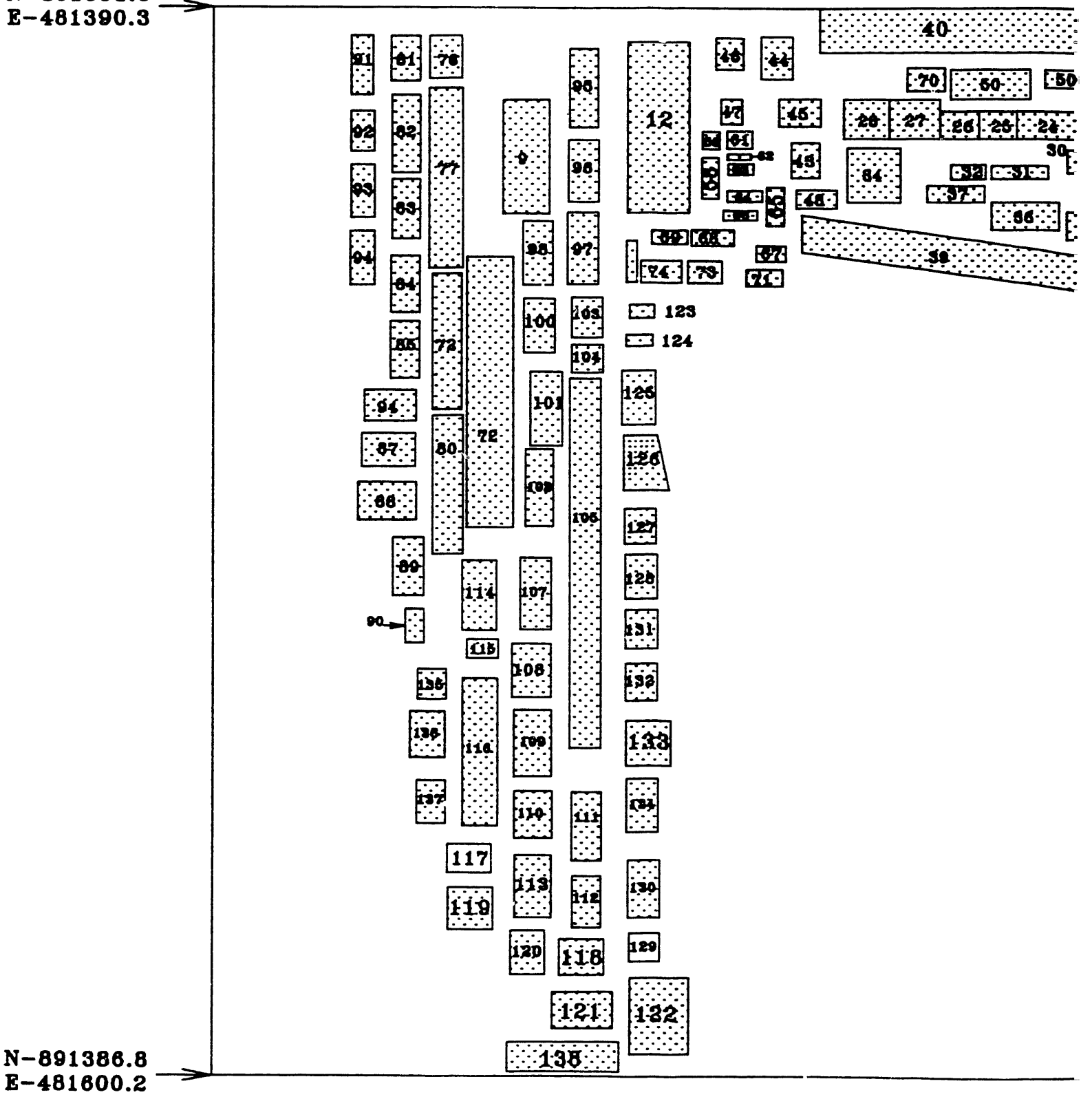
N-891691.5
E-481390.3
N-891386.8
E-481600.2
40
70
50
12
9
77
72
80
123
124
135

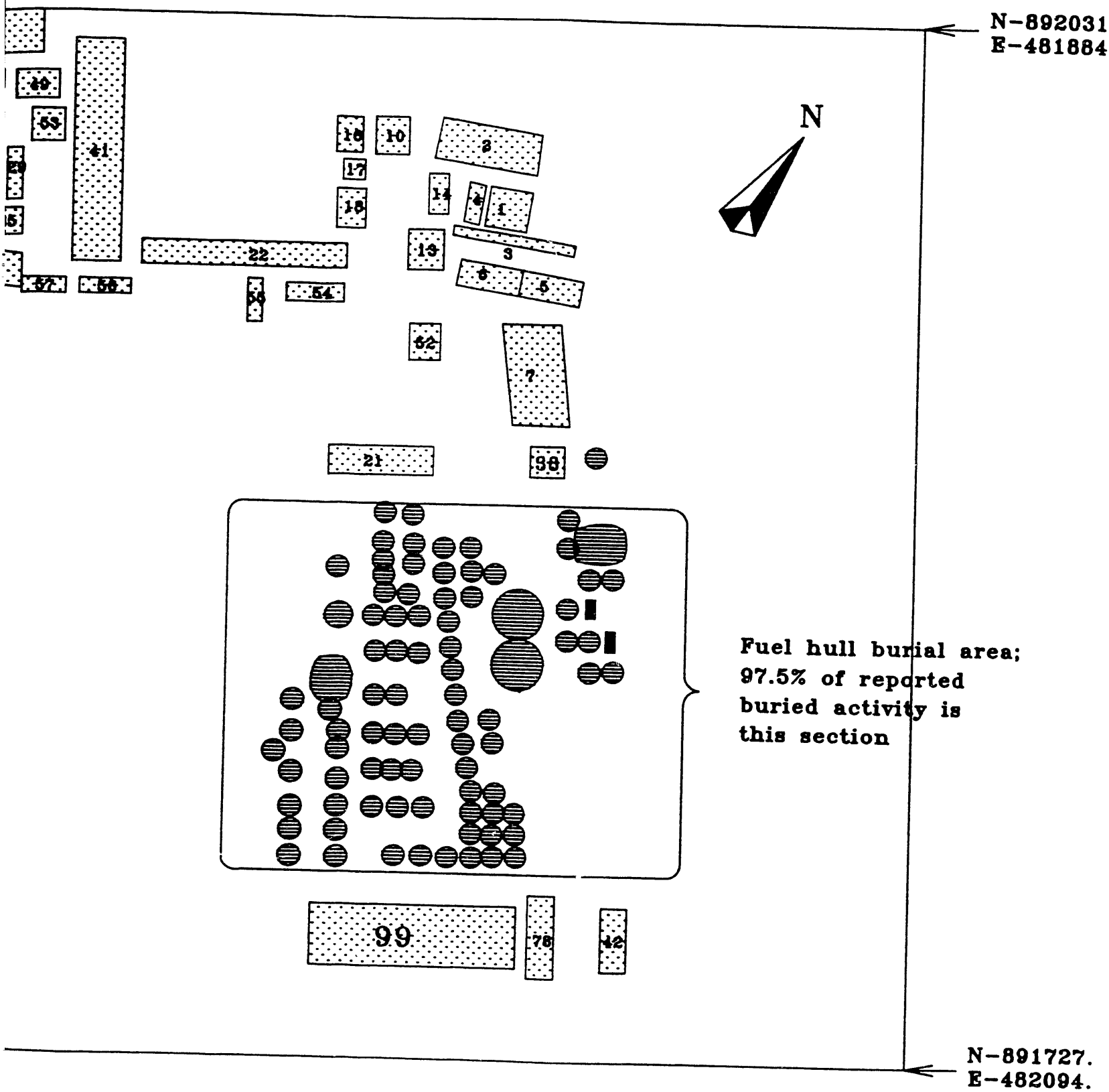

Figure 2.5 Location map of disposal pits and trenches at the FDA (From Nuclear Fuel Services, Inc., High level burial area map, drawing no. 40-A-A-1158).

The miscellaneous wastes disposed in the pits in the northeastern corner of the FDA included twenty-two one thousand gallon steel tanks containing spent tributyl-phosphate (TBP) solvent dissolved in n-dodecane, which is one of the primary components of kerosene (Blickwedehl et al., 1989). In November 1983, solvent was detected in a monitoring well located outside the north western corner of the FDA. The solvent plume has been detected at a distance of approximately 18 m from its original disposal location with migration to the north. The mechanism for solvent release from buried storage tanks is hypothesized to have been as follows (Blickwedehl et al., 1989): "After burying the waste, ground water would fill up the original disposal pits which were excavated in the low permeability unfractured till. Eventually, the water level reached the covers of the tanks, which were loosely attached, and flowed in. Water entering the tanks eventually displaced the lighter solvent. When the water level in the disposal pits reached the weathered till, the water and solvent floating on top of it moved laterally through the surficial fractured zone."

A trench has been constructed in 1990 along the north western and north eastern borders (See Figure 2.6) of the FDA to intercept and remove any solvent as well as other contaminants. A cross-sectional view of the trench is shown in Figure 2.7. The trench is approximately 20 ft (6m) deep and was constructed in intervals up to a total length of 804 ft (270 m)[3/]. The base of the trench slopes toward a central sump located at the northeastern corner of the FDA. Liquids seeping into the trench will flow under gravity towards the central sump and from there are pumped to a treatment and storage facility on the FDA. The volume of water pumped from the trench is recorded on a daily basis. A time record of measured trench inflows for the period of March to August, 1990 is shown in Figure 2.8. To date (June, 1991) no solvent or radioactive contaminants have been measured in the interceptor trench. A time record of daily precipitation recorded at the FDA during the same period of March to August, 1990 is shown in Figure 2.9. A comparison of the occurrence of peak precipitation events and trench inflows shows a reasonably good correspondence with a lag time of approximately 2 to 3 days of the response in trench inflow to precipitation events. It should be noted that the vertical axes in both Figures 2.8 and 2.9 are plotted using a logarithmic scale, in order to accommodate the large variation in daily precipitation and trench inflows. It can be seen that whereas the average precipitation stays fairly constant throughout the six-month period, the measured inflows into the interceptor trench decreased considerably following the first one to two months of operation even though the length of the trench was increased during the same period. The initially large, and then decreasing rate of trench inflow has been attributed by site personnel[4/] to a temporary drainage effect of the soil surrounding the trench following trench installation, combined with a diminishing contribution of surface run-off seepage through the trench cap as the clay cap settled with time. An alternative, or at least contributing factor, is the influence of evapotranspiration of the grass vegetation at the FDA. Evapotranspiration of up to 80 cm/year

---

[3/] Mr. Tom Weiss, WVNS, personal communication

[4/] Mr. Tom Weiss, WVNS, personal communication

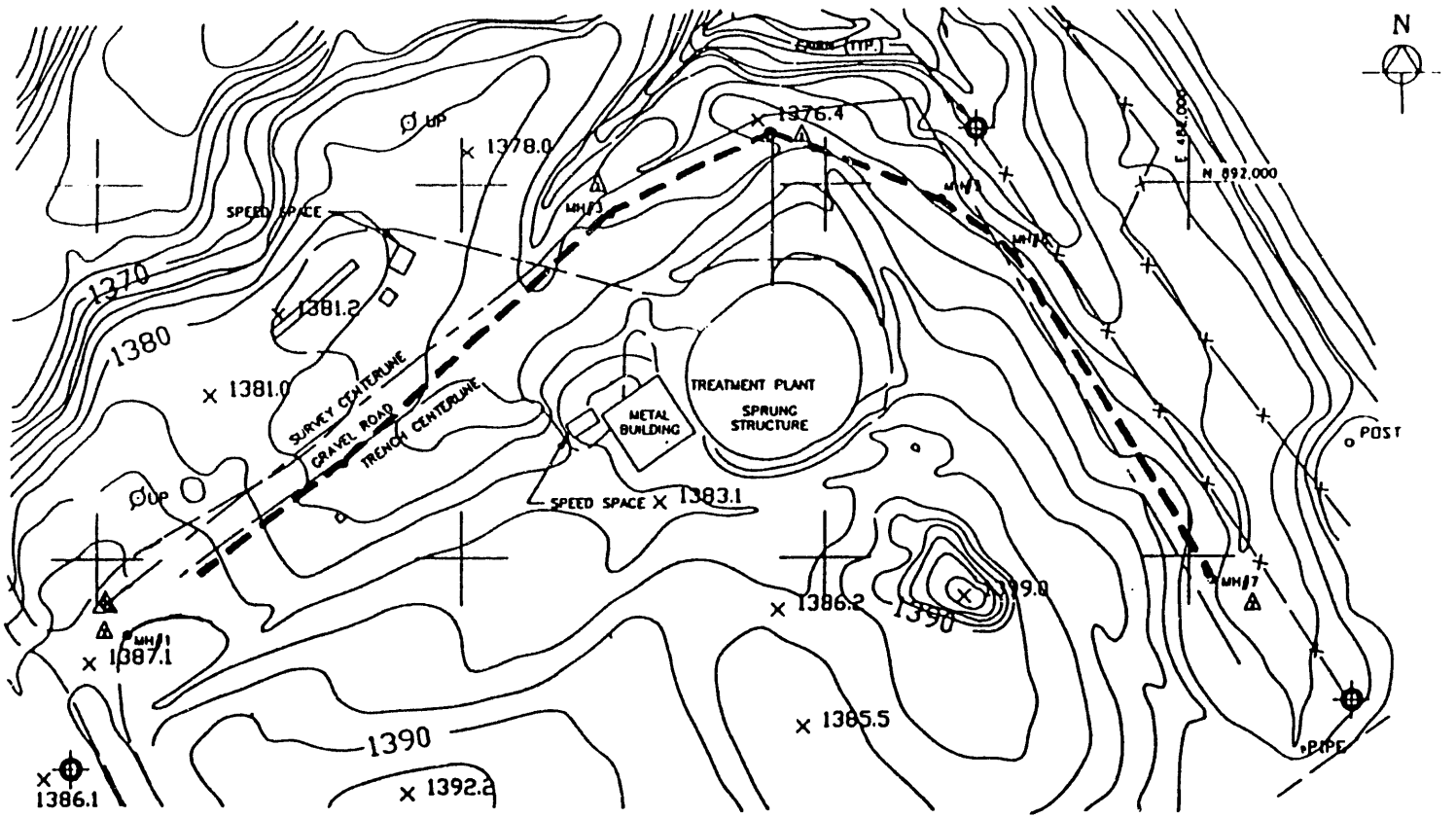

Figure 2.6 Position of the interceptor trench along the north-eastern and north-western boundary of the FDA.

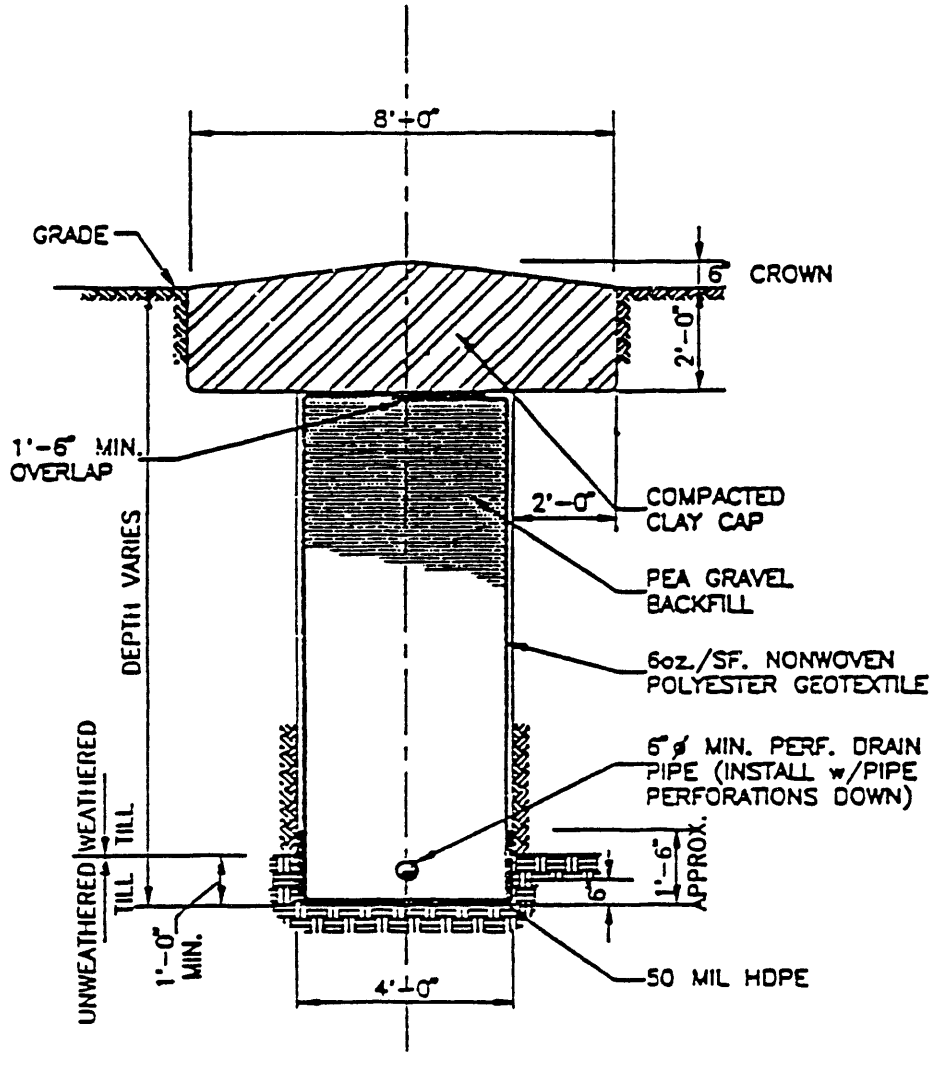

Figure 2.7 Cross-sectional view showing typical design of the interceptor trench.

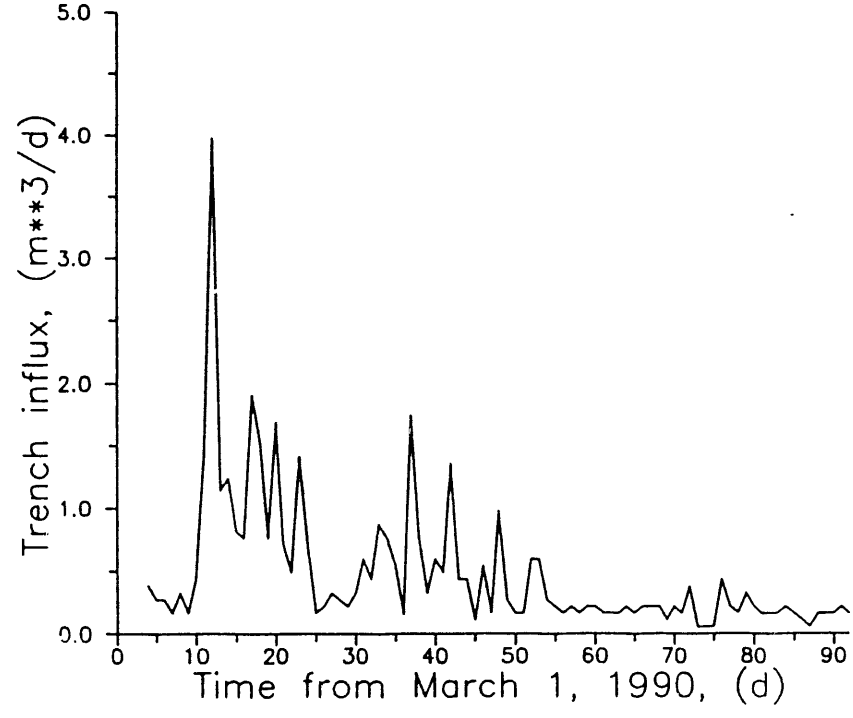

Figure 2.8 Observed inflows to interceptor trench for the period March to August, 1990.

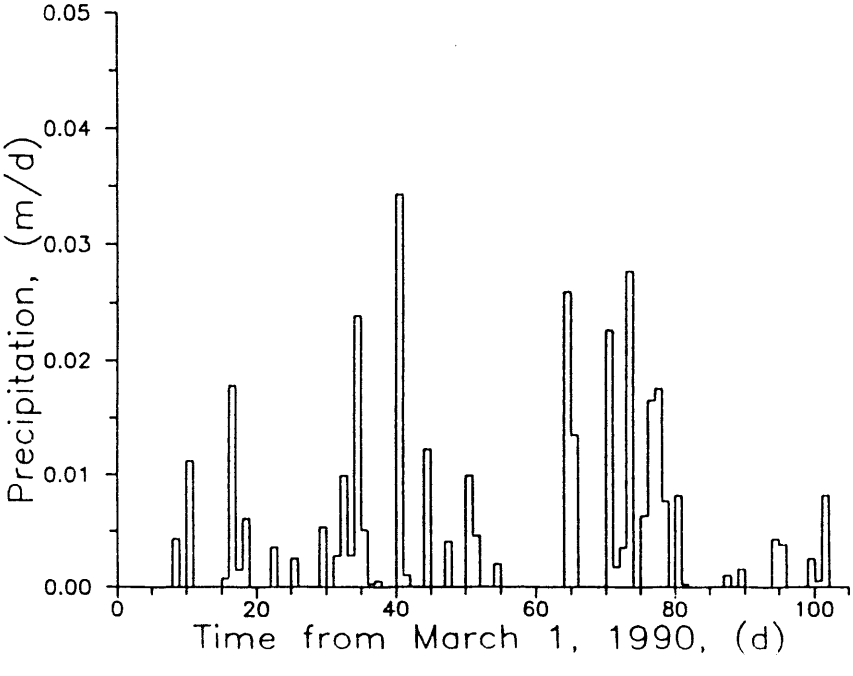

Figure 2.9 Daily precipitation recorded at the FDA during the period March to August, 1990.

could compensate for much of the precipitation during Spring and Summer and thereby eliminate much of the inflow into the trench.

2.5 GROUNDWATER MONITORING DATA

In the course of various hydrogeological investigations conducted over the last 10 years, a substantial number of groundwater monitoring wells have been installed in and around the FDA. These wells can provide useful auxiliary data for calibrating a groundwater flow model. The previous modeling studies conducted at the FDA and state licensed disposal area have relied primarily on available water level data from monitoring wells for model calibration. A limitation of using only water level data to calibrate a groundwater flow model is that when hydraulic conductivities are not known or in error, a model may reproduce observed water levels very well but can still fail to accurately simulate flow rates. The availability of direct data on trench inflow rates largely overcomes this limitation.

Even though many groundwater wells are present at the site, only a relatively few of them provide data that is useful for the present investigation. The two main criteria for evaluating the suitability of monitoring well data were: (1) the well would have to be installed in the upper part of the till to provide data on water table fluctuations in the near-surface zone; and (2) frequent monitoring data would have to be available for the March to May 1990 model simulation period. These two considerations eliminated many of the wells. However, the monitoring wells that have been installed and/or monitored as in the north-eastern corner of the FDA as part of the solvent plume monitoring effort (Blickwedehl et al., 1989) provided exactly the data required. Frequent monitoring data are available for a number of wells that were either installed specifically as part of the solvent investigation (Blickwedehl et al., 1989), or that were installed previously by the U.S.G.S but have been monitored frequently as part of the solvent plume migration study.

Observed water level variations in the period March - May 1990 for a number of these shallow wells are shown in Figure 2.10 with well locations indicated in Figure 3.1. Wells 89-13-W and 85-I-11 show water levels within 1 m of the soil surface during the entire period. Wells 89-29-E and 89-5-N show consistently lower water levels, although the water level in these wells continued to rise throughout the depicted time period. A number of factors probably contribute to the somewhat different behavior of the wells. One consideration is the different topographic locations of the wells, differences between wells may reflect three dimensional flow patterns at the site. Wells 89-13-W and 85-I-11 show similar average water levels, but well 85-I-11 displays much greater temporal variation. A likely reason for this is that the casing of well 85-I-11 has been observed to be cracked, allowing direct seepage of rainwater into the well[5/]. The rising water level in wells 89-29-E and 89-5-14 is somewhat anomalous, since it continues throughout the summer period (Figure 2.11). Over the approximately 1 year period shown in Figure 2.11, the lowest water levels occurred during the winter, while highest water levels

---

5/ Peter Newsome, Dames and Moore, personal communication.

occurred in the summer time. This is the reverse of what would be expected based on climatological information. The highest water levels would be expected in late winter and spring in response to snowmelt with dropping water levels through the summer. A possible explanation for the behavior exhibited by this, as well as other of the solvent plume exploratory wells, is that these wells may represent not water level variations in the upper part of the Lavery till (particularly in the weathered zone), but rather the water levels inside disposal trenches. The exploratory wells were intended to be installed inside solvent disposal pits (Figure 2.12) and the water level record may reflect a delayed response of the water level in these pits to rainfall events.

Besides these mentioned wells, shallow water level data are available from a number of 'RCRA' wells installed around the perimeter of the FDA (Figure 2.13). These RCRA wells included both shallow wells, screened in the upper most part of the Lavery Till and deeper wells, screened in the unweathered till. The shallow monitoring wells are wells no. 0906, 0907, 0908 and 1109A. Water level data for these wells during 1990 are given in Table 2.2. Wells 0906 and 0907 indicate water levels between 2 to 3 meters below the ground surface during most of the year, while wells 0908 and 1109 indicate generally deeper water levels.

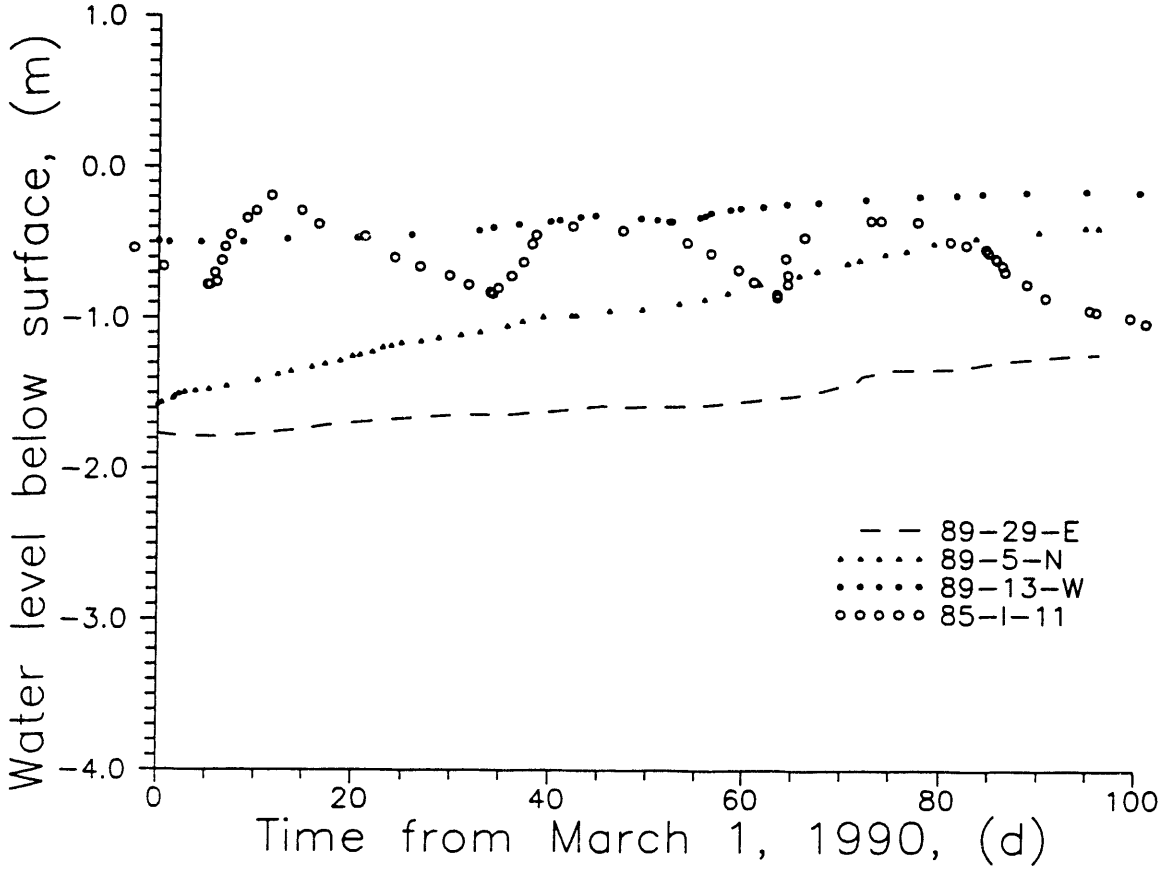

Figure 2.10 Observed water levels in Solvent Plume Exploratory wells during Spring, 1990.

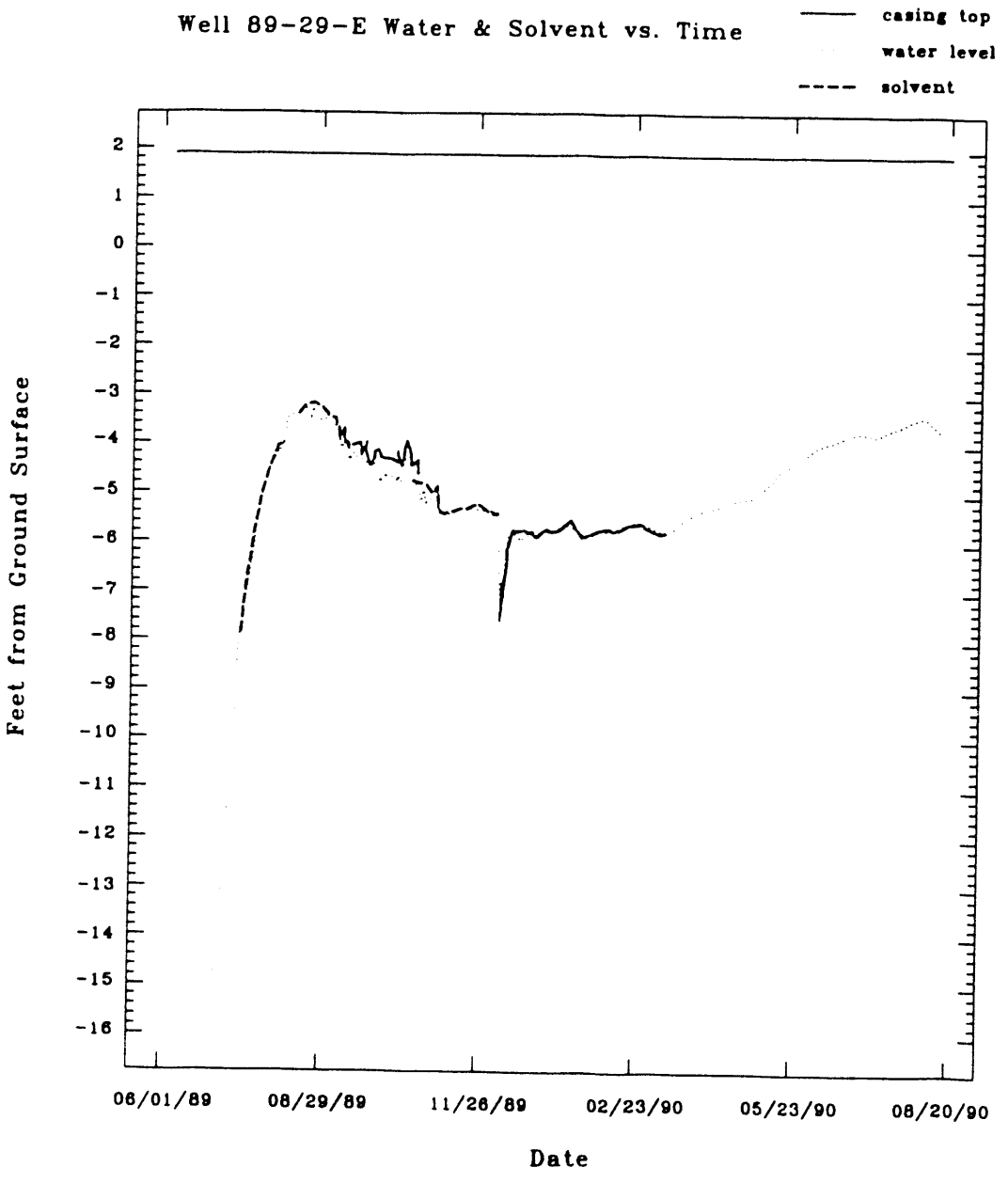

Figure 2.11 Observed water level variations for well no. 89-29-E.

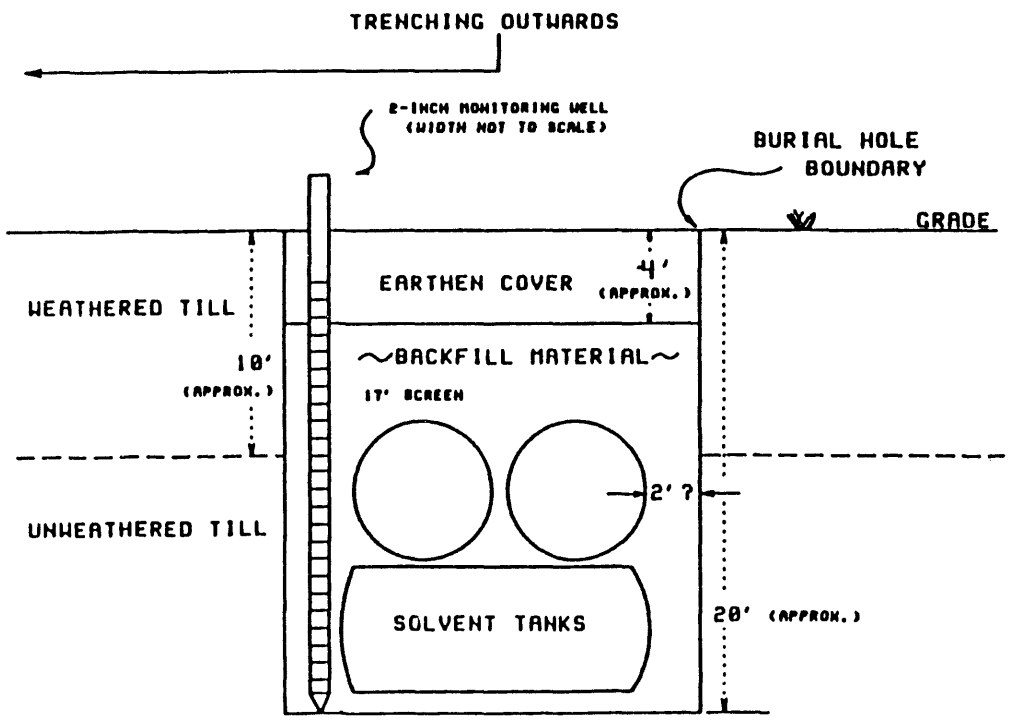

Figure 2.12 Schematic diagram showing well installation in solvent disposal pits (from Blickwedehl et al., 1989).

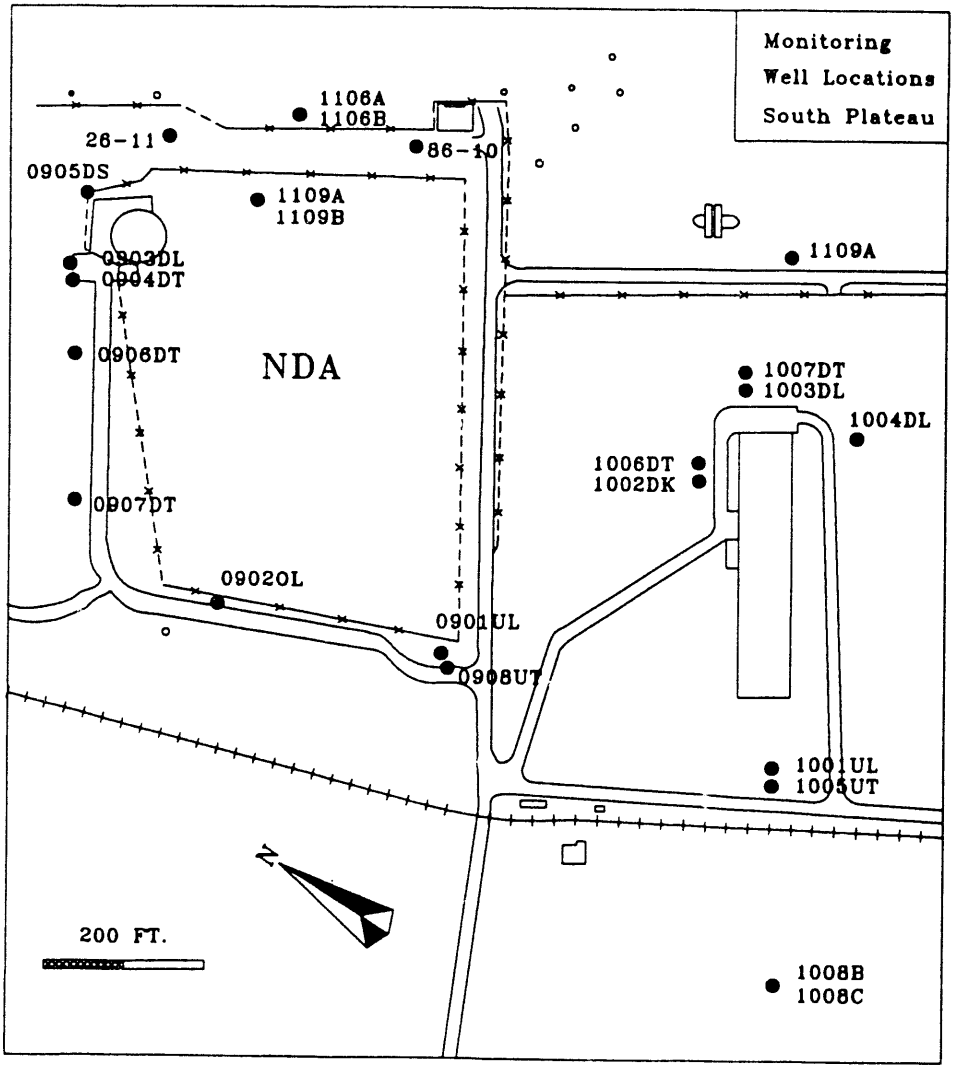

Figure 2.13 Location of NDA RCRA monitoring wells.

Table 2.2 Shallow water level data for FDA RCRA monitoring wells[1)]

	Well ID No.			
	0906	0907	0908	1109A
Screened Interval	1.5-3.0[2)]	1.8-4.9	1.8-6.4	1.8-4.9
Measurement Date				
1/02/90	2.24[2)]	2.94	-	-
1/19/90	1.76	2.47	-	-
1/24/90	1.96	2.35	-	-
2/06/90	1.32	2.14	-	-
2/16/90	1.17	1.99	-	-
2/20/90	-	-	-	-
6/01/90	-	-	5.48	-
7/18/90	1.31	1.96	-	-
7/26/90	2.0	3.12	-	-
7/30/90	1.98	-	5.18	-
8/2,3/90	-	-	5.18	-
8/14,17/90	2.33	3.20	5.83	2.75
8/30/90	-	-	-	2.70
9/05/90	2.47	2.78	5.85	4.68
9/19/90	-	-	-	3.97

1) Data obtained from memorandum from C.J. Roberts, WVNS to T.J. Rowland, USDOE, dated 10/29/90.

2) Meters below ground surface.

3 GROUNDWATER FLOW MODEL

3.1 MODELED CROSS-SECTIONS

Two separate vertical cross-sections have been chosen in this study to simulate transient groundwater flow in the FDA. The location of the cross-section is shown in Figure 3.1. The first cross-section (A-A′) is oriented from southwest to northwest across the FDA and represents a sub-section of the larger profile modeled by Prudic (1986) and by Bergeron and Bugliosi (1988). The entire cross-section modeled by Bergeron and Bugliosi is shown in Figure 3.2, and can be seen to extend across both the FDA and the state-licensed disposal area. The subsection simulated in the present study is shown as the cross-hatched area in Figure 3.2. The first cross-section was chosen to coincide with the profile of Bergeron and Bugliosi (1986), in order to allow verification of the present model against their steady state result. In addition, the available results of Bergeron and Bugliosi could be used to assign boundary conditions for the present model. The second cross-section (B-B′) of Figure 3.1 is oriented from southwest to northeast across the FDA. It crosses underneath the treatment and disposal facility ("Sprung Structure") on the FDA and terminates at the interceptor trench. The motivation for selecting this second cross-section is discussed later on in this report, following presentation and evaluation of simulation results for the first cross-section. The vertical profiles of the two sections are shown in Figures 3.3 and 3.4. They show the dimensions of the modeled areas, vertical sequence of different soil materials (weathered, transition and unweathered till), as well as the assumed initial position of the water table in the FDA area. It can be seen that in comparison with the modeling of Prudic (1986) and Bergeron and Bugliosi (1988), a relatively shallow cross-section is modeled. The reason for this is that the present investigation is focused on transient flow through the near-surface layers at the FDA, with less interest in movement through the deeper, unweathered till.

3.2 GOVERNING EQUATIONS

Groundwater flow at the FDA burial site near West Valley is simulated and analyzed using the VAM2D computer code (Huyakorn et al., 1991). VAM2D is a two-dimensional finite element code for simulation of groundwater flow and solute transport in variably saturated porous media. The governing equation for transient water flow in a variably saturated soil is written as:

$$\frac{\partial}{\partial x_i}\left[K_{ij}k_{rw}\left(\frac{\partial \psi}{\partial x_j} + e_j\right)\right] = \left(S_w S_s + \frac{dS_w}{d\psi}\right)\frac{\partial \psi}{\partial t} - q \qquad (3.1)$$

where

- ψ is the pressure head (L);
- K_{ij} is the components of saturated hydraulic conductivity tensor (L/T);
- k_{rw} is the relative permeability with respect to water phase;
- x_i (i=1, 2) are spatial coordinates (L);

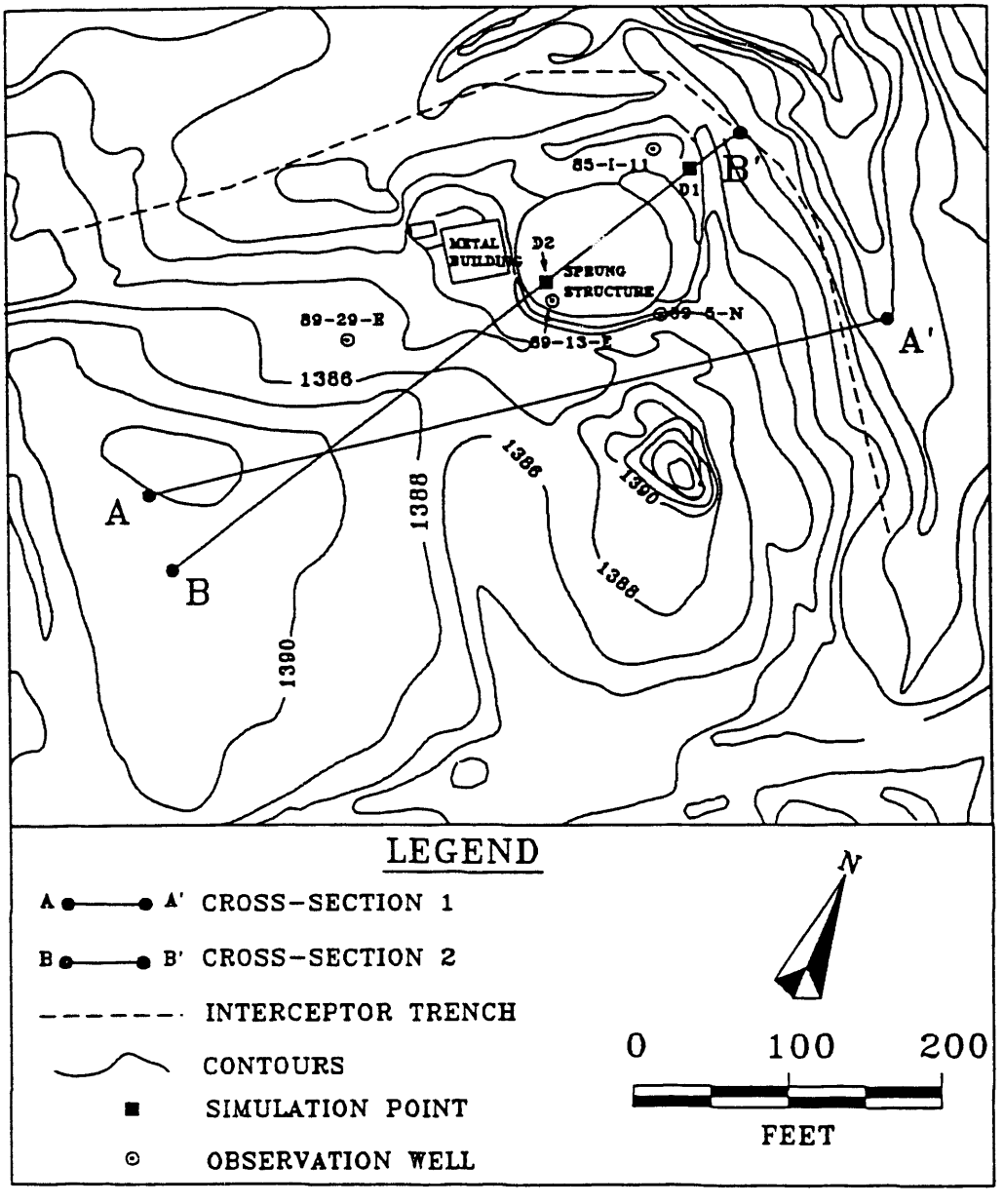

Figure 3.1 Locations of simulated cross-sections and interceptor trench at the Facility Disposal Area of the Western New York Nuclear Service Center.

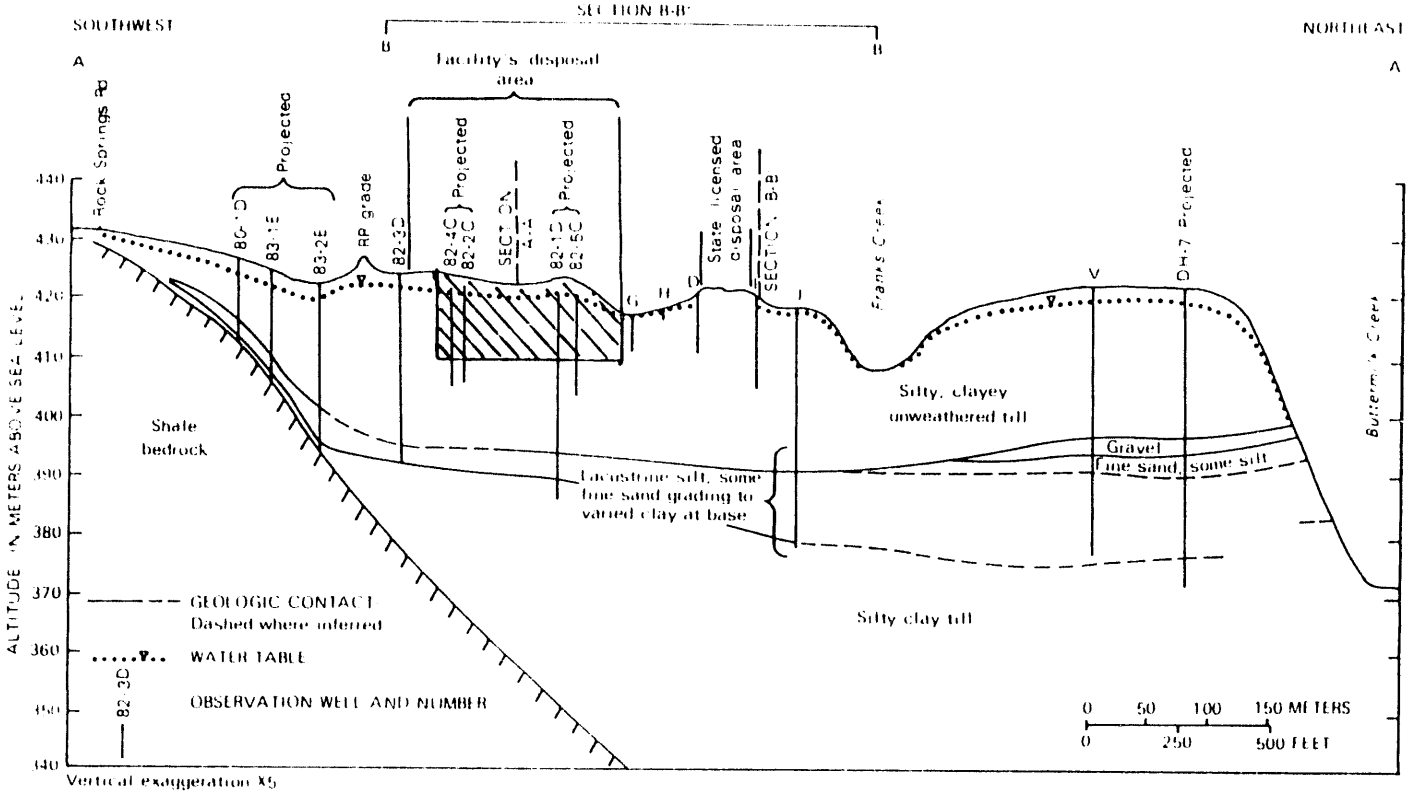

Figure 3.2 Vertical cross-section through FDA and state-licensed disposal area used by Bergeron and Bugliosi (1988).

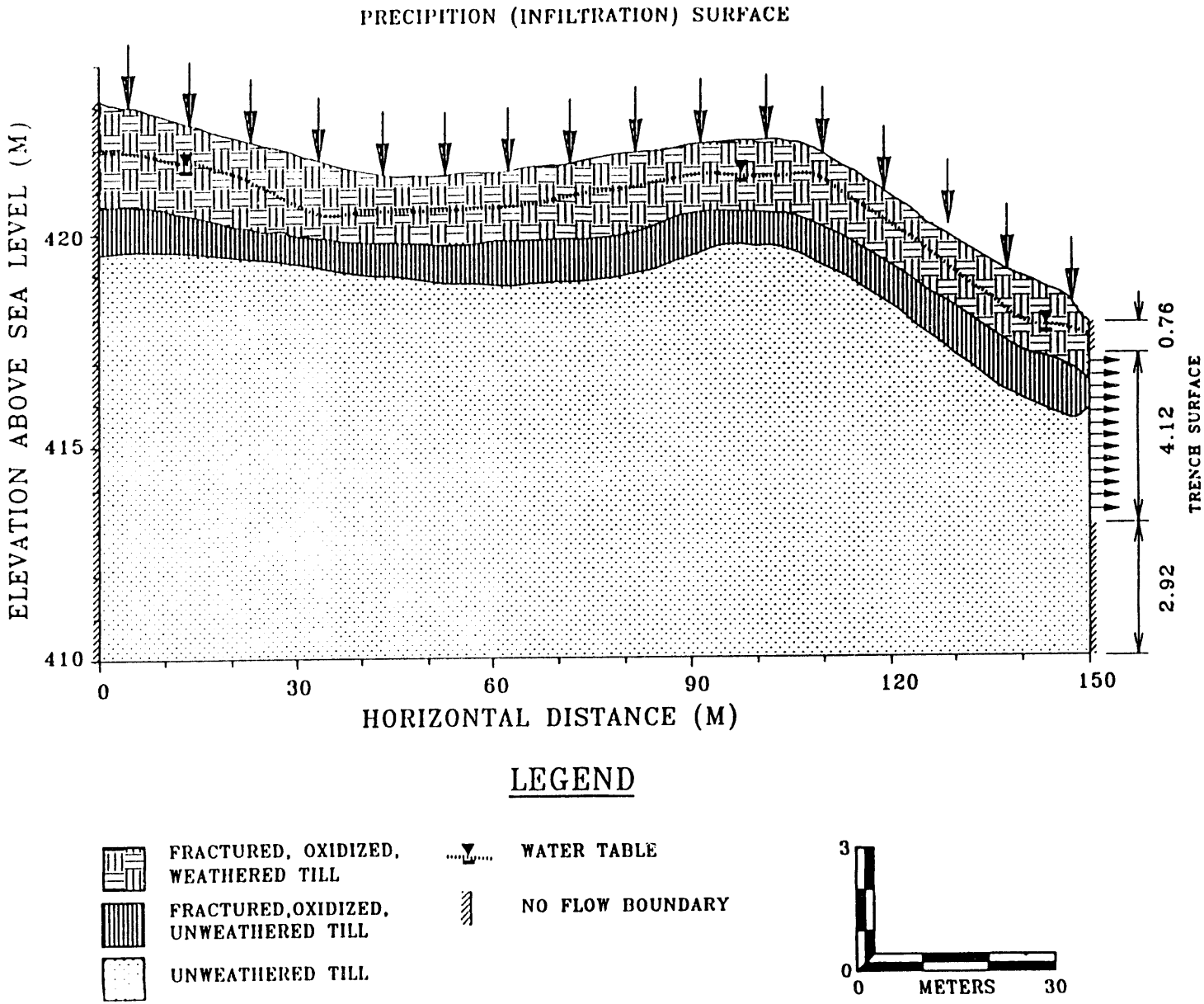

Figure 3.3 Section 1 (A-A′) of the FDA site showing position of fractured, weathered and unweathered till layers, assumed initial water table, and boundary conditions. (Location of section is shown in Figure 3.1.)

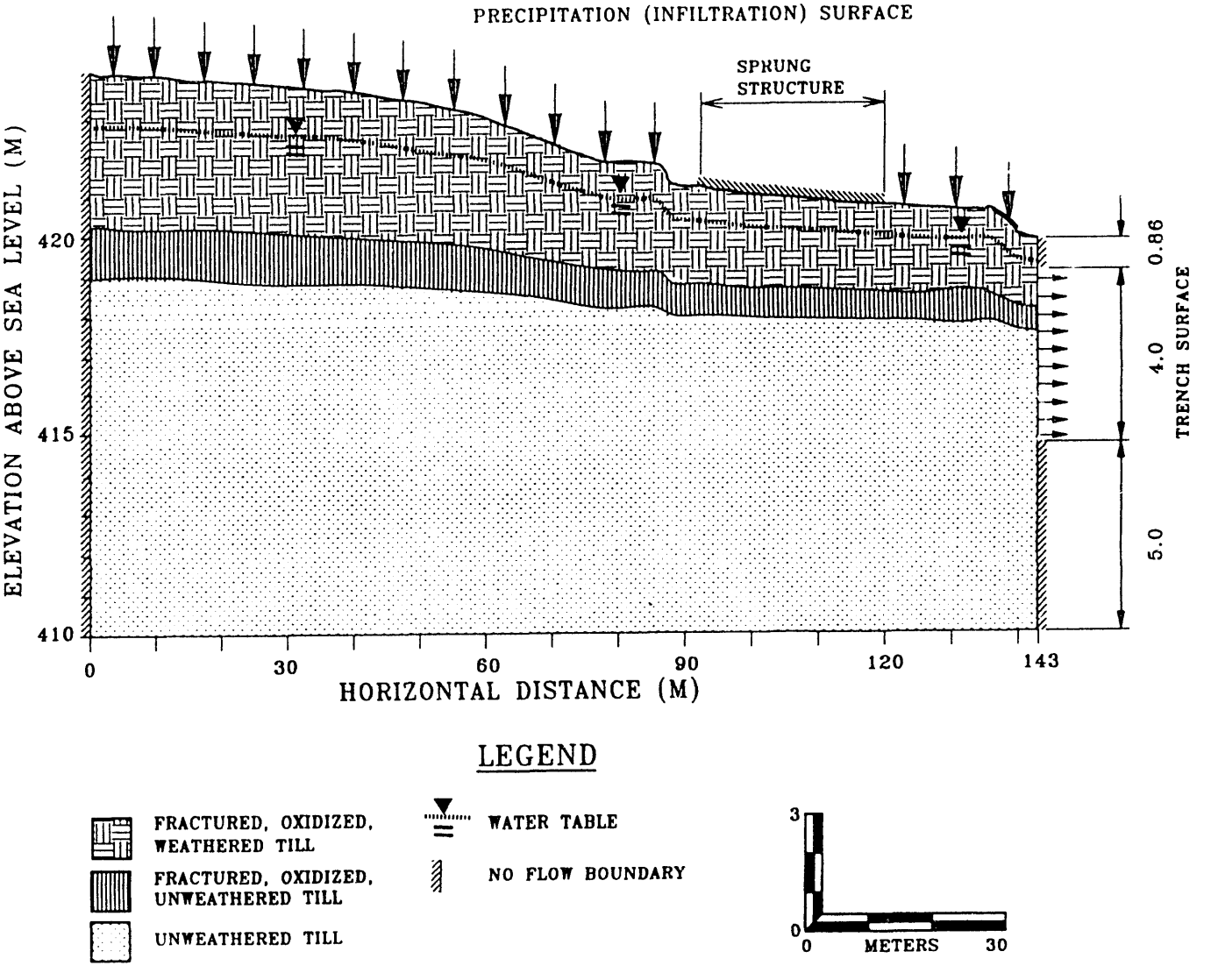

Figure 3.4 Section 2 (B-B′) of the FDA site position of fractured, weathered and unweathered till layers, assumed initial water table, and boundary conditions. (Location of section is shown in Figure 3.1).

e_i is the unit vector assumed to be vertically upward;
S_w is water phase saturation;
t is time (T);
q is the volumetric flow rate via sources (or sinks) per unit volume of the porous medium (L^3/T);
S_s is the specific storage coefficient (L^{-1}) defined as

$$S_s = \rho_w g \, (\phi C_r + C_w) \tag{3.2}$$

where

ρ_w is the density of water (M/L^3);
g is the gravitational acceleration constant (L^2/T);
ϕ is the effective porosity;

C_r and C_w are coefficients of compressibility of the porous medium and water (LT^2/M), respectively. It may be noted that although (3.1) is written in terms of the pressure head, ψ, the VAM2D code allows selection of either pressure head or hydraulic head, $h = \psi + z$ (where z is the elevation above datum), as primary dependent variables in solving the flow equations. The simulations presented here actually used the hydraulic head formulation which has certain advantages when used in conjunction with a curvilinear, rather than strictly rectangular grid.

The governing equation for variably saturated flow (Equation 3.1) is the Richards equation for porous media. The VAM2D code does not have capability to account explicitly for fractured media, such as the upper weathered till layer. Very few, if any, simulation codes are available that have this capability, particularly when dealing also with transient and variably saturated flow conditions. Since VAM2D has many of the other capabilities required to model this site (surface infiltration conditions, seepage trench face), and detailed quantitative data on fracture properties such as aperture, required to operate a discrete fracture model, are not available, it was considered justified to use the VAM2D code for the simulations described herein. The effects of fractures in the upper, weathered till layer are accounted for indirectly through the assignment of the hydraulic constitutive relations which now represent effective curves for the composite fractured-porous medium.

3.3 SOIL HYDRAULIC CONSTITUTIVE RELATIONS

In order to solve the variably saturated flow problem, it is necessary to specify the relationships of relative permeability versus water phase saturation, and pressure head versus water phase saturation. Two alternative function expressions are used in the code to describe the relationship of relative permeability versus water saturation. These functions are given by (Brooks and Corey, 1966; van Genuchten, 1980):

$$k_{rw} = S_e^n \tag{3.3}$$

and

$$k_{rw} = S_e^{1/2} [1-(1-S_e^{1/\gamma})^\gamma]^2 \tag{3.4}$$

where n and γ are soil specific parameters; S_e is a dimensionless effective saturation, defined as:

$$S_e = \frac{S_w - S_{wr}}{1 - S_{wr}} \tag{3.5}$$

where S_w is the water saturation and S_{wr} is the residual water saturation, which is a soil specific coefficient.

The relationship of pressure head versus water saturation is described by the following function (Mualem, 1976; van Genuchten, 1980):

$$\frac{S_w - S_{wr}}{1 - S_{wr}} = \begin{cases} \dfrac{1}{[1+(\alpha\,|\,\psi - \psi_a\,|\,)^\beta]^\gamma} & for\ \psi < \psi_a \\ 1 & for\ \psi \geq \psi_a \end{cases} \tag{3.6}$$

where α (L^{-1}) and β are empirical parameters; ψ_a is the air entry pressure head (L). The parameters β and γ are usually related by $\gamma = 1\text{-}1/\beta$.

Data on relative permeability as a function of water content and of water content as a function of pressure head are available from U.S. DOE (1986), and are given also in Appendix A. The data are, for the pressure head range of interest, plotted in Figures 3.5 and 3.6 respectively, together with fitted curves used in the VAM2D simulations. The relationship between water content and pressure head is shown in Figure 3.5, with data points corresponding to measured data and the fitted curve corresponding to the filled van Genuchten relation (Eq. 3.3). The relative permeability - water content relation is shown in Figure 3.6. The continuous curve in this figure corresponds to the Brooks-Corey relative permeability function (Eq. 3.3) which was used in the simulations. The hydraulic constitutive relations shown in Figures 3.5 and 3.6 show the highly nonlinear behavior expected of fractured clay media. The overall water content can be seen to decrease only very slightly with decreasing pressure head until pressure head values are -50 m and lower. The shape of the water retention characteristic indicates the dominance of the properties of the till clay matrix. Fractures will drain at pressure heads relatively close to zero. Since fractures contribute relatively little to the total porosity, the

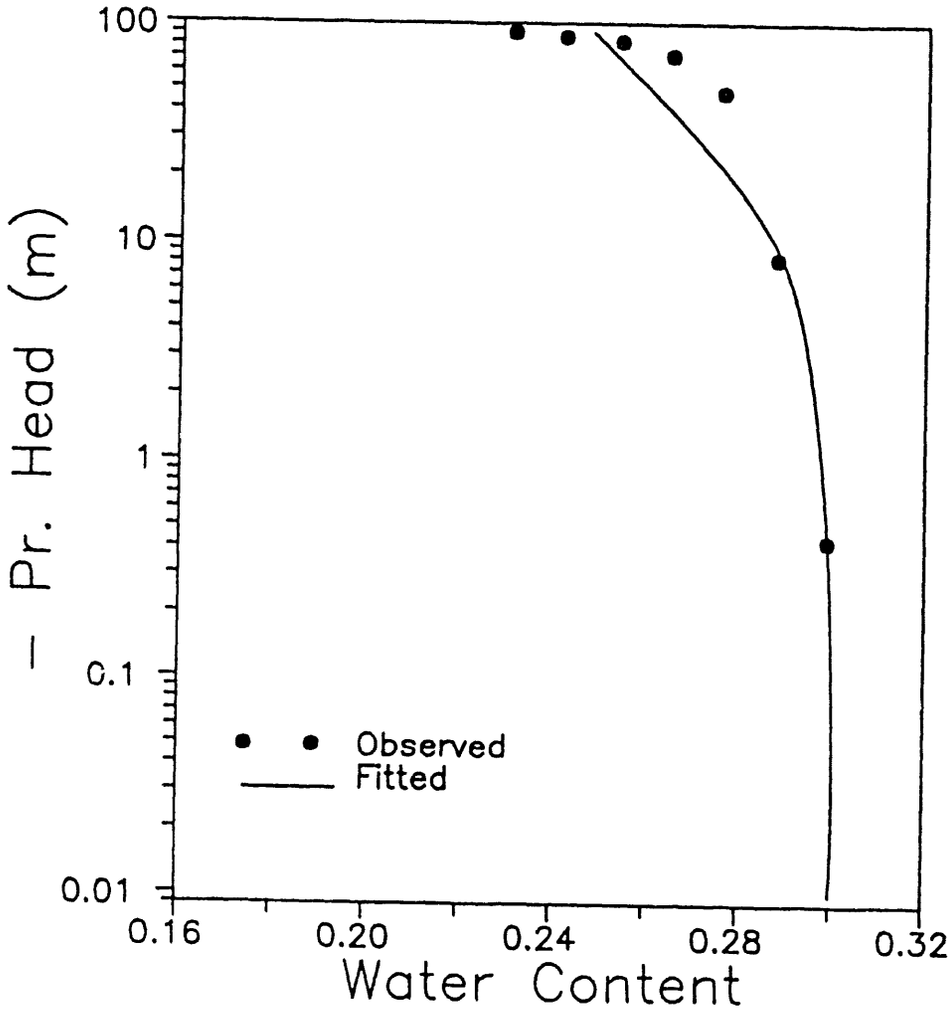

Figure 3.5 Water content versus capillary pressure head relations used in VAM2D model. Observed data from U.S. DOE (1986).

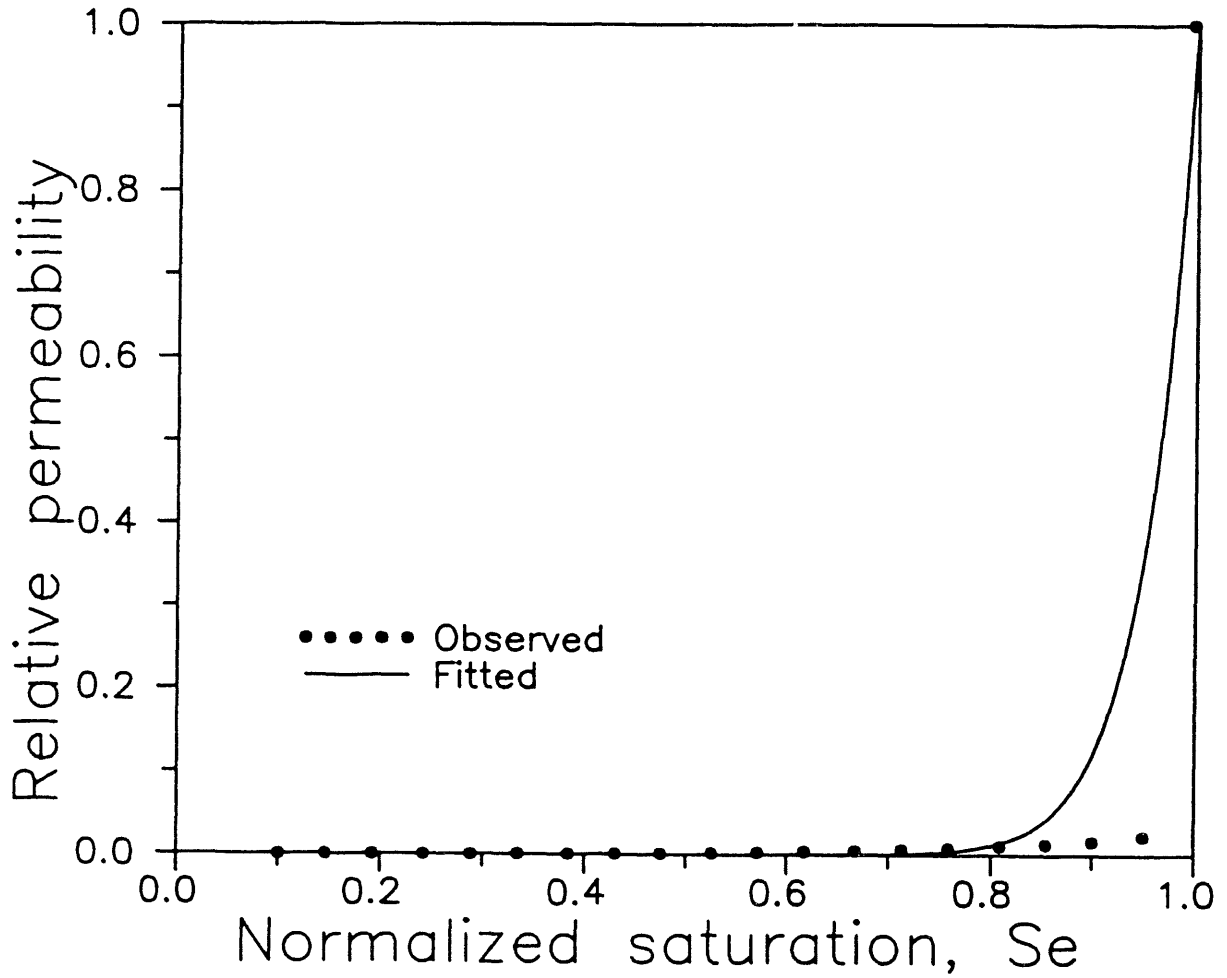

Figure 3.6 Relative permeability versus water saturation curves used in VAM2D modeling. Observed data from U.S. DOE (1986).

overall water content of the soil still remains close to saturation, until the matrix starts to drain at much lower pressure heads. Since actual pressure heads in the unsaturated zone at the FDA are expected to not fall below a few meters, Figure 3.5 indicates that even as the water table falls during dry periods, the till matrix itself will stay close to saturated. In contrast to the water retention characteristic, the relative permeability data in Figure 3.6 show the strong influence of fractures on the hydraulic conductivity. A slight decrease in overall saturation, corresponding to the emptying of fractures, results in a very steep drop of the hydraulic conductivity. The solid curve in Figure 3.6 represents the relationship assigned to the weathered till. Although this curve is quite steep near saturation, it is still less so than the observed data. Some smoothing of the curve was used to reduce numerical problems in the simulation. The relative permeability curves assigned to the transition layer between the weathered and unweathered till, and to the underlying unweathered till are shown also in Figure 3.6. These zones were assigned smoother curves by adjusting the value of the exponent n in Eq. 3.3 under the assumption that they behave more nearly like porous media. It may be pointed out however, that in the simulations these lower layers stayed saturated throughout the modeling period and the model simulations are thus independent of the unsaturated hydraulic properties of these zones; the only material characteristics that affect flow are the saturated hydraulic conductivity values.

3.4 INITIAL AND BOUNDARY CONDITIONS

The initial and boundary conditions implemented in VAM2D to solve a variably saturated flow problem are in general, as follows:

Initial conditions:

$$\psi(x_i, 0) = \psi_o(x_i) \tag{3.7}$$

Boundary conditions:

i) Prescribed head

$$\psi(x_i, t) = \bar{\psi}(t) \text{ on } B_1 \tag{3.8}$$

ii) Prescribed flux

$$v_i n_i = -v_n(t) \text{ on } B_2 \tag{3.9}$$

iii) Seepage face

$$\psi(x_i, t) = 0 \text{ (at the seepage face), and fluid only leaves the system.} \tag{3.10}$$

iv) Evaporation and infiltration

$$| v_i n_i | \leq | E_s^* (t) | \tag{3.11a}$$

and

$$\psi_L \leq \psi \leq 0 \tag{3.11b}$$

where

- ψ_o is the initial head value;
- B_1 is the portion of the flow boundary with ψ prescribed as $\bar{\psi}$;
- v_i is the Darcy velocity component;
- B_2 is the portion of the flow boundary with the outward normal velocity $-v_n$ prescribed;
- n_i is the outward unit normal vector of the boundary;
- E_s^* is the maximum potential surface flux under prevailing atmospheric conditions;
- ψ_L is the minimum pressure head allowed under the prevailing soil conditions.

The boundary conditions used in this flow simulation for the two modeled sections shown in Figures 3.2 and 3.3, are as follows:

1. No-flow boundaries along the left side because the hydraulic gradient at this boundary is essentially vertical (Prudic, 1986).
2. On the right side, the trench face is treated as a seepage face boundary, and the portions above and below the trench are treated as no-flow boundaries.
3. Ground surfaces are treated as infiltration boundaries, with transient infiltration fluxes calculated using observed precipitation data during the simulation period, as outlined above.
4. The bottom surfaces are subject to prescribed-head conditions, with head values taken from the steady state simulation results of Prudic (1986) and Bergeron and Bugliosi (1988), assuming that approximately steady state conditions prevail at this depth.

The initial conditions used for the two sections were generated by the VAM2D code using the above boundary conditions with a constant infiltration flux (2 cm/yr) along the soil surface and zero pressure head conditions at the location of the interceptor trench.

3.5 FINITE ELEMENT GRID DESIGN

In the VAM2D modeling of transient flow in the FDA site, the two-dimensional domains for Sections 1 and 2, depicted in Figures 3.2 and 3.3, respectively, were discretized into two separate curvilinear finite element grids, shown in Figures 3.7 and 3.8. The first grid (Figure 3.7) was designed to simulate flow along Section 1 (A-A′, see Figure 3.1). The second finite-element grid (Figure 3.8) was developed to evaluate flow along Section 2 (B-B′) in Figure 3.1.

Very fine grid spacings were generated for the two grids when compared to those in the previous simulation studies of the same site (e.g., Prudic, 1986; U.S. DOE, 1986; Bergeron and Bugliosi, 1988). A total of 1,540 and 1,460 elements are used for the two sections, respectively. The maximum horizontal element dimensions are $\Delta x = 2$ meters, and the maximum vertical element spacings are $\Delta y = 1$ meter. Smaller nodal spacings are used near the ground surface and near the trench to obtain good accuracy and resolution near these time dependent infiltration and seepage face boundaries.

Prescribed head (Eq. 3.8) and prescribed flux (Eq. 3.9) boundary conditions are quite straight-forward and do not require further elaboration. The seepage face boundary condition applies at boundaries where instantaneous drainage takes place, physically it describes a condition where the pressure head is fixed at $\psi = 0$ when the soil is saturated and no-flow conditions occur when the soil is unsaturated. These conditions control seepage from the Lavery till into the interceptor trench.

The evaporation-infiltration condition (Eq. 3.11) describes a condition in which the flux (Eq. 3.11a) at the soil surface is prescribed as long as the specified pressure head condition (Eq. 3.11b) is satisfied. During periods of evaporation, water is removed at a prescribed rate until the pressure head at the soil surface falls below the critical value ψ_L. When this occurs, the boundary condition changes to a prescribed head condition with ψ_L. During subsequent time steps, it is continually checked that the actual evaporation flux is less than the potential evaporation rate. When the actual flux becomes greater than E_s, the boundary condition changes back to a prescribed flux condition. Rainfall conditions are handled in an analogous manner; initially the flux into the soil is equal to the prescribed rainfall rate, E_s. When the rainfall rate exceeds the saturated hydraulic conductivity of the soil, the boundary condition switches to a prescribed head condition with $\psi = 0$ at the soil surface. When the rainfall rate is reduced and causes unsaturated conditions at the soil surface, the boundary condition reverts back to one of a prescribed flux. Physically, this infiltration condition corresponds to a situation where run-off starts when the soil surface becomes saturated. The total amount of run-off is then equal to the difference between the total rainfall and the amount of water actually admitted into the soil. Use of this boundary condition is particularly advantageous in situations such as the present where data on total precipitation rate are available, but the amounts of run-off and net infiltration are not known. Using (Eq. 3.11), the modeler does not need to make assumptions regarding the partitioning of precipitation into infiltration and run-off, rather the computer code makes these corrections automatically during the simulation, as a function of the hydraulic properties assigned to the soil. While the approximation via (Eq. 3.11) represents a substantial simplification of the surface processes under ambient atmospheric control, they also represent the physically closest approximation possible without resorting to a complete rainfall-runoff modeling approach, and require knowledge only of the total precipitation rate.

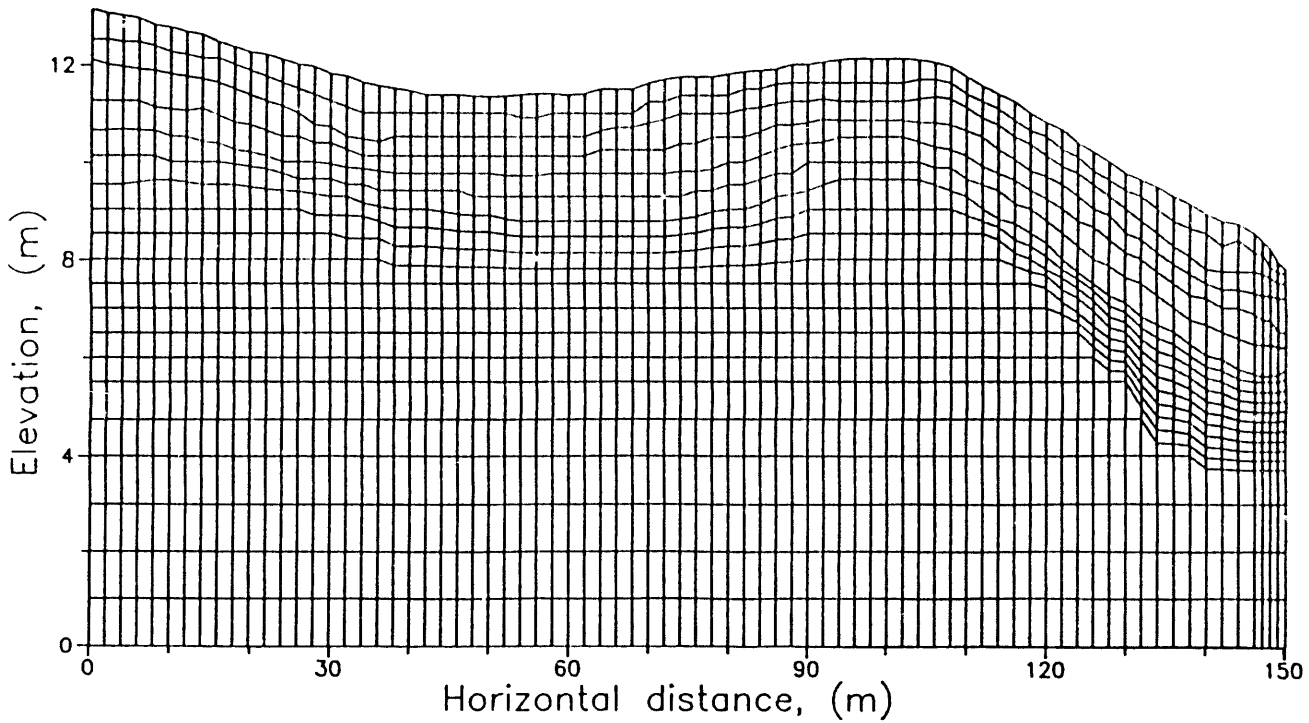

Figure 3.7 VAM2D curvilinear finite element grid used ir the simulation of groundwater flow along Section 1.

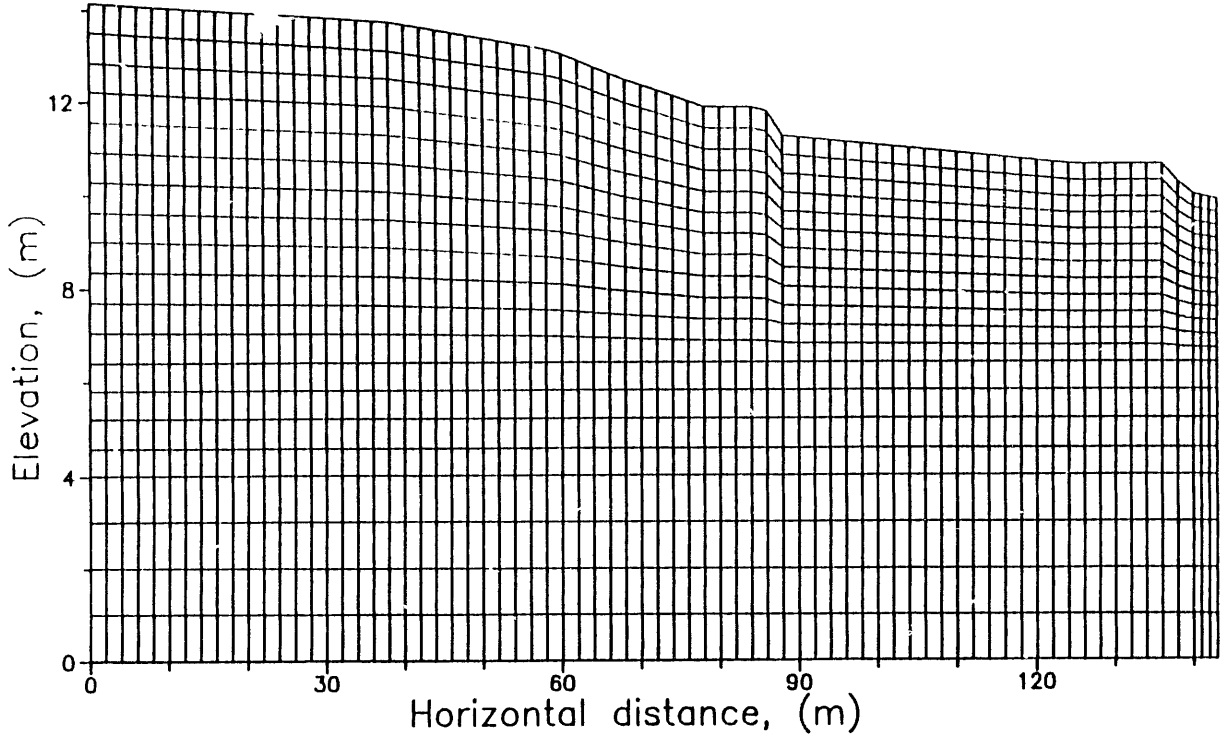

Figure 3.8 VAM2D curvilinear finite element grid used in the simulation of groundwater flow along Section 2.

3.6 TIME STEPPING SCHEME AND SIMULATION INTERVAL

The high degree of nonlinearity in the unsaturated hydraulic properties of the upper, fractured till layer combined with the daily variations of the infiltration rate along the soil surface required the use of relatively small time steps in order to avoid convergence difficulties as well as to obtain sufficient resolution in the approximation of the soil surface infiltration boundary. The presence of a seepage face boundary at the trench face imposes an additional degree of nonlinearity. The transient flow simulations were conducted using an adaptive time stepping scheme in which the time step size is adjusted by the code depending on the ease or difficulty of convergence of the numerical flow solution. The maximum time step size was set to $\Delta t_{max} = 0.1$ days, in order to ensure accurate representation of daily varying precipitation rates. Initial simulation runs using larger values of Δt_{max} showed significant sensitivity of simulation results to the selected Δt_{max} values.

The use of rather small timesteps combined with the need to conduct numerous model calibration runs introduces practical constraints in terms of the selection of the optimal simulation time interval. A related, and at least as important, consideration is the availability of accurate data for model calibration. Daily trench inflow measurements provided the main calibration data for the transient flow model, with data available for the period of March to August, 1990 at the time the simulations were conducted. Construction of the trench was ongoing during the same period, so that the total measured inflow at different times represents different total trench lengths. Information on the time periods of trench construction were provided by Mr. Tom Weiss of the West Valley Project Office and are summarized in Table 3.1 below.

Table 3.1 Completion Schedule of Interceptor Trench[6/]

Date	Activity
Jan. 1 - March 2, 1990	Constructed first 100 ft. of trench
March 2 - March 22, 1990	Data collection, no construction
March 22 - March 28, 1990	Trench extended to 200 ft.
March 28 - June 11, 1990	Data collection, no construction
June 11 - October 17, 1990	Trench extended to 456 ft.
October 19 - December, 1990	Trench extended to 804 ft., flooding of central collection sump

6/ Mr. Tom Weiss, WVNS, personal communication.

Roughly speaking, the data collected between March 2 and June 11, 1990, is expected to be reliable, with only a one week period of trench construction activity during the last week of March. On the other hand, trench construction activities were ongoing more or less continually during the second half of the year [7]. Moreover, the central sump in the trench from which the water is pumped flooded during the very wet fall of 1990, making it impossible to accurately determine daily inflows for the latter part of the year[8]. Based on these combined considerations, a 3-month simulation interval, covering the time period from March - May, 1990 was selected for model calibration.

As mentioned before, the measured total trench inflows may contain contributions from surface runoff which has infiltrated through the trench cap, as well as subsurface seepage from the FDA through the side of the trench. The relative contribution of these two processes is unknown and also may have changed with time. Observations from site personnel suggest that the high initial inflow rates (see Figure 2.8) reflect mostly direct seepage through the trench cap and that the diminishing inflow rate with time reflects actual subsurface inflow through the sides of the trench. A confounding factor is that throughout the simulation time period of March-May, evapotranspiration increases. The effect of evapotranspiration is to remove water from the soil and therefore, it too will result in a decreasing inflow into the trench. Given only data on the total trench inflow it is therefore very difficult to partition this inflow into a component representing infiltration from surface runoff through the trench cap and actual subsurface flow through the trench sides. The distinction is important though since VAM2D simulates only the latter component. In calibrating the flow model subjective decision must therefore be made as to what proportion of trench inflow is due to lateral subsurface seepage. In evaluating flow modeling results presented hereafter, we considered the case in which lateral subsurface seepage into the trench represented either 50% and 80% of the observed total trench inflow. These fractions were chosen some what arbitrarily; they serve to illustrate the agreement between simulated and observed results for the two different conditions.

---

[7] Mr. Tom Weiss, WVNS, personal communication.

[8] Mr. Tom Weiss, WVNS, personal communication.

4 GROUNDWATER FLOW MODELING RESULTS

In view of limitation and uncertainty of the data available for flow studies in the FDA site, specifically on fracture characterization near the surface, a series of transient flow simulations have been made in this study to evaluate the sensitivity of the model to variations in hydraulic properties and to obtain some insight into the transient behavior of groundwater flow along the two cross-sections. Since the effective hydraulic conductivity of the upper, fractured till layer is poorly known and it was expected also that lateral flow through this layer and simulated inflow into the trench would be quite sensitive to the permeability of the upper till layer, the model was calibrated primarily by adjusting the hydraulic conductivity of the fractured till in order to obtain a good match with observed trench inflow. Additionally, predicted water table elevations were compared against the observation well monitoring data presented in Section 2.5 for the additional calibration.

4.1 CROSS-SECTION 1

4.1.1 Steady-State Flow Simulation

As mentioned before, the first modeled cross-section represents a subsection of the larger two-dimensional models of Prudic (1986) and Bergeron and Bugliosi (1988). As a first verification test of the present model, a steady state flow simulation was therefore conducted in order to reproduce the earlier result of Bergeron and Bugliosi. A three-layer isotropic system consisting of weathered till, transition zone, and unweathered till was simulated, with thicknesses of the weathered till layer and transition zone, as well as saturated hydraulic conductivities for each layer taken from Bergeron and Bugliosi (1988). The saturated hydraulic conductivity of tne unweathered till was taken to be 2×10^{-5} m/d (2.3×10^{-8} cm/s), the fractured till was assigned a 10x greater conductivity while the transition layer was assigned an intermediate value of 1×10^{-4} m/d. The conductivity of all layers was assumed to be isotropic. For this steady state case, a constant and uniform infiltration rate of 2 cm/yr was used as the surface boundary condition. The unsaturated hydraulic properties used by Bergeron and Bugliosi (1988) are not reported; the parameters discussed in Section 3.3. were therefore used in the present simulations. Hydraulic parameters used in the steady state simulation are listed in Table 4.1. Steady state hydraulic head contours obtained from the VAM2D simulation are shown in Figure 4.1. Figure 4.2 gives the head distribution along the same cross-section from the best-fit steady-state simulation of March 1983 conditions by Bergeron and Bugliosi (1988). Note that the elevation base in the VAM2D model corresponds to 410m MSL. A comparison of the hydraulic heads of Figures 4.1 and 4.2 indicates that the VAM2D simulation produced essentially the same prediction of the hydraulic head profile in the flow system. Slight deviations occur only near the right-hand side boundary, corresponding to the location of the interceptor trench. In the VAM2D simulation this was modeled as a seepage face boundary, whereas no boundary at all was present at this location in the earlier model of the Bergeron and Bugliosi. This result verifies the correct operation of the VAM2D code and the consistency of the present model with previous modeling studies.

Table 4.1 Physical parameters used in the simulation of steady-state surface infiltration case for Cross-Section 1.

Soil Layer		Unweathered Till	Unweathered Fractured Till	Weathered, Fractured Till
Material number		1	2	3
Hydraulic Conductivity (m/d)	K_x	$2x10^{-5}$	$1x10^{-4}$	$2x10^{-4}$
	K_y	$2x10^{-5}$	$1x10^{-4}$	$2x10^{-4}$
Porosity	ϕ	0.25	0.28	0.30
Relative Permeability Eq. (3.3)	S_{wr}	0.0	0.0	0.0
	n	4.0	10.0	20.0
Capillary Pressure Eq. (3.6)	α	0.0634	0.0634	0.0634
	β	1.1026	1.1026	1.1026
	ψ_a	0.0	0.0	0.0
Specific Storage	S_s	0.0	0.0	0.0

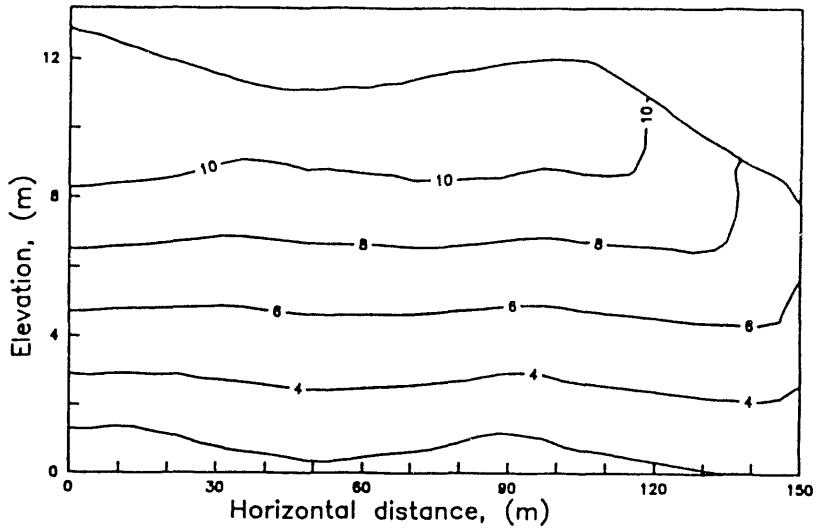

Figure 4.1 Distribution of hydraulic head in Section 1 calculated from steady-state infiltration rate on ground surface.

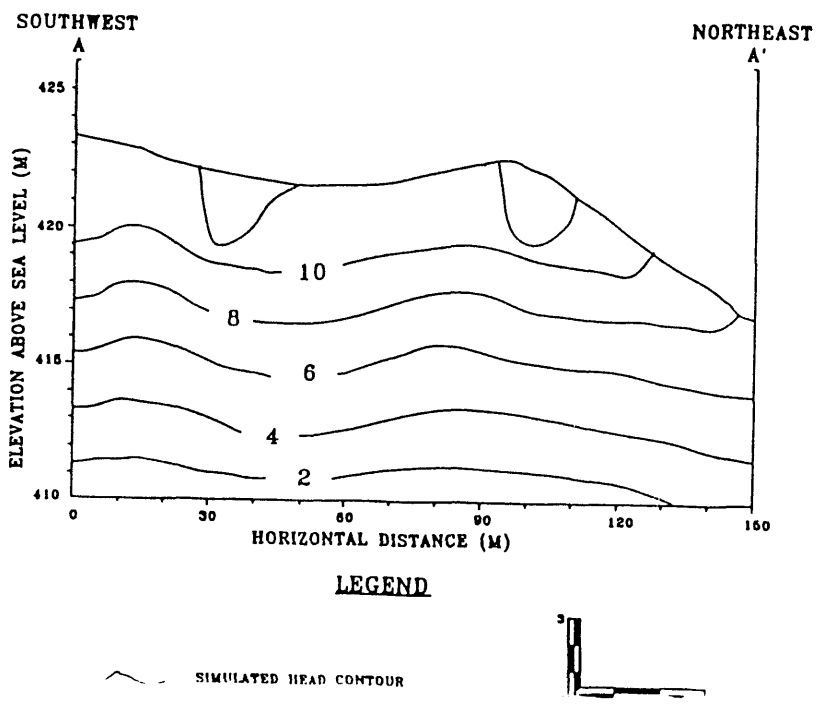

Figure 4.2 Distribution of hydraulic head in Section 1 based on the best-fit steady-state simulation of March 1983 conditions (from Bergeron et al., 1988).

4.1.2 Transient Simulations

Following the steady state simulation described in the previous section, the same cross-section was then modeled in a transient sense, using the observed precipitation record to give daily varying infiltration rates. No changes were made in the model other than the surface boundary condition, on the notion that if the steady state models of Prudic (1986) and Bergeron and Bugliosi (1988) are realistic representations of the actual site, they should yield reasonable results also when used in a transient mode. As mentioned, data on observed trench inflows provided the principal means of evaluating this and subsequent model simulation runs. In order to utilize the trench inflow data for this purpose, it was necessary to make the assumptions that inflow is more or less uniform along the entire length of the trench. It is therefore permissible to divide the total volume of water measured in the trench by the length of the trench to get the inflow rate per unit trench length for comparison with the 2D cross-sectional model. Initial model comparisons were made assuming 50% of the observed trench inflow is actually caused by subsurface seepage from the FDA. The calculated inflow rate per unit trench length was therefore divided further by a factor of 2.0 to obtain values for comparison with simulated results.

Results for the transient simulation are presented in Figures 4.3 to 4.6. Figure 4.3 shows the distribution of daily precipitation and the actual infiltration as simulated by the model. It should be noted that the vertical axis is plotted on a logarithmic scale. The graphs show that on many days with rainfall, the actual infiltration was substantially less than the total rainfall. The difference between the two is the predicted run-off. It can be seen that during wet periods, the infiltration levels off at a rate of 2.4×10^{-5} m/d which is the simulated infiltration rate when the soil is fully saturated. Figure 4.4 shows cumulative infiltration against cumulative precipitation for the 90-day simulation period. This figure demonstrates even more clearly that the infiltration lags far behind the total precipitation. The total infiltration is only 0.5 cm or 1.5% of total precipitation at the end of the three month period. Observed and simulated daily inflows into the interceptor trench are compared in Figure 4.5. The same data are shown in a cumulative plot in Figure 4.6. Simulated trench inflows are much smaller than observed and also fail to reproduce the temporal variation of daily inflows. The comparison of cumulative trench inflows (Figure 4.6) only confirms this. The graph of cumulative observed trench inflows in Figure 4.6 in addition shows that the inflow rate into the trench diminishes considerably after the first 20 to 30 days. It is likely that this is due to increased evapotranspiration at the site. However, it is also possible that the reduction in inflow rate reflects the fact that actual inflows were not uniform along the length of the trench. Between March 22 and 28 the length of the trench was extended from 100 to 200 feet. The concurrent apparent reduction in inflow rate could indicate that the contribution from the new section of the trench was less than that of the original 100 feet.

Overall, the results of this transient simulation compare quite poorly with available data. Total precipitation was so much higher than the saturated conductivities of the different till layers, that the model predicted essentially fully saturated conditions throughout the simulation period. Still, even though the soil in the simulation was completely saturated, drainage into the

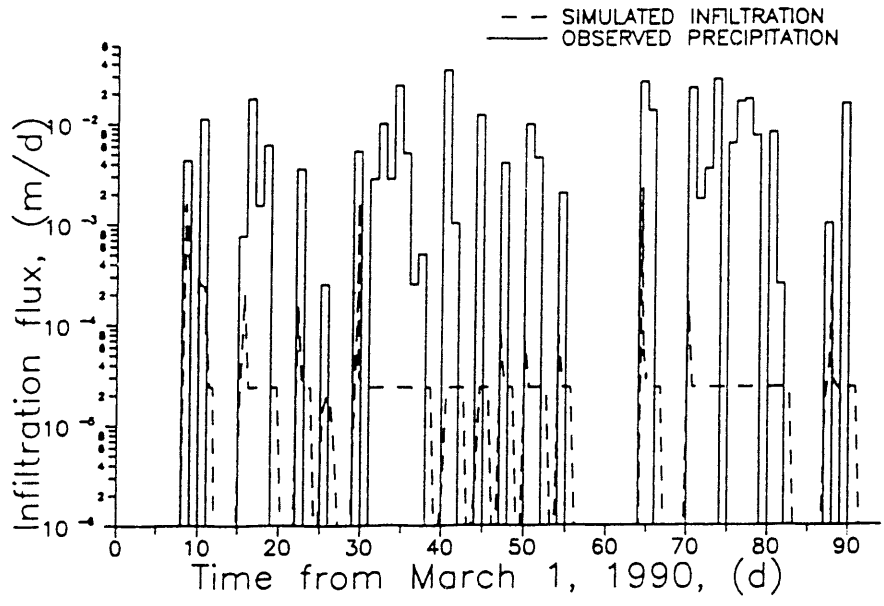

Figure 4.3 Comparison of simulated infiltration flux and observed precipitation rate along Section 1; Cross-Section 1, first transient simulation.

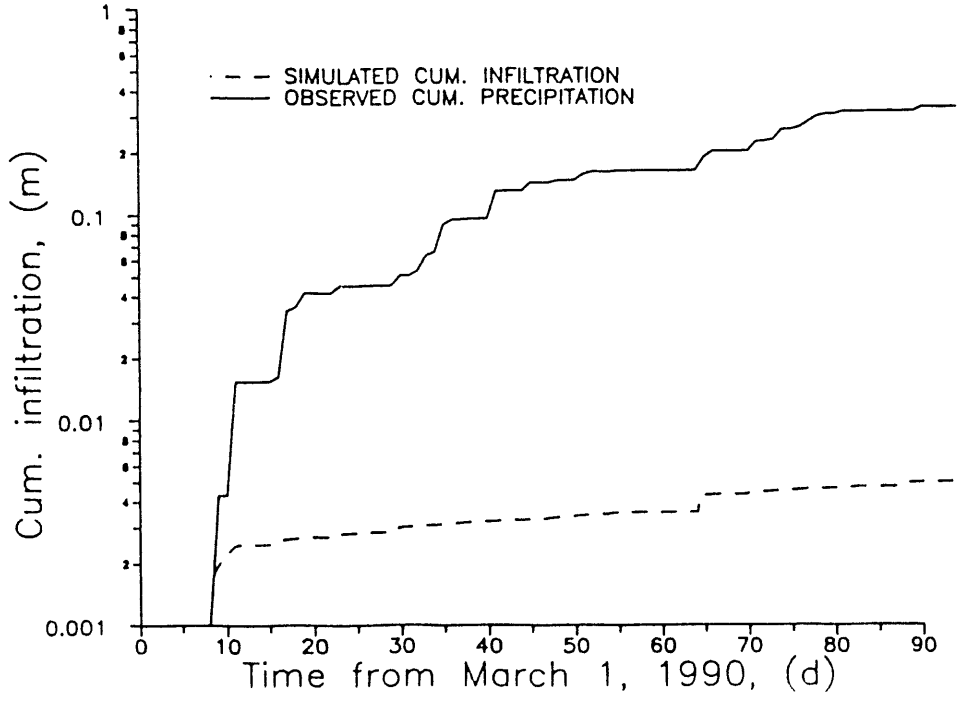

Figure 4.4 Comparison of simulated cumulative infiltration and observed cumulative precipitation along Section 1; Cross-Section 1, first transient simulation.

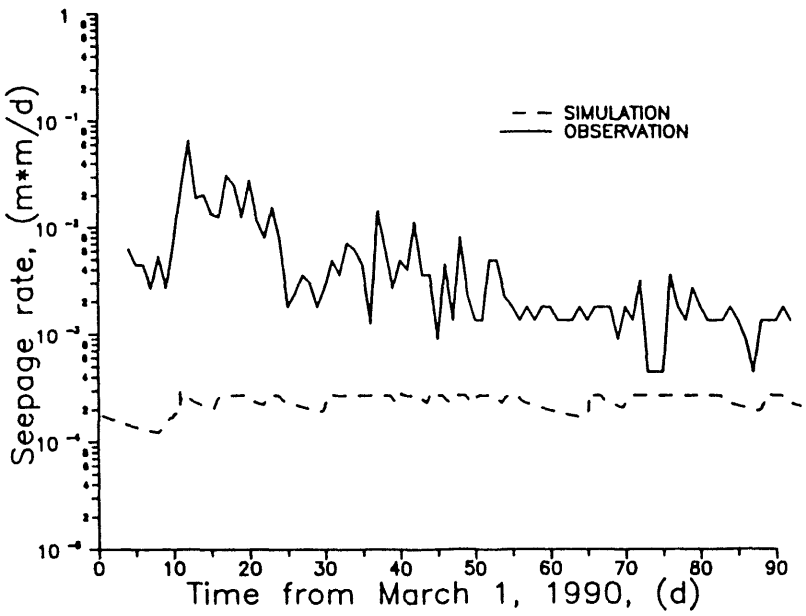

Figure 4.5 Comparison of simulated and observed daily inflow rates into interceptor trench; Cross-Section 1, first transient simulation.

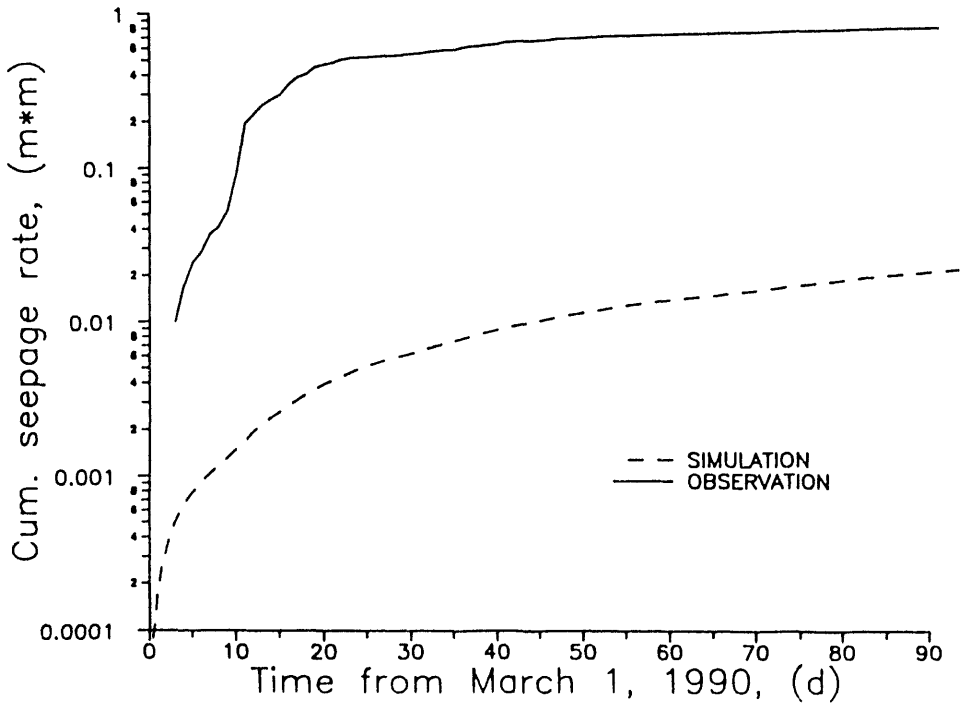

Figure 4.6 Comparison of and observed simulated cumulative inflow into interceptor trench; Cross-Section 1, first transient simulation.

interceptor trench was still much less than observed. This indicates that the chosen permeability values were too low. Useful further insight into the model behavior can be obtained by inspection of the simulated flow velocity profile. A representative velocity profile is shown in Figure 4.7. Arrows indicate both the direction and magnitude of flow at different locations. This figure shows a strong dependence of topography on flow paths in the near surface zone. Whereas flow in the deeper unweathered till is strictly vertically downward, groundwater flow in the surface, fractured layer closely follows the local topography. It can be seen that drainage into the trench occurs only from the sloping region extending approximately 50 m away from the trench. The slight surface ridge at an x-coordinate of 100 m in the modeled cross-section acts as a flow divide. There is lateral flow towards the surface depression at x = 50 m, causing locally continuous fully saturated conditions. Since water in the 2D cross-sectional model cannot flow away sideways, it is removed only by downward flow through the underlying unweathered till. Since only a relatively small portion of the domain drains into the trench, flow in the model is controlled mostly by downward movement into and through the low permeability unweathered till. Apart from short duration peaks following dry periods, the rate of infiltration into the soil (2.4×10^{-5} m/d) is very close to the hydraulic conductivity of the unweathered till, which was taken to be 2×10^{-5} m/d.

Since the initial transient simulation indicated that the assumed hydraulic conductivity values were too low to permit sufficiently rapid drainage into the interceptor trench, a second simulation was performed with saturated hydraulic conductivity of the fractured till layer increased twenty-five times from 2×10^{-4} m/d to 5×10^{-3} m/d. This modification resulted in a higher simulated infiltration and increased flow into the trench as shown in Figures 4.8 to 4.11. While inflow into the trench is predicted much better than in the first case, the best agreement occurs at later times; inflows during the first 25 days are still significantly underpredicted. The evaluation of how well the model reproduces the observed daily trench inflow, depends on the significance that is given to contribution of vertical seepage through the trench cap. During the first twenty four days of the simulation, simulated inflow rates are up to 10 times smaller than observed which could be attributed to the initially high rate infiltration through the trench cap. At the same time, the model can be seen to overpredict trench inflow after the first two months. This could be caused by the effect of evapotranspiration, which will reduce trench inflow but is ignored in the simulations. Figure 4.11 shows that on a time-integrated basis the model underpredicts the cumulative inflow by a factor of 3. Inspection of the velocity profile for this simulation also showed that while the magnitude of flow velocities was greater than before, the delineation of flow paths was essentially still the same as shown in Figure 4.7. The accumulation of water in topographically lower areas is an artifact of modeling the site in two-dimensions. The model does not permit sideways movement of water, which will obviously occur in reality. The selected profile for cross-section 1 therefore does not allow a realistic representation of actual groundwater flow at the site. For this reason cross-section 1 was abandoned and further simulations were performed using cross-section 2.

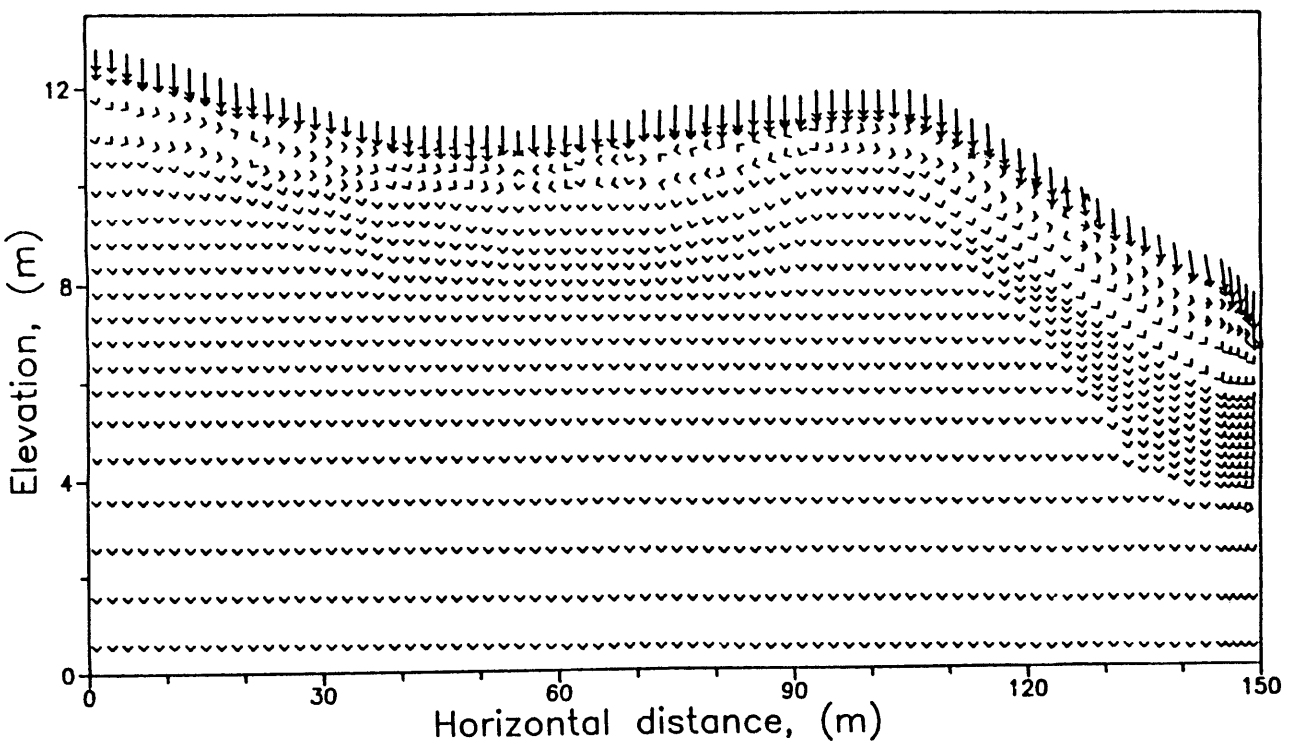

Figure 4.7 Simulated velocity distribution of groundwater flow in Cross-Section 1 at t = 11 d.

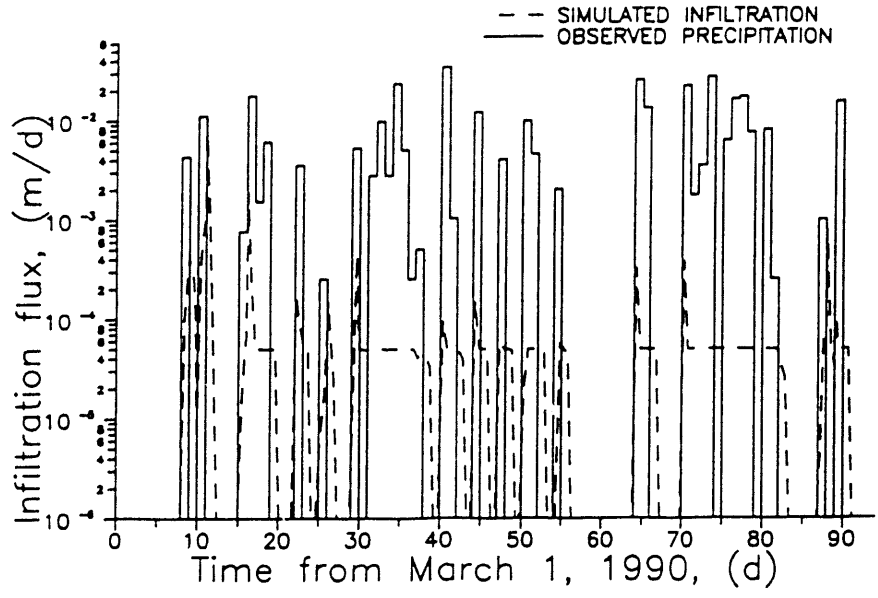

Figure 4.8 Comparison of simulated infiltration flux and observed precipitation rate; Cross-Section 1, second transient simulation.

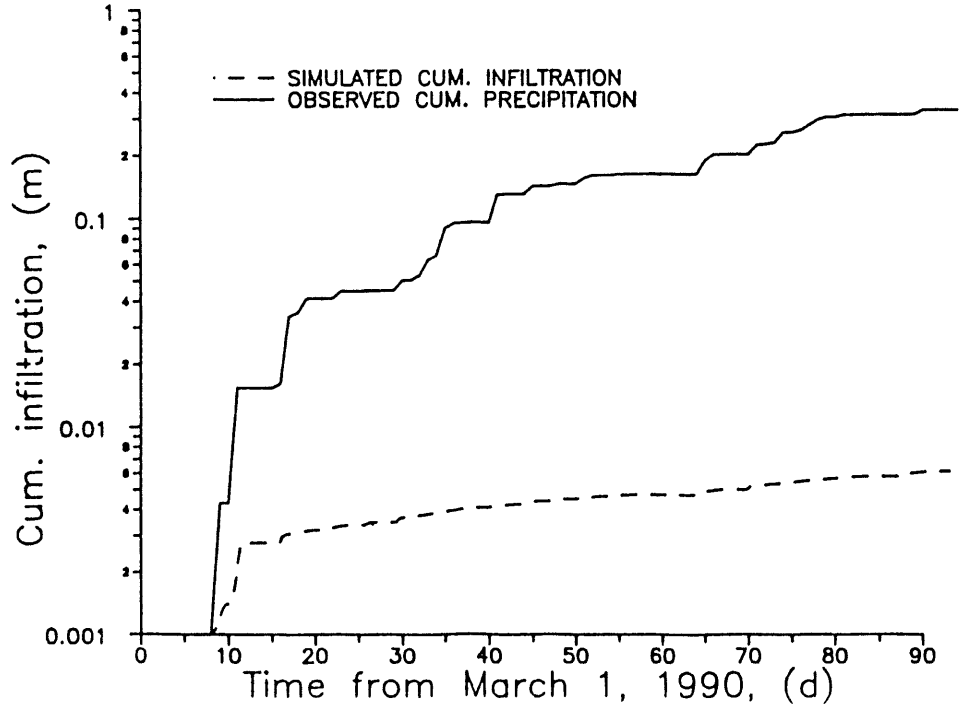

Figure 4.9 Comparison of simulated cumulative infiltration and observed cumulative precipitation; Cross-Section 1, second transient simulation.

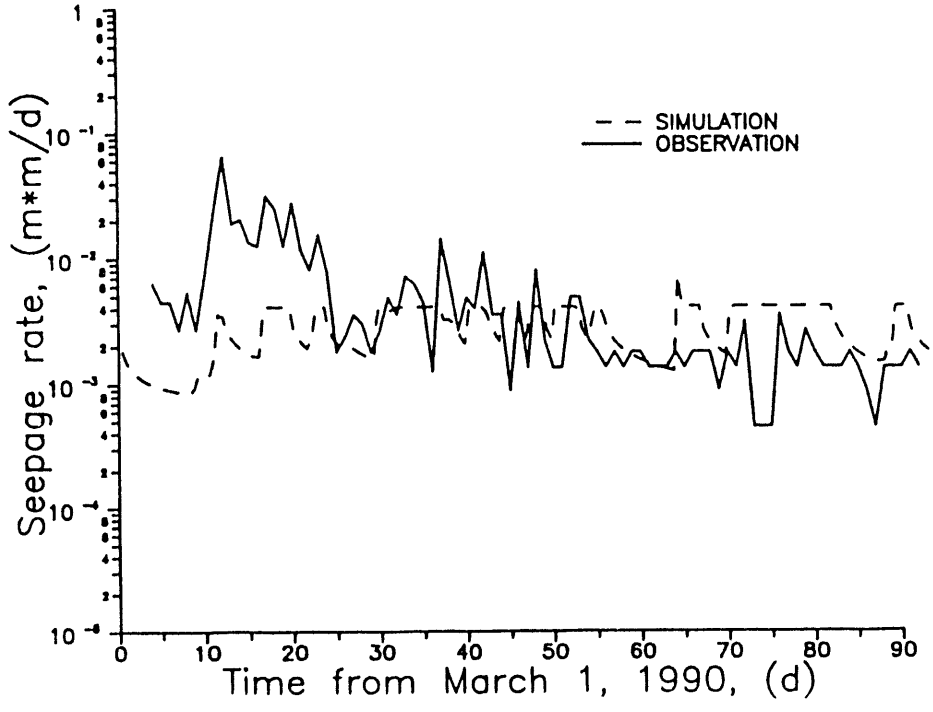

Figure 4.10 Comparison of simulated and observed daily inflow rates into interceptor trench; Cross-Section 1, second transient simulation.

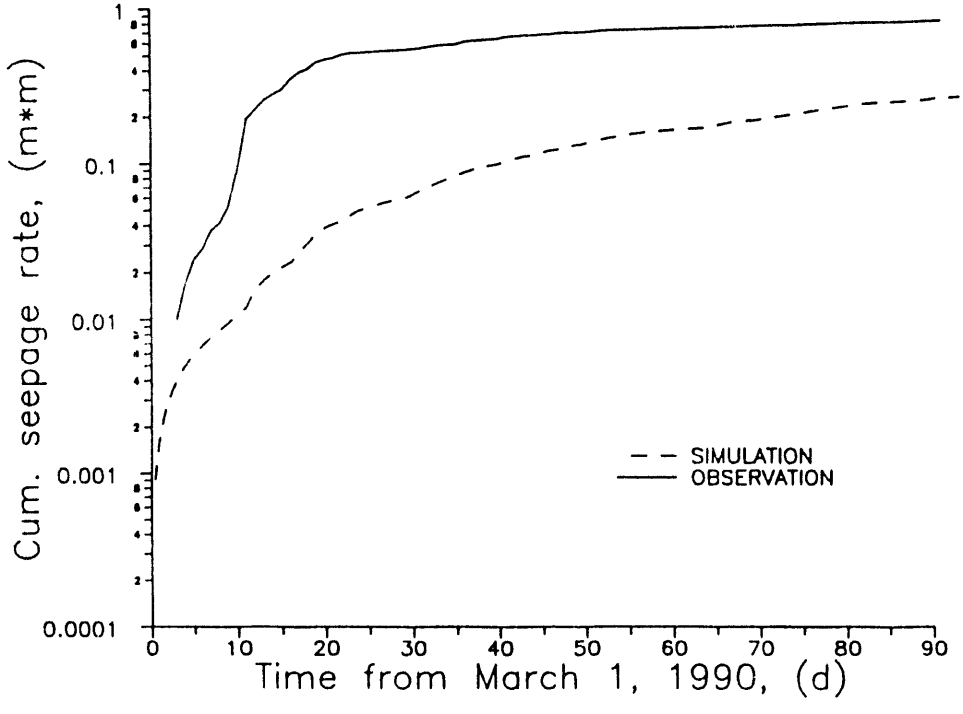

Figure 4.11 Comparison of simulated and observed cumulative inflow into interceptor trench; Cross-Section 1, second transient simulation.

4.2 CROSS-SECTION 2 SIMULATIONS

4.2.1 Assignment of Initial Conditions

Cross-section 2 follows the transect B-B' in Figure 3.1. This cross-section is laid out more or less diagonally across the FDA following the surface topography. It passes underneath the storage facility on the site (Sprung Structure) and terminates at the interceptor trench near the central sump pump. The profile of cross-section 2 is depicted in Figure 3.4 showing the assignment of boundary conditions and depth of the surface fractured till and the transition layer from fractured to unweathered till. The presence of the building is handled by assigning this portion of the cross-section a no-flow surface boundary condition, while infiltration conditions are used elsewhere along the surface boundary.

Initial conditions for the transient simulations were determined in a manner analogous to that used for cross-section 1; a steady-state simulation was performed with a constant infiltration rate of 2 cm/yr and hydraulic parameters for the different soil layers as listed in Table 4.2. The difference with initial steady state simulation of cross-section 1 is that, based on the results of the cross-section 1 simulations, a higher saturated conductivity values was assigned to the top, fractured till layer. This value was 10^{-3} m/d, instead of the value of 2×10^{-4} m/d used initially for cross-section 1. This steady state simulation was used to determine the initial water table position (see Figure 3.4) for the subsequent transient simulations.

4.2.2 Transient Simulation 1

The first transient simulation of cross-section 2 used the hydraulic parameter values as listed in Table 4.2. Results of the simulation are presented in Figures 4.12 to 4.15. Figures 4.12 and 4.13 show observed precipitation and computed infiltration on daily and cumulative bases, respectively. Observed and simulated trench inflows for this simulation are shown in Figures 4.14 and 4.15. "Observed" trench inflow here still refers to 50% of the actual measured rate, assuming this is the inflow fraction due to subsurface seepage. The results show that simulated infiltration and trench inflows are considerably lower than observed values. The simulated trench inflow rate agrees with observed rates only during the final 20 or 80 days of the simulation period (Figure 4.14). On a cumulative basis, the simulated total trench inflow in nearly 10 times smaller than the observed value. Considering also the effect of evapotranspiration on actual trench inflows during the latter part of the simulation period which was not accounted for, it seems justified to conclude that this simulation underpredicts lateral seepage into the trench. The main reason for this would be that the hydraulic conductivity assigned in the model to the fractured till is too low, thereby not allowing sufficiently rapid drainage of infiltrating water into the trench.

Table 4.2 Physical parameters used in the simulation of initial head distributions in Section 2.

Soil Layer		Unweathered Till	Unweathered Fractured Till	Weathered, Fractured Till
Material number		1	2	3
Hydraulic Conductivity (m/d)	K_x	$2x10^{-5}$	$1x10^{-4}$	$1x10^{-3}$
	K_y	$2x10^{-5}$	$1x10^{-4}$	$1x10^{-3}$
Porosity	ϕ	0.25	0.28	0.30
Relative Permeability Eq. (3.3)	S_{wr}	0.0	0.0	0.0
	n	4.0	10.0	20.0
Capillary Pressure Eq. (3.6)	α	0.0634	0.0634	0.0634
	β	1.1026	1.1026	1.1026
	ψ_a	0.0	0.0	0.0
Specific Storage	S_s	0.0	0.0	0.0

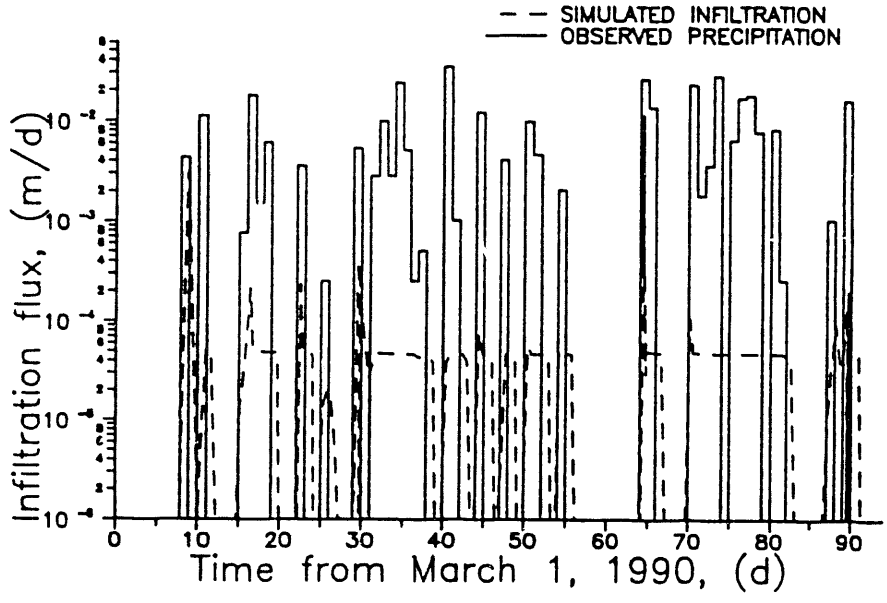

Figure 4.12 Comparison of simulated infiltration flux and observed precipitation rate; Cross-Section 2, first transient simulation.

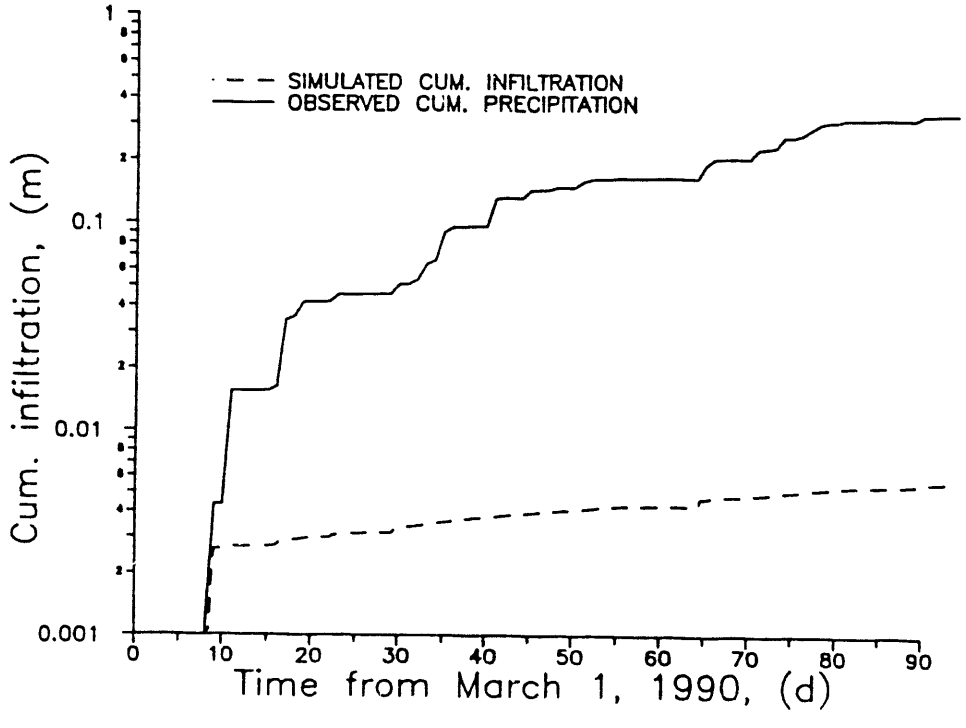

Figure 4.13 Comparison of simulated cumulative infiltration and observed cumulative precipitation; Cross-Section 2, first transient simulation.

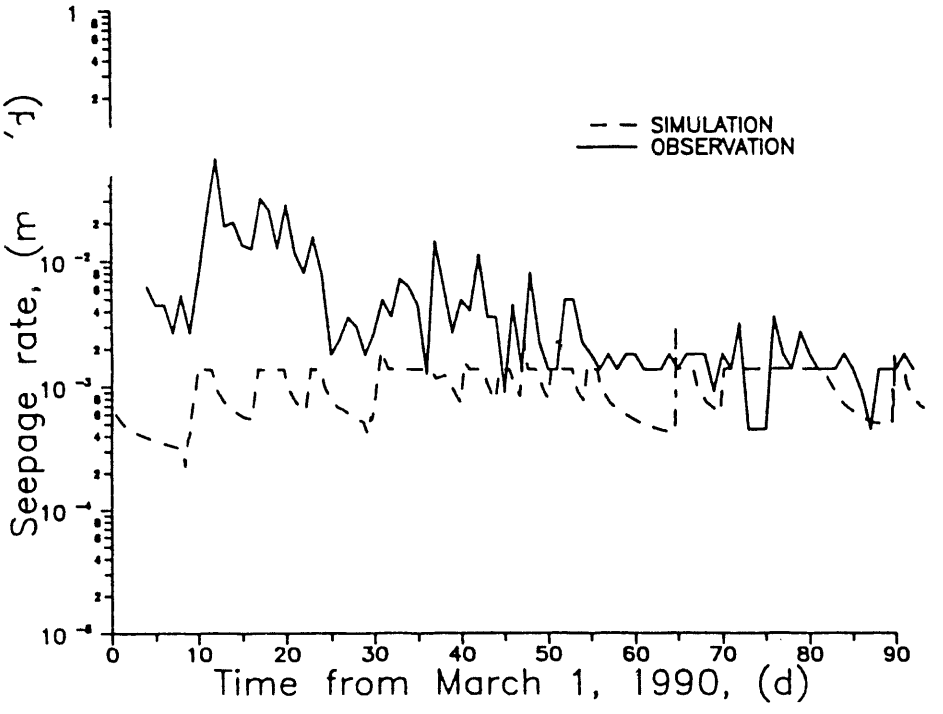

Figure 4.14 Comparison of simulated and observed daily inflow rates into interceptor trench; Cross-Section 2, first transient simulation.

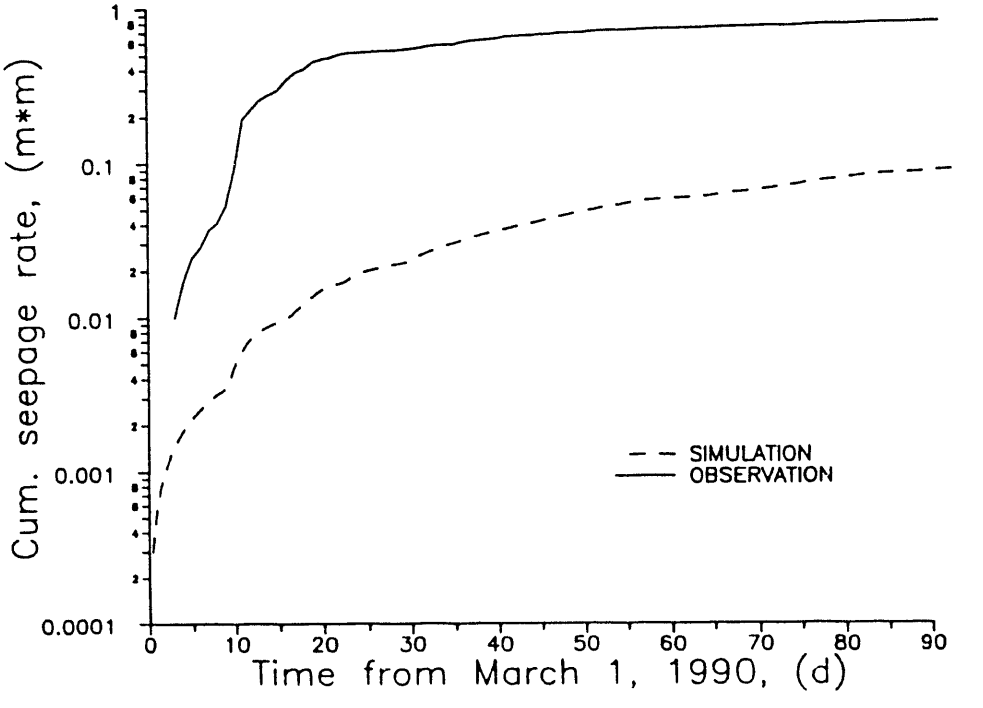

Figure 4.15 Comparison of simulated and observed cumulative inflow into interceptor trench; Cross-Section 2, first transient simulation.

4.2.3 Transient Simulation 2

The saturated conductivity of the fractured layer was therefore further increased from 1 x 10^{-3} to 5 x 10^{-3} m/d. Results for this next simulation are presented in Figures 4.16 to 4.19, showing again a comparison of total precipitation and infiltration into the soil, and observed and predicted inflows to the trench. Compared to the results shown in Figures 4.18 and 4.19, the five-fold increase in permeability causes a doubling of the net infiltration. The resulting flow into the trench now matches the observed data now much better (Figures 4.18 and 4.19). Inflows during the first month of the simulation are still under-predicted; agreement is quite good for the second month, while the model over predicts inflows during the third month (May, 1990). The latter phenomenon is probably due to the reduction of actual inflow caused by evapotranspiration. Groundwater velocity profiles corresponding to t = 9 days and t = 60 days in the simulation are shown in Figures 4.20 and 4.21, respectively. Day 9 of the simulation corresponds to the initial time period of high infiltration, while t = 60 days corresponds to a day of no infiltration. The graphs indicate that lateral groundwater flow to the interceptor trench occurs mainly through the highly permeable surface fractured layer; below the upper few meters of the till, movement is predominantly downward. The flow pattern in the fractured till layer is significantly different from that shown before in Figure 4.7. It can be seen that seepage into the trench originates not only from areas immediately adjacent to the trench, but from across the entire 150 m long cross-section. Cross-section #2 does not contain any topographic obstructions to lateral flow to the trench and the increased hydraulic conductivity assigned to the fractured till also facilitates lateral flow. While the present simulation resulted in reasonably good agreement with observed trench inflows, the model also predicted that the water table would be right at or very close to the surface during the entire simulation period. This is because daily rainfall rates are still substantially higher than the saturated conductivity value assigned to the fractured till layer. Unsaturated flow physics incorporated into the VAM2D code dictate that infiltration will occur at the precipitation rate, and surface run off will not occur until the soil becomes fully saturated. Given the frequency and magnitude of precipitation, the model can therefore only predict that the soil remains essentially saturated throughout the simulation period. Water level data from available monitoring wells on the other hand (Section 2.5) indicate that while the water table can be close to the surface during wet periods, the water table position was consistently overpredicted by the model. Given the precipitation intensity at the site, the only way to obtain unsaturated conditions in the upper part of the fractured till is to postulate the existence of a (relatively thin) surface layer with a hydraulic conductivity lower than that of the underlying fractured till. Physically such a lower permeability layer could have resulted from surface compaction due to various human activities at the site, or a variety of other factors (for instance, reduced permeability due to soil swelling causing closure of fractures at the soil surface following rainfall) that would tend to reduce the effective permeability of the top most part of the soil.

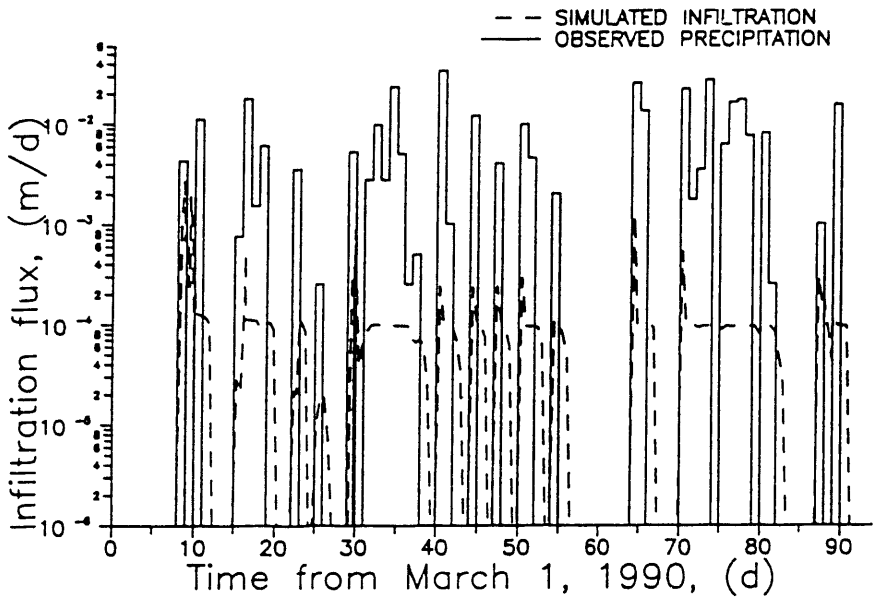

Figure 4.16 Comparison of simulated infiltration flux and observed precipitation rate; Cross-Section 2, second transient simulation.

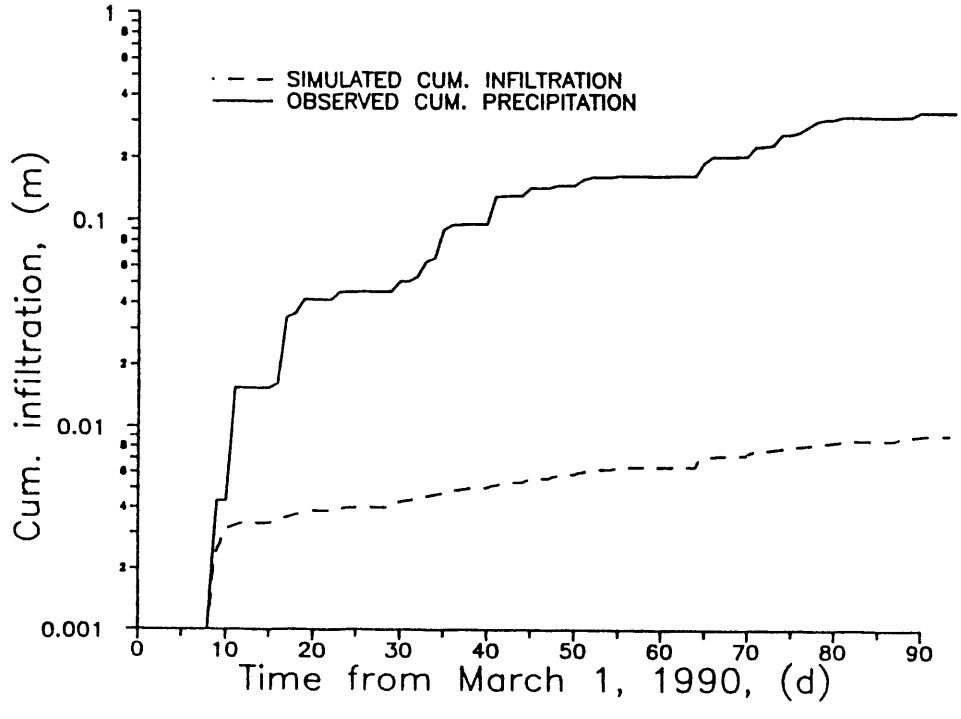

Figure 4.17 Comparison of simulated cumulative infiltration and observed cumulative precipitation; Cross-Section 2, second transient simulation.

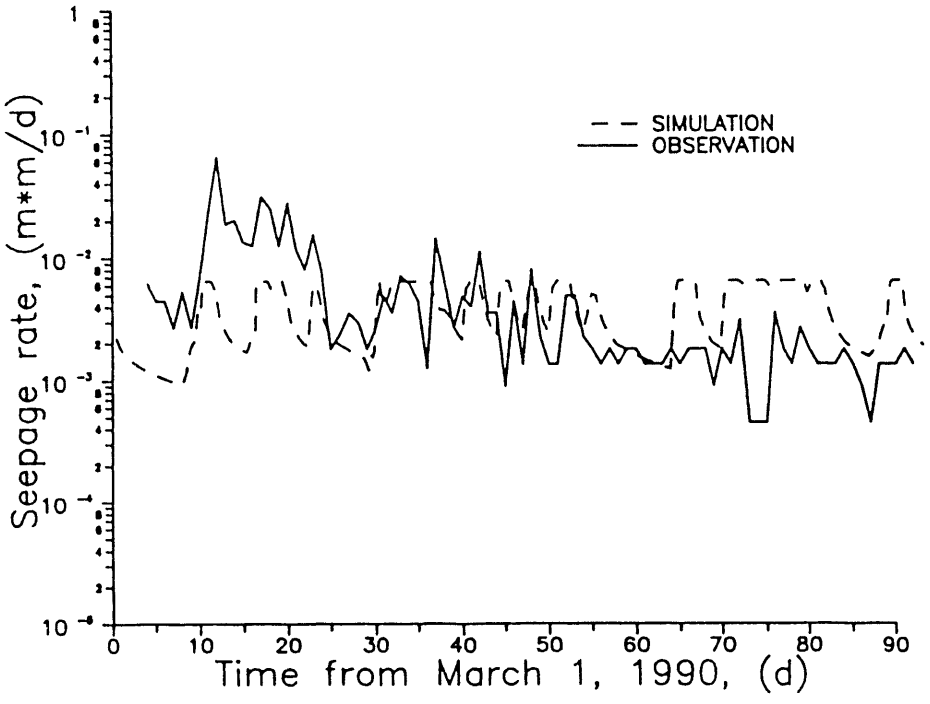

Figure 4.18 Comparison of simulated and observed daily inflow rates into interceptor trench; Cross-Section 2, second transient simulation.

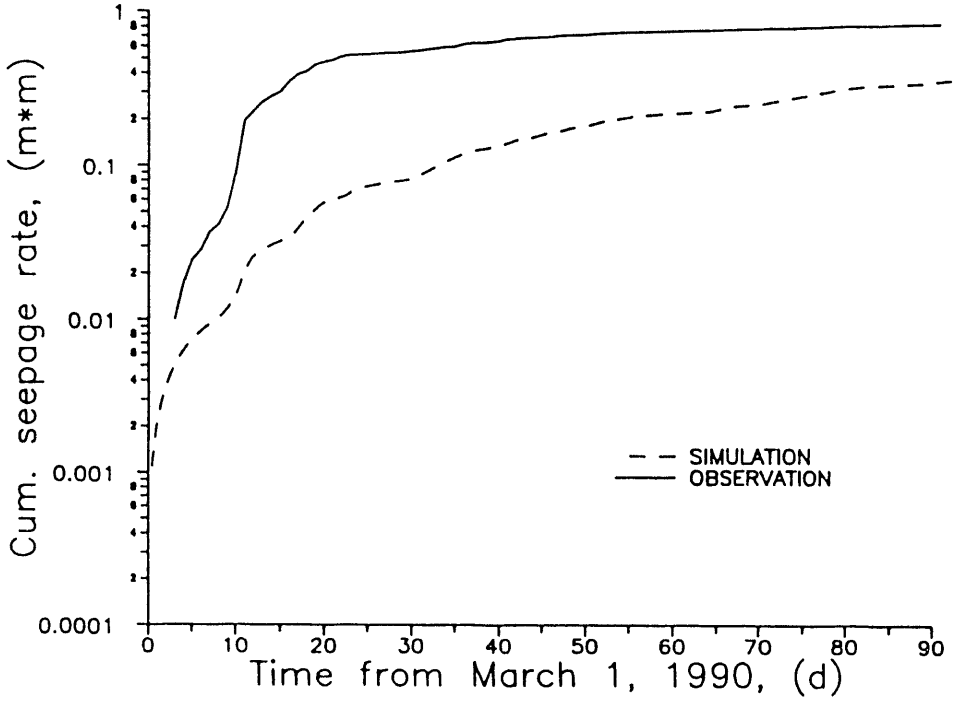

Figure 4.19 Comparison of simulated and observed cumulative inflow into interceptor trench; Cross-Section 2, second transient simulation.

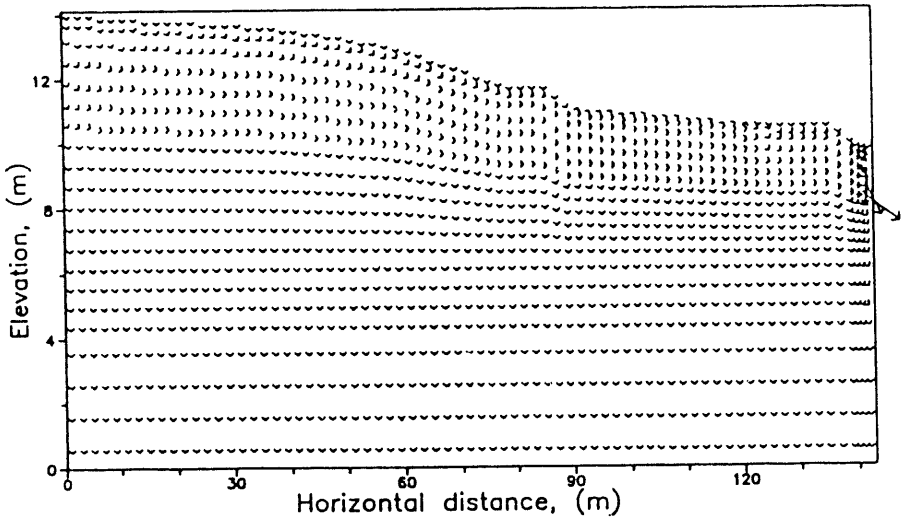

Figure 4.20 Groundwater flow velocities at t = 9 d; Cross-Section 2, second transient simulation.

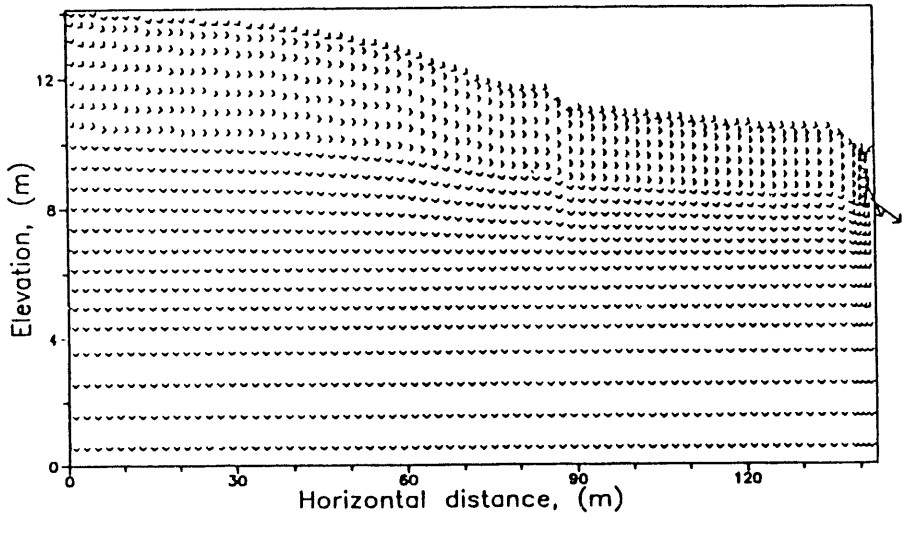

Figure 4.21 Groundwater flow velocities at t = 60 d; Cross-Section 2 second transient simulation.

4.2.4 Transient Simulation 3

To further calibrate the model and improve the agreement with observed water table positions, the presence of a lower permeability surface cover, overlying the high permeability fractured till was incorporated into the model. The thickness of the surface cover was somewhat arbitrarily set to 20 cm and it was assigned a saturated hydraulic conductivity of 5×10^{-4} m/d. This surface cover regulates the amount of water that can infiltrate into the soil and the hydraulic conductivity contrast with the fractured till below it ensures that the upper part of the fractured till remains unsaturated. To emphasize this contrast, the hydraulic conductivity of the fractured till was further increased to a value of 5×10^{-2} m/d. Values of the hydraulic parameters assigned to the separate soil layers in the present simulation are listed in Table 4.3. Figures 4.22 and 4.23 show daily and the comparison of simulated and observed cumulative infiltration. Even though the surface cover reduced the hydraulic conductivity at the soil surface compared to the previous simulation, infiltration in the present simulation is still higher. This is because the higher permeability of the fractured till allows the infiltrated water to drain away into the interceptor trench more quickly, thereby allowing more water to infiltrate over time. However, at the end of the three-month simulation period, the net infiltration into the soil is still no more than 5% of the total precipitation. As a result of the higher infiltration, simulated inflow into the trench is also increased compared to the earlier simulations (Figures 4.24 and 4.25). Compared to the previous simulations the curve of simulated trench inflow is shifted further upward. Figure 4.24 shows that for the case in which 50% of the observed trench inflow is caused by subsurface seepage from the FDA, the simulations now reproduce quite well the high initial inflow during the first 3 weeks of the simulation period, but consistently overpredict trench inflow at later times. This simulation also overpredicts the cumulative amount of trench inflow at the end of the three month period (Figure 4.25). The overall agreement between observed and simulated trench inflows can be improved by allowing a greater proportion of observed inflows to be contributed by subsurface seepage from the FDA. For instance, Figures 4.26 and 4.27 show the comparison between observed and simulated for the case in which 80% of the observed trench inflow is attributed to seepage from the FDA. This does not change the simulation results, it merely shifts the curve representing observed data upward, thereby improving the overall agreement with the inflow predicted in the final simulation. Groundwater flow velocity profiles for the simulation are shown in Figures 4.28 and 4.29. Compared to Figures 4.20 and 4.21 they show essentially the same flow paths with dominantly lateral flow through the fractured till. The magnitude of the flow rate through the fractured layer is increased though to accommodate the higher rate of seepage into the interceptor trench.

Finally, Figures 4.30 and 4.31 show a comparison of simulated water table elevations against observed levels in wells 89-13-W and 85-I-11. Of the available observation wells reviewed in Section 2.5, these two wells are situated closest to the modeled cross-section (transect B B′ is Figure 3.2). Predicted water levels at the two points D_1 and D_2 (Figure 3.1) along the cross-section nearest the two observation wells are plotted in Figures 4.30 and 4.31. The average water level in well 85-I-11 corresponds reasonably well to the average predicted level. However, the observed and simulated time-variation of water levels shows a poor agreement. Because of the mentioned cracking of the casing of this well and possibility of direct rainfall inflow into the well, the observed data for this well may not be very reliable. Better

Table 4.3 Physical parameters used in the final transient simulation of groundwater flow along Section 2.

Soil Layer		Unweathered Till	Unweathered Fractured Till	Weathered, Fractured Till	Compacted Soil Cover
Material number		1	2	3	4
Hydraulic Conductivity (m/d)	K_x	2×10^{-5}	1×10^{-4}	5×10^{-2}	5×10^{-4}
	K_y	2×10^{-5}	1×10^{-4}	5×10^{-2}	5×10^{-4}
Porosity	ϕ	0.25	0.28	0.30	0.30
Relative Permeability Eq. (3.3)	S_{wr}	0.0	0.0	0.0	0.0
	n	4.0	10.0	20.0	4.0
Capillary Pressure Eq. (3.6)	α	0.0634	0.0634	0.0634	0.0634
	β	1.1026	1.1026	1.1026	1.1026
	ψ_a	0.0	0.0	0.0	0.0
Specific Storage	S_s	0.0	0.0	0.0	0.0

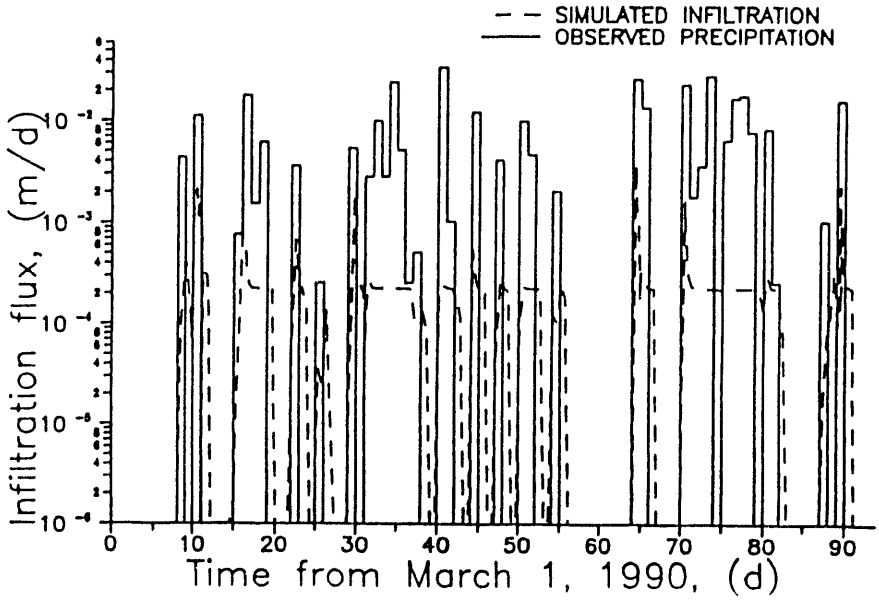

Figure 4.22 Comparison of simulated infiltration flux and observed precipitation rate; Cross-Section 2, final transient simulation.

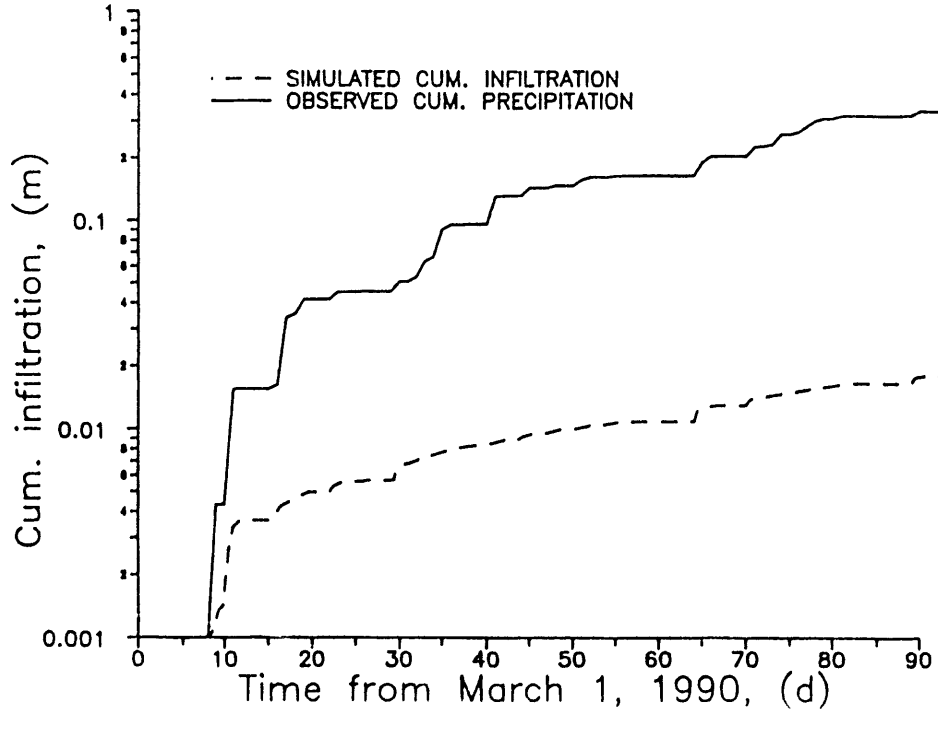

Figure 4.23 Comparison of simulated cumulative infiltration and observed cumulative precipitation; Cross-Section, final transient simulation.

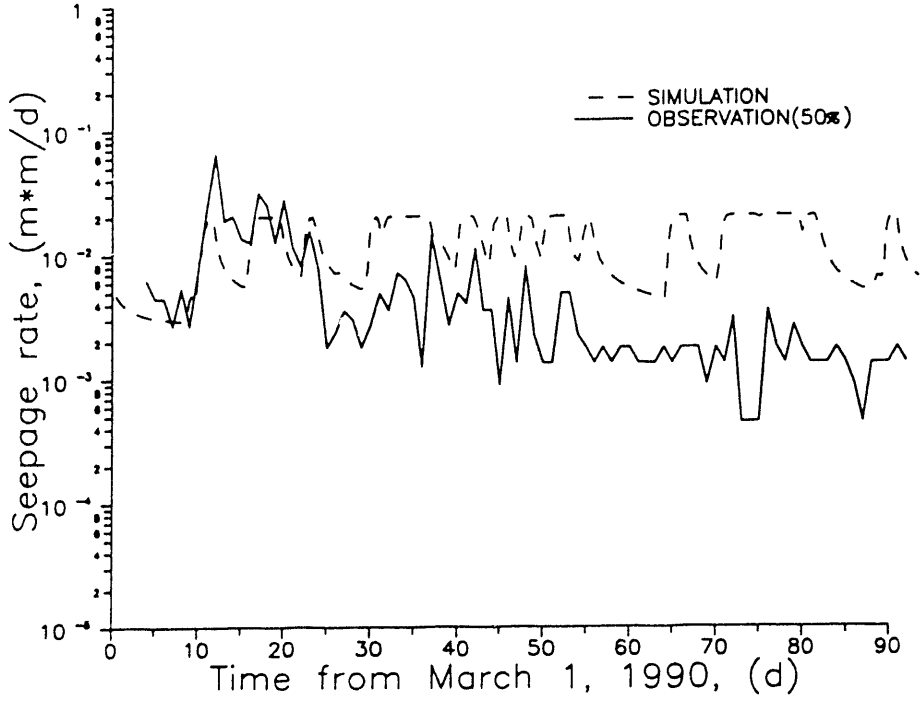

Figure 4.24 Comparison of simulated and observed daily inflow rates into interceptor trench; Cross-Section 2, final transient simulation. Observed data for case in which 50% of total trench inflow is caused by subsurface seepage.

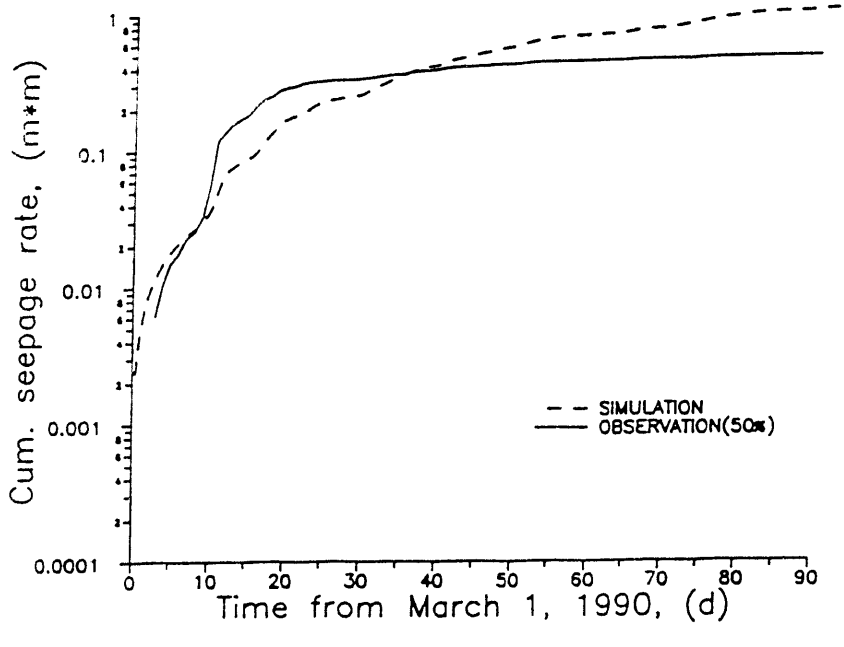

Figure 4.25 Comparison of simulated and observed cumulative inflow into interceptor trench; Cross-Section 2, final transient simulation. Observed data for case in which 50% of total trench inflow is caused by subsurface seepage.

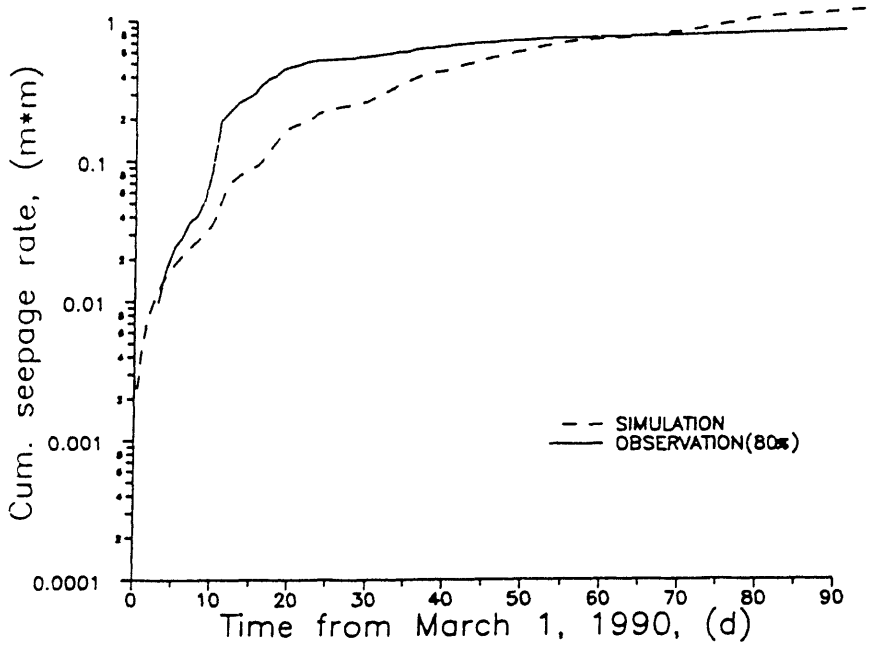

Figure 4.26 Comparison of simulated and observed daily inflow rates into interceptor trench; Cross-Section 2, final transient simulation. Observed data for case in which 80% of total trench inflow is caused by subsurface seepage.

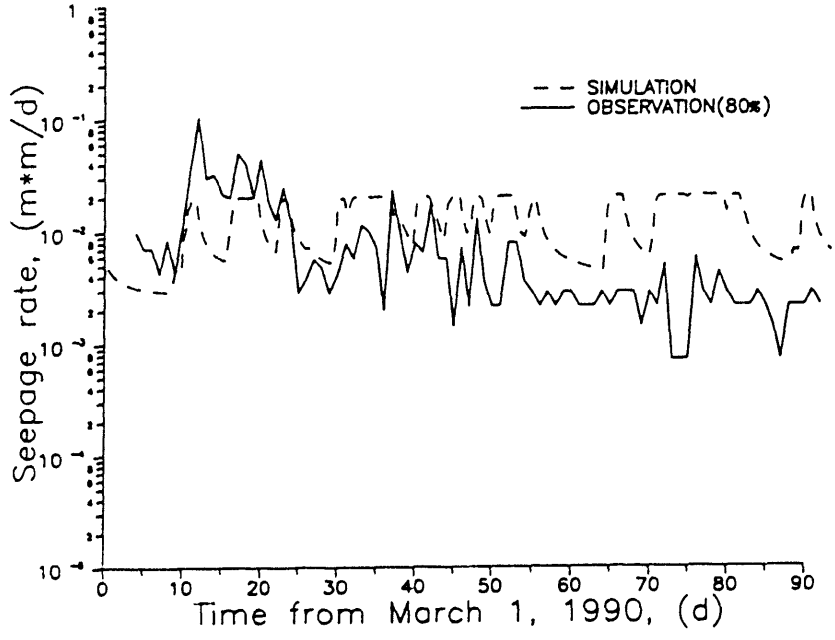

Figure 4.27 Comparison of simulated and observed cumulative inflow into interceptor trench; Cross-Section 2, final transient simulation. Observed data for case in which 80% of total trench inflow is caused by subsurface seepage.

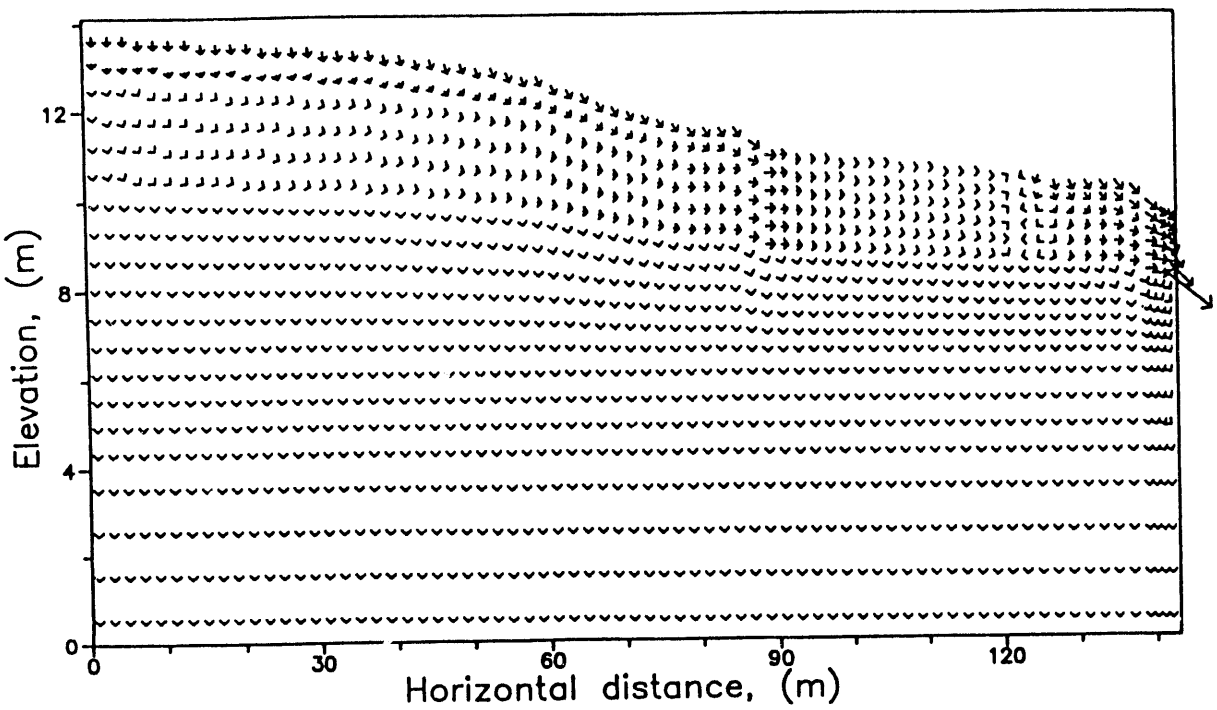

Figure 4.28 Groundwater flow velocities at t = 9 d; Cross-Section 2, final transient simulation.

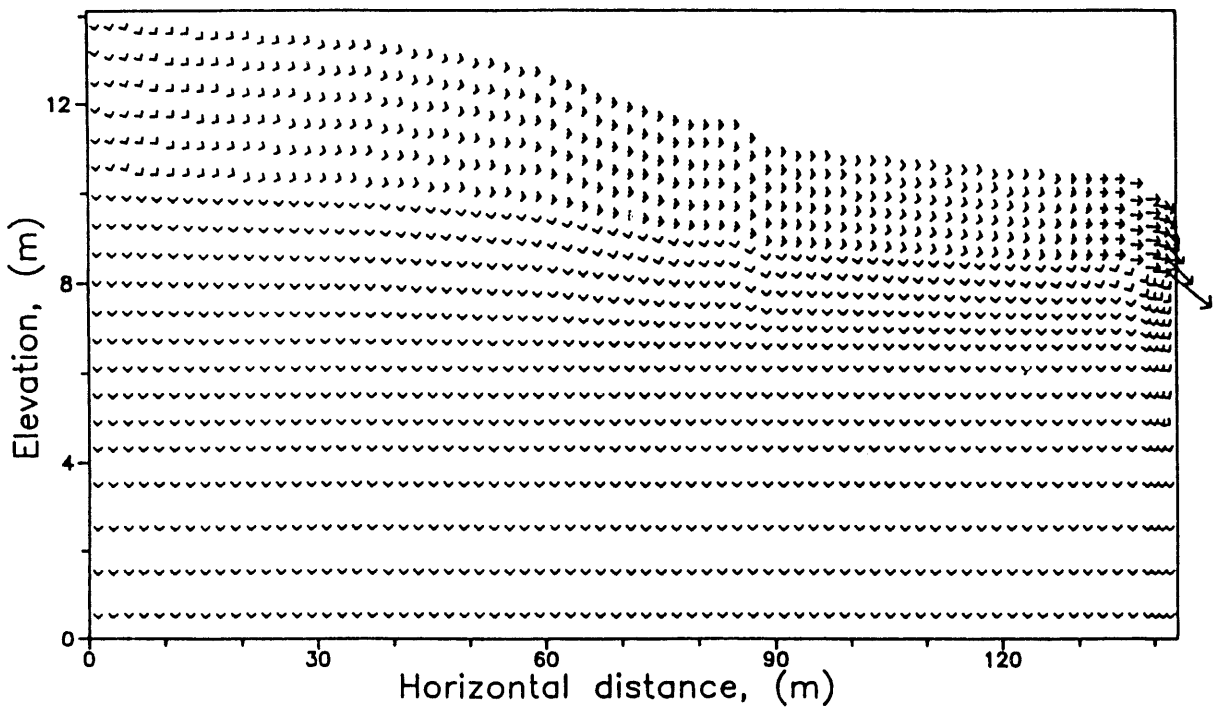

Figure 4.29 Groundwater flow velocities at t = 60 d; Cross-Section 2 final transient simulation.

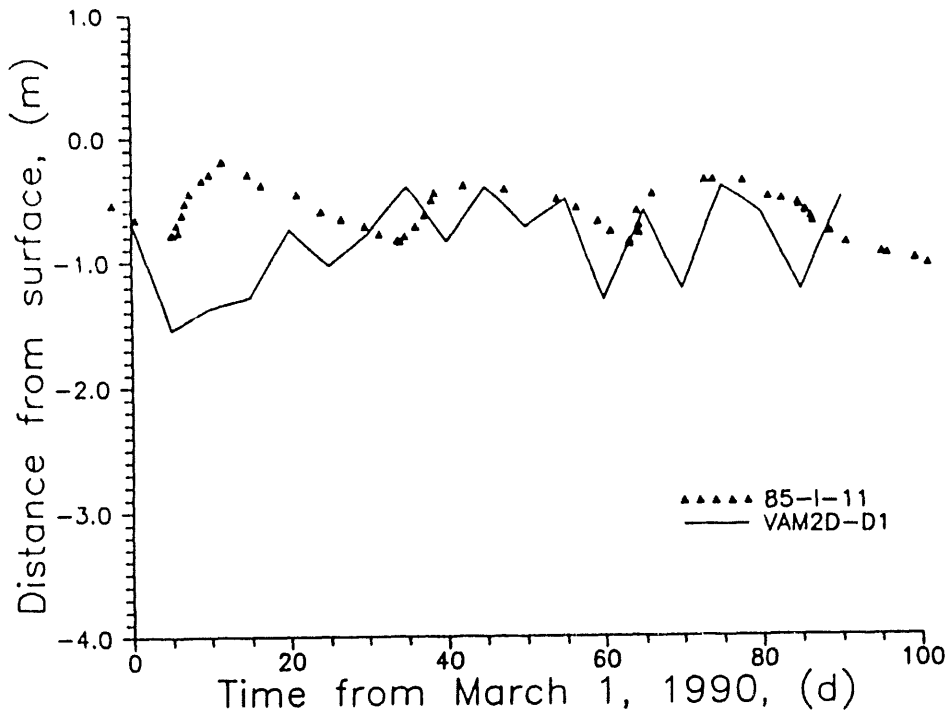

Figure 4.30 Comparison of simulated water table with observation data from Well 85-I-11; Cross-Section 2, final transient simulation.

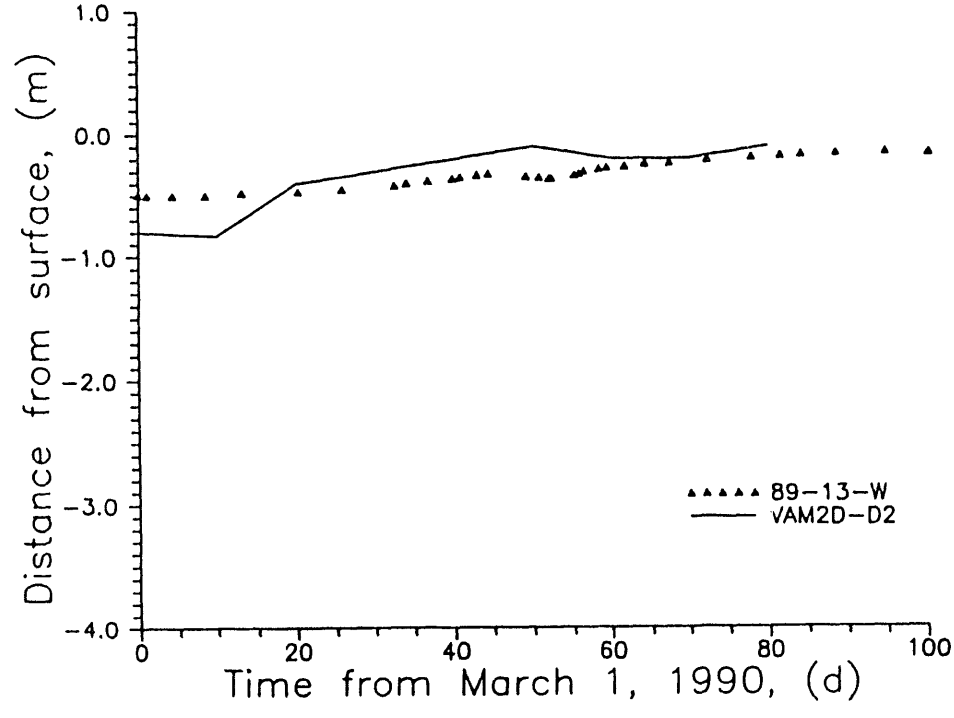

Figure 4.31 Comparison of simulated water table with observation data from Well 89-13-W; Cross-Section 2, final transient simulation.

agreement is obtained for well 89-13-W. This well is actually located inside the 'Sprung Structure' at the site, which is modeled as a no-precipitation boundary in the simulation. Because there is no direct infiltration near this well, much of the time variation of water levels is damped out, which agrees well with the observations at well 89-13-W. A comparison of predicted water levels with observation data from the 'RCRA' wells (Table 2.2) shows that none of these wells have recorded data for the March-May simulation period. Observed water levels from wells 0906 and 0907 in February, i.e., prior to the simulation period are somewhat deeper than simulated levels during the March-May period.

As further analysis of the transient flow simulations, it is useful to extrapolate the results from the 3-month simulation period to an annual basis and discuss them in terms of the total water balance for the site. The results from the final simulation are used here. At the end of the simulation, the total amount of water infiltrated into the soil was around 1.5 cm. Considering that the simulation interval covers a wet period of the year, the net infiltration as a yearly basis could be estimated to be 2 to 3 times the March - May period, i.e. on the order of 3-4.5 cm/year. Assuming that the hydraulic conductivity of the unweathered till of 2×10^{-5} to 3×10^{-5} m/d is accurate, the amount of water removed by downward flow is approximately 2 cm/year. The remaining infiltrated water (1 to 2.5 cm/year) drains into the interceptor trench. The above amounts are all expressed as volumes per unit area; the total volumetric flow into the trench would be obtained by multiplying by the drainage area of the interceptor trench. The corresponding average rate of lateral flow through the fractured till may be estimated as follows:

$$V = \textit{Trench inflow rate} \times \frac{\textit{Length of Flow Section}}{\textit{Fracture Zone Thickness}}$$

For an annual trench inflow rate (per unit area) of 1.5 cm, a flow section length of 150 m and effective thickness of the fractured layer of 3 m, the resulting average flow rate is calculated to be around 75 cm/year. Assuming further more that this flow is mainly through fractures, with a fracture porosity on the order of 10%, the average lateral seepage velocity through the fractured till is around 7.5 m/year. For the second simulation (Section 4.2.3), the average lateral flow rate is roughly 50% smaller. In this case the lateral seepage velocity is thus around 3.5-4 m/year. Note that this value agrees well with the observed average rate of migration of the solvent plume of 9.6 ft/yr = 2.9 m/yr (Blickwedehl et al., 1989).

4.3 EFFECTS OF ANISOTROPY

All simulation results presented above pertain to cases with isotropic hydraulic conductivities in all soil layers. In reality, the hydraulic conductivity of the fractured till layer is expected to be highly anisotropic due to the predominantly vertical orientation of fractures. To evaluate the significance of hydraulic anisotropy in the fractured till layer, variants of the simulation scenarios presented in the preceding sections, in which the vertical hydraulic conductivity was set to be 10 x greater than the horizontal conductivity were also modeled. Results of the simulations were found to be very insensitive to the higher vertical conductivity in all cases. The reason is that vertical flow is controlled by the permeability of the unweathered

till. The rate of flow out the bottom of the modeled cross-sections was approximately the same in all cases considered, varying between 2 x 10^{-5} and 3 x 10^{-5} m/d. These values are on the same order as the saturated hydraulic conductivity assigned to the unweathered till. Variations in hydraulic conductivity of the fractured till however did affect predicted flow into the trench. Plots of the groundwater flow velocities during the simulations clearly showed that virtually all of the water draining into the trench originates as lateral flow from the fractured till layer, with only very minor contributions from the transition layer and unweathered till. Consequently, the values used for hydraulic conductivity of the fractured till should be interpreted as representing estimates of the effective lateral (K_x) saturated conductivity of this zone. While actual vertical conductivities are likely to be considerably higher than the horizontal values, the present modeling did not allow estimation of these values. For simplicity therefore, the till was treated as an isotropic medium in the simulations presented here.

5 RADIONUCLIDE TRANSPORT MODELING

5.1 MODELING APPROACH

Following the groundwater flow analysis, an assessment was made of the radionuclide migration from a typical disposal pit at the site. Although subject to considerable uncertainty, data (precipitation, trench inflow, water levels) is available to calibrate a site groundwater flow model. Much more limited data is available for a radionuclide migration analysis. The locations of disposal pits and trenches, i.e., source locations are known and records are available of the wastes disposed at the site. However, the rate at which radionuclides are being released from the different waste forms into the subsurface environment is unknown. Apart from the solvent plume which represents a special case, no monitoring data is available either to assess the actual extent, if any, of present radionuclide movement to allow model calibration. The radionuclide transport analysis presented in this section therefore does not purport to represent actual present or future radionuclide migration at the site, rather it is intended to investigate potential radionuclide migration under certain assumed conditions. Specifically, the modeling is designed to evaluate the effect of lateral groundwater flow through the upper, fractured till on radionuclide migration from a typical fuel hull disposal pit. The fuel hull disposal pits are of particular interest as possible sources for radionuclide release since they contain the bulk (95% or more; Nicholson and Hurt, 1985) of the total activity buried at the site. The construction and disposals in the fuel hull pits have been described by Nicholson and Hurt (1985) and have been reviewed in Section 2.4. The locations of the fuel hull pits are indicated in Figure 2.5.

The following radionuclides were considered in the transport simulations: Sr-90, Cs-137 and Pu-239. Inventories of these radionuclides in the fuel hull pits are given in Table 2.1. Of the long-lived plutonium species Pu-239 and Pu-240, only Pu-239 was simulated since it has a greater half life than Pu-240. Other factors assumed equal, Pu-239 should therefore have the greatest potential for migration.

The groundwater flow modeling was used as the basis for the transport analysis, however with a number of significant modifications. A two-dimensional cross-section was again modeled with the same geometrical features of surface topography, thickness of fractured zone and location of the outflow seepage face (interceptor trench) as flow model section #2. To accommodate the full depth (50 feet) of the fuel hull pits, the lower boundary of the grid was extended 10 m downward from that used in the flow simulations. The base of the grid used in the transport analyses thus corresponds to an elevation of 410 m above sea-level. Figure 3.1 shows that the location of cross-section 2 used in the flow simulations does not actually pass through the area where the fuel hull pits are located. The modeled cross-section in the transport analyses is intended to represent some 'average' soil profile, with no specific actual location in the field. While there are a total of approximately 80 fuel hull burial holes, in the present modeling a single source was simulated, representing one typical burial pit. The position of this source in the model is shown in Figure 5.1. The distance of the source to the right-hand side boundary of the model is 45 m which is approximately the average distance of the fuel hull pits to the interceptor trench in the field. Figure 5.1 also indicates that the top of the source is at

1.5 m below the top of the unweathered till. This reflects the NRC technical specification that the top of the waste had to be at least four feet below the top of undisturbed till (Nicholson and Hurt, 1985) with the latter assumed to be the top of the unweathered till. The finite element grid used in the transport simulations contained 4512 nodes and is shown in Figure 5.2. Comparison with Figure 3.8 shows that the transport grid used is much more refined that the grid used for the flow modeling, particularly around the source, in order to minimize any numerical inaccuracies.

To accommodate the timescales involved in the radionuclide transport analysis (on the order of hundreds of years), steady state flow conditions were assumed for transport with a long term net infiltration rate of 3.5 cm/year. Hydraulic properties of the different till layers were those used in the final transient flow simulation, i.e., with high permeability fractured zone and reduced permeability surface cover. The resulting steady state flow field is depicted in Figure 5.3. In this steady state flow model, close to 50% of the infiltration is accounted for by downward flow through the unweathered till and the remaining 50% is removed by lateral flow through the fractured till into the trench on the right-hand side model boundary. Resulting lateral flow rates (Darcy velocity) through the fractured zone in the vicinity of the modeled disposal pit are on the order of 0.7 m/year. The modeled steady state conditions probably are on the high side of actual, current flow through the fractured till. For transport modeling purposes, the flow conditions are thus conservative in the sense that they will tend to overestimate advective radionuclide movement through the fractured till.

5.2 TRANSPORT PARAMETER ESTIMATION

An important consideration in the radionuclide transport analysis is the applicability of the VAM2D porous medium transport model to describe transport through the fractured till, and related to this, the determination of appropriate transport parameter values. Although the VAM2D code does not account for the presence of fractures, a previous analysis (Kool and Wu, 1991) has shown that under steady state flow conditions the code can be used with reasonable success to predict contaminant transport through fractured media, provided that retardation factors and especially dispersivities are determined in an appropriate manner to reflect the effective transport characteristics of the fractured medium. The needed effective transport characteristics include: porosity, retardation factors and dispersivity. These may be estimated from porous matrix and fracture parameters using relationships reviewed by Kool and Wu (1991). For the present analysis it was assumed that the total porosity in the fractured till is the same as the matrix porosity and that the effective retardation factor in the fractured till is the same as the matrix retardation factor, i.e., retardation in fractures is ignored. Effective dispersivities for the fractured till were estimated using the following relationship (Kool and Wu, 1991):

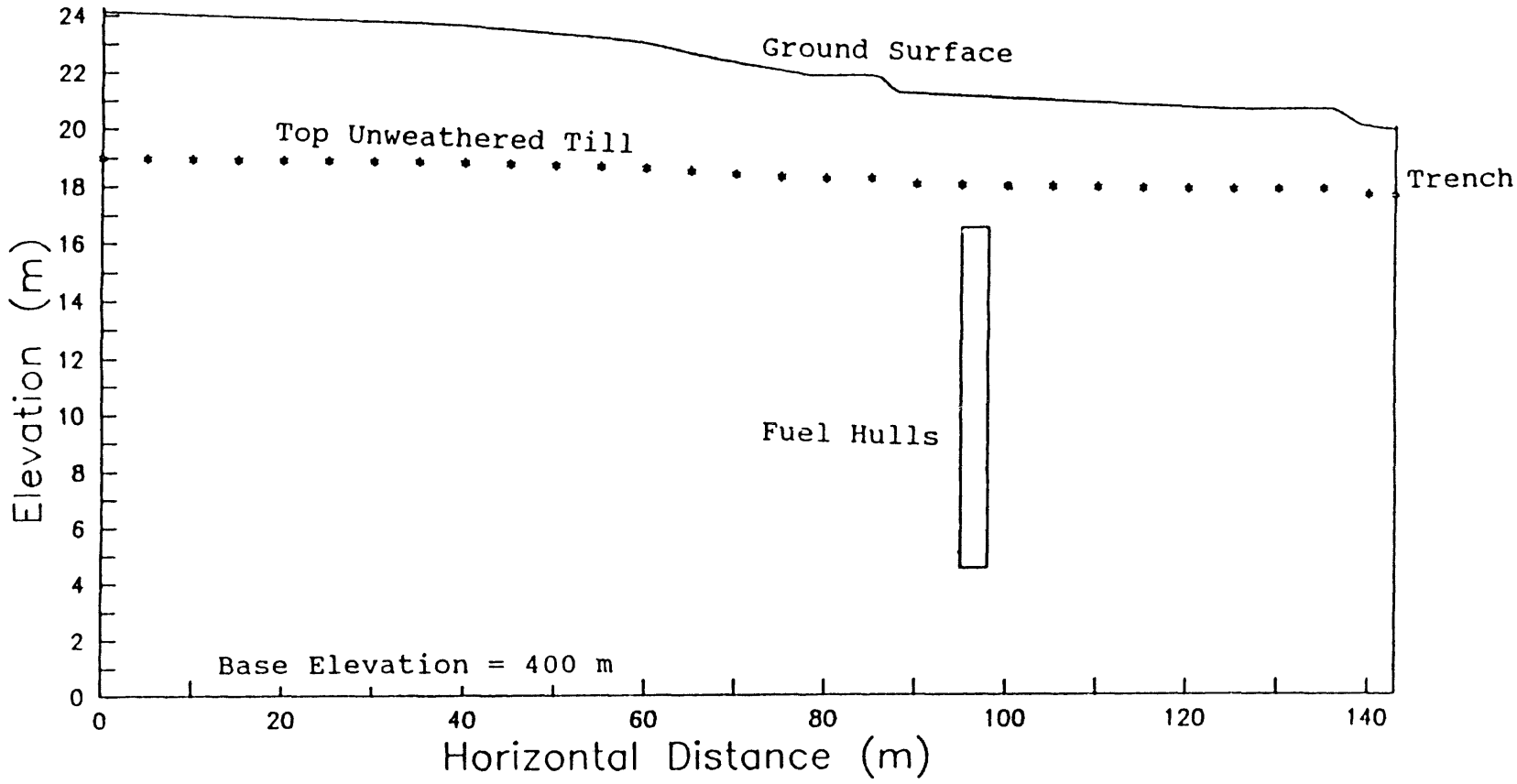

Figure 5.1 Schematic cross-sectional view of the radionuclide source, representing a typical fuel hull burial bit.

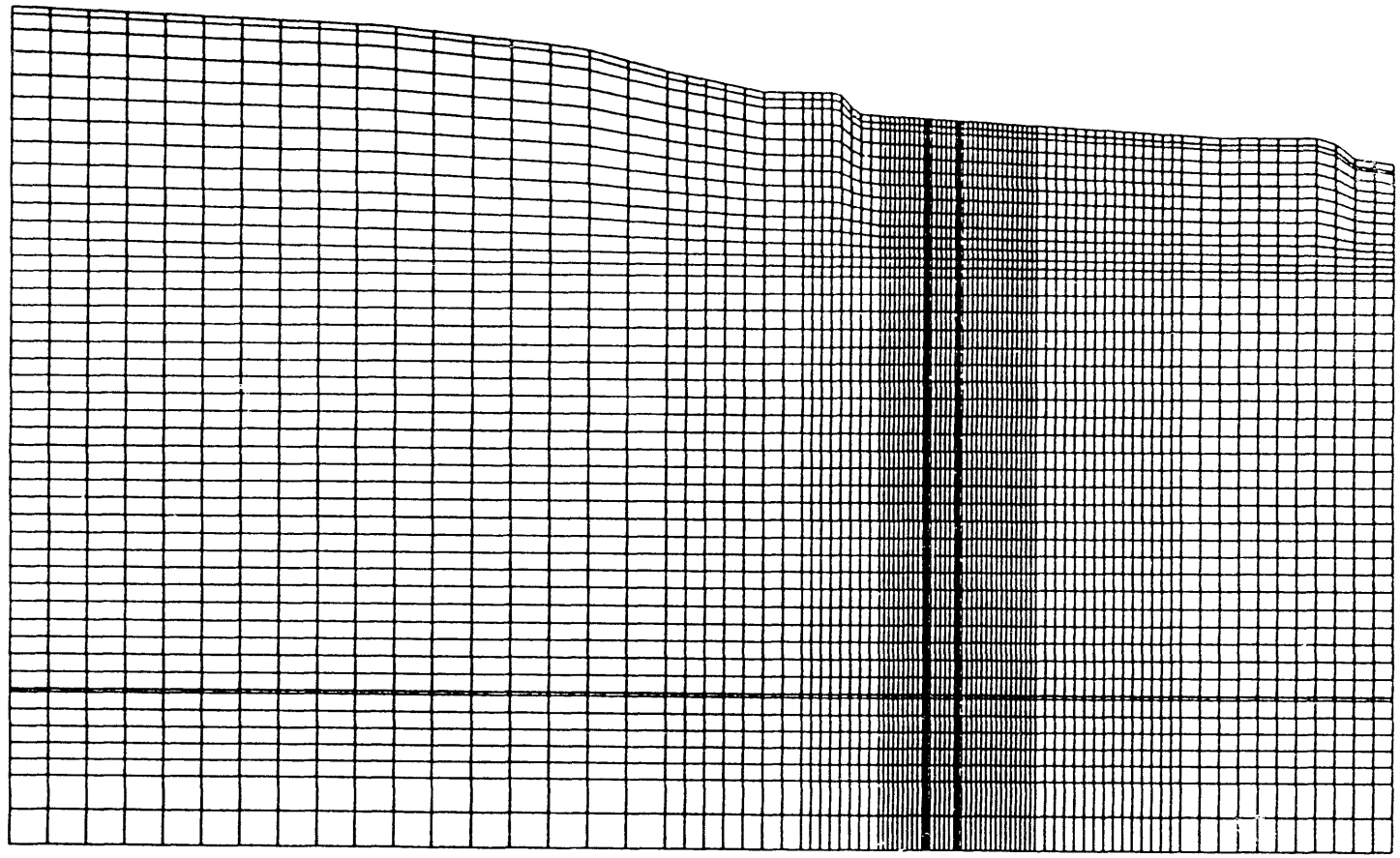

Figure 5.2 Finite element grid, consisting of 4370 elements, used in the transport simulations.

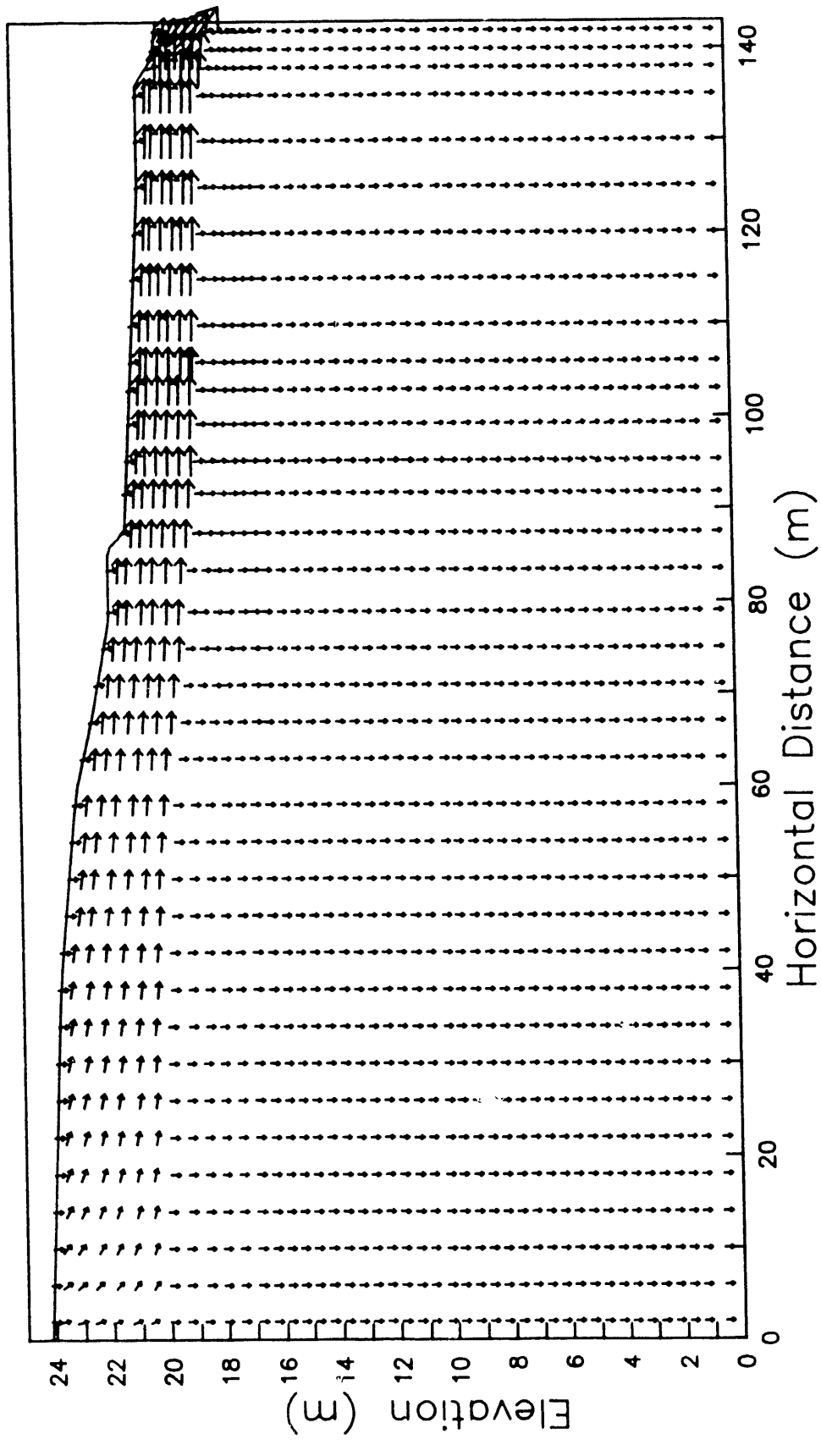

Figure 5.3 Steady state groundwater flow field used in the radionuclide transport simulations.

$$\alpha_i = \frac{\phi_m (L_i - b_i)^2}{3\phi_T^2 D_m} \left[\frac{R_m}{R_e}\right]^2 |V_i| \qquad (5.1)$$

where

α_i = Effective dispersivity in i-th direction
ϕ_m = Matrix porosity
ϕ_T = Total (matrix + fracture) porosity
D_m = Diffusion coefficient
R_m = Matrix retardation factor
R_e = Effective retardation factor
L_i = Half spacing between fractures in i-th direction
b_i = Half aperture of fractures in the i-th direction
v_i = Groundwater flow rate in i-th direction
i = Direction index, either horizontal (x) or vertical (z)

Using the following approximations: $\phi_m = \phi_T = 0.3$; $L_i = 0.2$m; $b_i \approx 0$; apparent diffusion coefficient $\phi D_m = 40$ cm^2/yr (Prudic, 1986); $R_m = R_e$; $V_x = 1$ m/yr; effective dispersivities of the fractured till were calculated to be $\alpha_x = 3.3$ m and $\alpha_z = 0.1$ m. These dispersivity values illustrate how the presence of fractures greatly increases the effective dispersivity. In contrast, for the unweathered till a dispersivity of only 0.01 m was used.

Transport simulation further require radionuclide decay rates and sorption partition coefficients. The latter were obtained from Nicholson and Hurt (1985, Table 7). Nicholson and Hurt list a range of k_d values for each radionuclide. The values used are for the anoxic, ultrasonic desegregated treatment, which yielded the lowest k_d values. No k_d values for Pu-239 are reported for the Lavery till. The k_d value for Pu-239 was therefore estimated from the k_d for Am-241 using a ratio of k_d (Pu-239) : k_d (Am-241) - 1:6, this being the average ratio of Am-241 and Pu-239 sorption coefficients reported by Nishita and Haug (1981) for various soil materials. The transport parameter values used in the radionuclide simulations are summarized in Table 5.1. It was furthermore assumed that the backfill in the disposal pit has the same hydraulic and transport characteristics as the transition material between unweathered and fractured till.

A primary unknown in the transport assessment is the actual rate of radionuclide release from the waste containers into the subsurface environment. For modeling purposes the following assumptions were made:

1) Release starts at the present time, using values in Table 2.1 for the initial pit radionuclide inventory.

Table 5.1 Transport parameter values used in radionuclide migration simulations.

Parameter	Units	Value
Chemical specific		
Half-life ($t_{1/2}$):		
Sr-90	yr	28.1
Cs-137	"	30.2
Pu-239	"	24,400
Partition coefficient (k_d):		
Sr-90	mℓ/g	7.0
Cs-137	"	48.0
Pu-239	"	62.4
Diffusion coefficient (D_m):		
Sr-90	cm^2/yr	40.0
Cs-137	"	40.0
Pu-239	"	40.0
Soil Specific		
Dispersivity (α_x,α_z):		
Unweathered	m	0.01, 0.01
Transition	"	0.02, 0.02
Fractured	"	3.3, 0.1
Porosity (ϕ_T):		
Unweathered	-	0.25
Transition	-	0.28
Fractured	-	0.30
Bulk Density (ρ_b):		
Unweathered	g/ml	1.65
Transition	"	1.65
Fractured	"	1.65

2) The leach rate follows first-order kinetics i.e., radionuclide release is proportional to the amount of radionuclide remaining in the waste with a leach coefficient of 10^{-6}/day.

In the VAM2D model, all grid nodes lying inside the disposal pit were designated as source nodes with the total pit radionuclide inventory equally divided among all of these nodes. Each of the nodes was further assigned a initial daily radionuclide mass flux equal to 10^{-6} times thecalculated nodal mass. All other nodes in the model domain were assigned zero initial concentration values. During the simulation, the release rate is automatically adjusted by the computer code to account for radioactive decay and mass removal due to leaching.

5.3 RESULTS

Simulated radionuclide distributions for Sr-90, Cs-137 and Pu-239 at selected times from the present are depicted by means of contours plots in Figures 5.4-5.9. The plotted contours correspond to a water phase concentration level of 10^{-3} μCi/L for Sr-90 and Cs-137 and 10^{-3} μg/L for Pu-239; slight irregularities represent some oscillations present in the numerical simulations. In all cases it can be seen that there is very little radionuclide migration beyond the disposal pit itself. For Sr-90 and Cs-137 the greatest extent of radionuclide migration occurs between 20 and 50 years, after this the plume contracts again as a result of radioactive decay. For these two radionuclides, radioactive decay is more rapid than the assumed rate of leaching from the waste. The simulations for Pu-239 were continued for a 500-year time period. Although Pu-239 has such a long half-life that radioactive decay is not very significant during this period, the extent of Pu-239 movement is still very limited. This can be attributed to the fact that Pu-239 is more strongly sorbed (k_d = 62.4) than Sr-90 (k_d = 7.0) or Cs-137 (k_d = 48.0).

The extent of radionuclide movement as shown in the figure is actually still somewhat exaggerated because numerical dispersion was not completely suppressed in the simulation. Under the assumptions employed in the transport model, radionuclides that are buried in the unweathered till below the fractured zone, remain in this zone and show very limited migration. Movement in the unweathered till is dominated by diffusion which itself is very slow, and the movement of radionuclides is further reduced by sorption. In the scenario depicted in Figures 5.4-5.9, the radionuclides remain in the unweathered till and simply do not move into the fractured till layer; whether or not there is much lateral flow through the fractured till, the fractured till does not represent a significant pathway for radionuclide movement in the simulations.

Key assumptions leading to this conclusion are that all of the waste is originally buried well below the surface fractured zone, and that the steady state flow assumption used in the transport analysis, does realistically describe long-term average flow conditions.

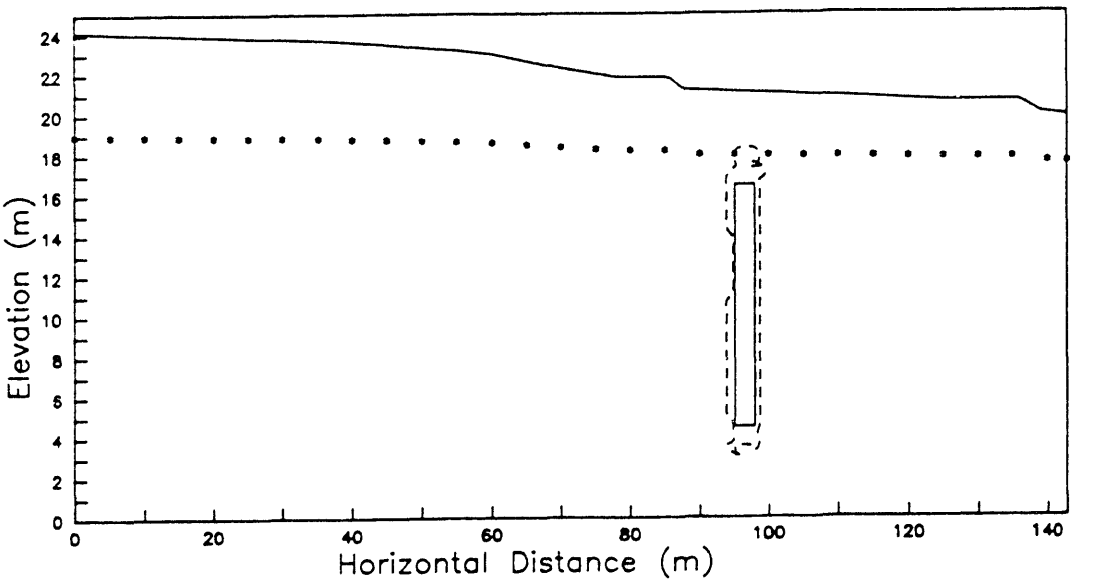

Figure 5.4 Sr-90 migration after 20 years; concentration contour represents 10^{-3} μCi/L level.

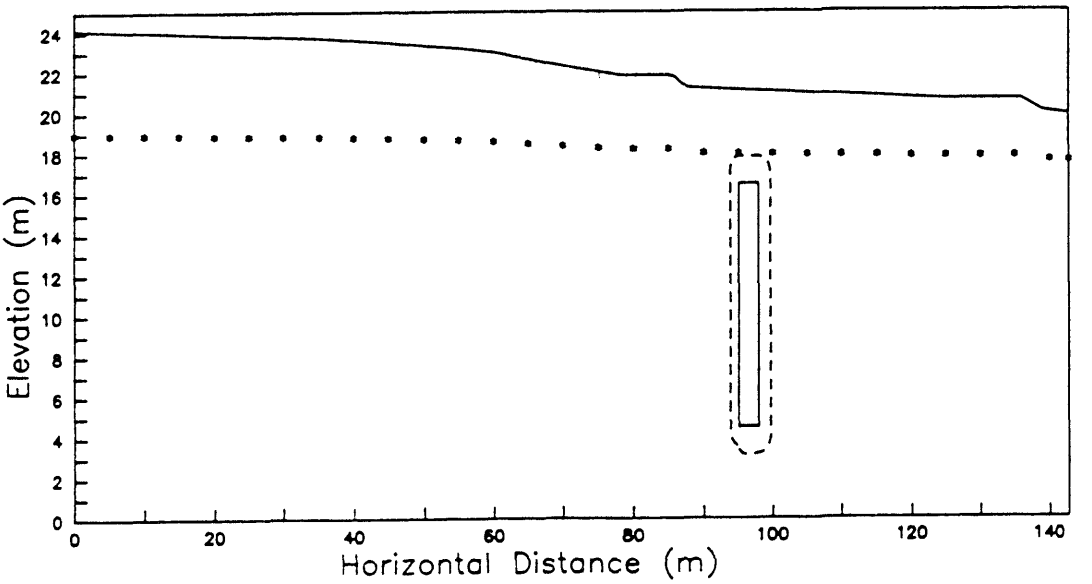

Figure 5.5 Sr-90 migration after 200 years; concentration contour represents 10^{-3} μCi/L level.

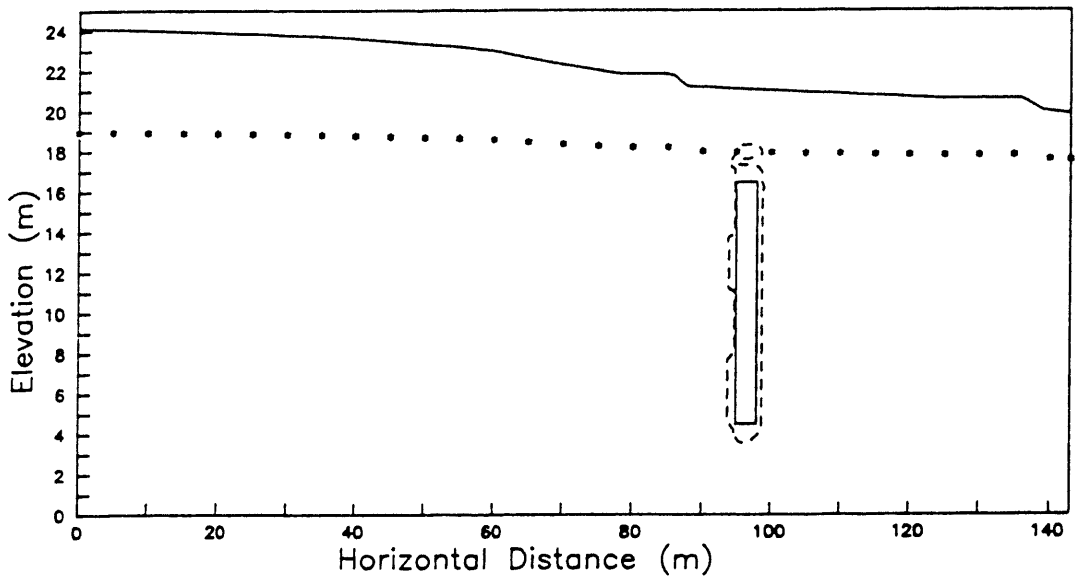

Figure 5.6 Cs-137 migration after 20 years; concentration contour represents 10^{-3} μCi/L level.

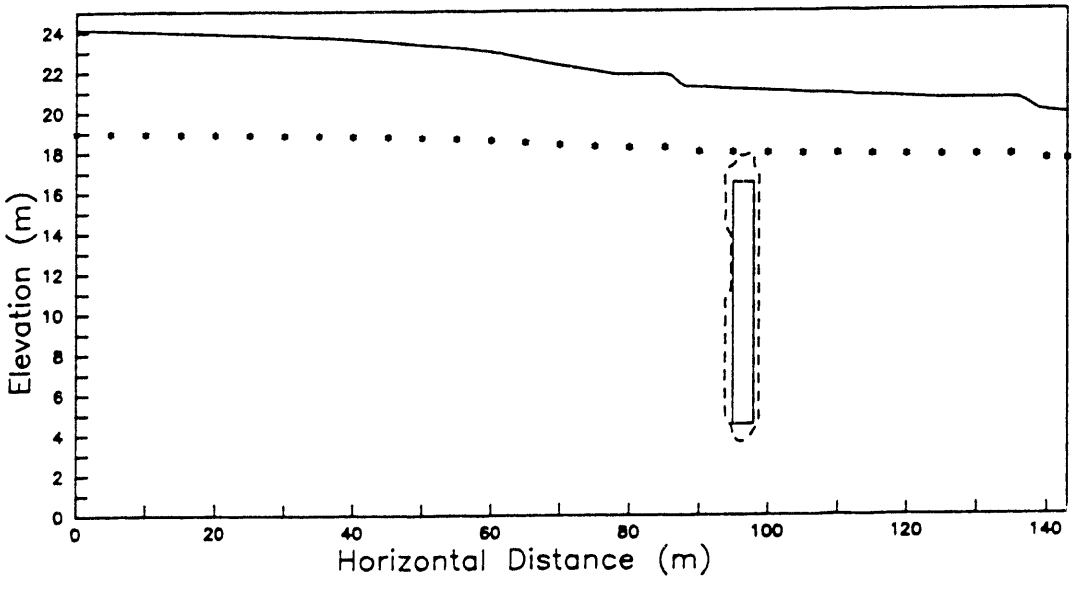

Figure 5.7 Cs-137 migration after 200 years; concentration contour represents 10^{-3} μCi/L level.

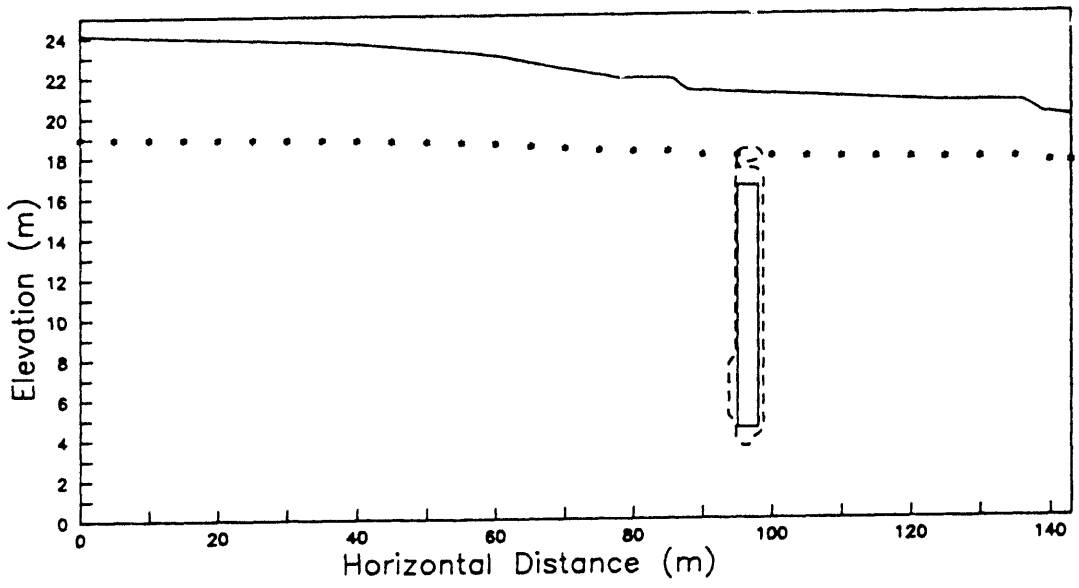

Figure 5.8 Pu-239 migration after 50 years; concentration contour represents 10^{-3} μg/L level.

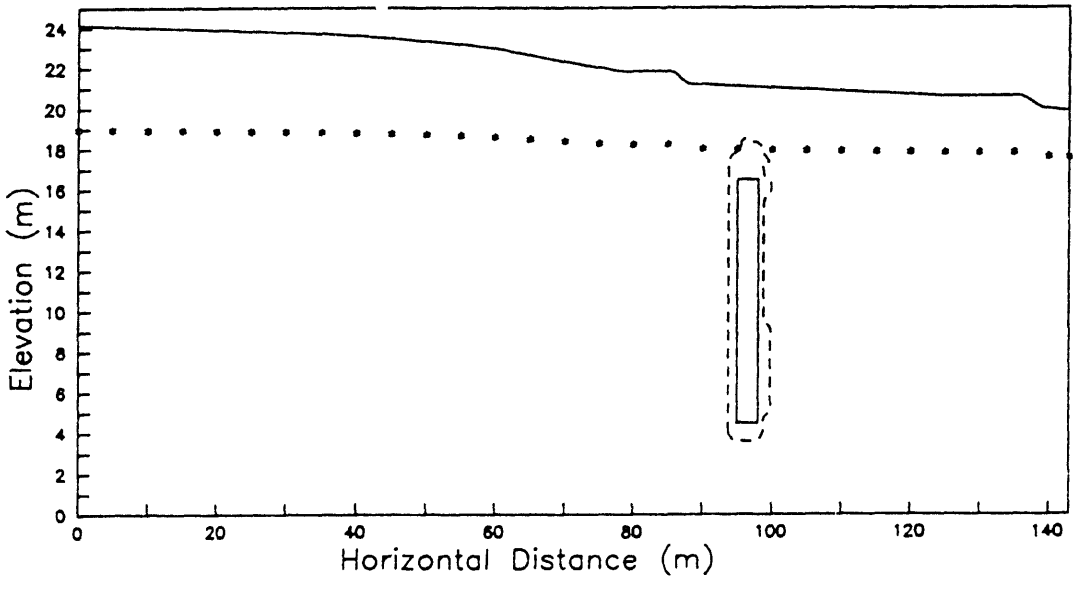

Figure 5.9 Pu-239 migration after 500 years; concentration contour represents 10^{-3} μg/L level.

It has been reported though that the top of the disturbed zone in NRC burial specifications, in practice was taken to be the depth of surface disturbance, rather than the top of the unweathered till[8/]. This would imply the possible burial of wastes well within the depth of the fractured layer. Another possible scenario that could introduce radionuclides into the fractured till zone is one in which rising water levels following an extended dry period fill up disposal pits and rise to within the fractured till, carrying contaminants with them. It is therefore still of interest to consider the transport of radionuclides through the fractured till as a second transport modeling scenario. The original transport scenario was modified by extending the source upward into the fracture zone to four feet below the soil surface, and then conducting the transport simulations again for Sr-90, Cs-137 and Pu-239. The total radionuclide inventory in the pit was kept the same as before. Results of this analysis are shown in Figures 5.10 - 5.15. Radionuclide distributions after 20 and 200 years are shown for Sr-90 and Cs-137 and 50 and 500 years for Pu-239. As before the 10^{-3} μCi/L concentration level is shown for Sr-90 and Cs-137, and the 10^{-3} μg/L concentration level is shown for Pu-239. The second simulation scenario demonstrates the potential for much greater radionuclide migration through the fractured till compared to the uweathered till. The results also show much more clearly the differences in mobility between the different radionuclide species. Sr-90 is the least strongly sorbed species; after 200 years the strontium plume has migrated approximately 25 m through the fractured till. For Cs-137 and Pu-239 the distances are 6m and 15m after 200 and 500 years respectively. It is noteworthy also that the simulations predict that radionuclides would move right up to the soil surface through a combination of diffusive and dispersive movement even through the net flow rate in the upper part of the soil is downward.

[8/] T. deBoer, NYSERDA, personal communication

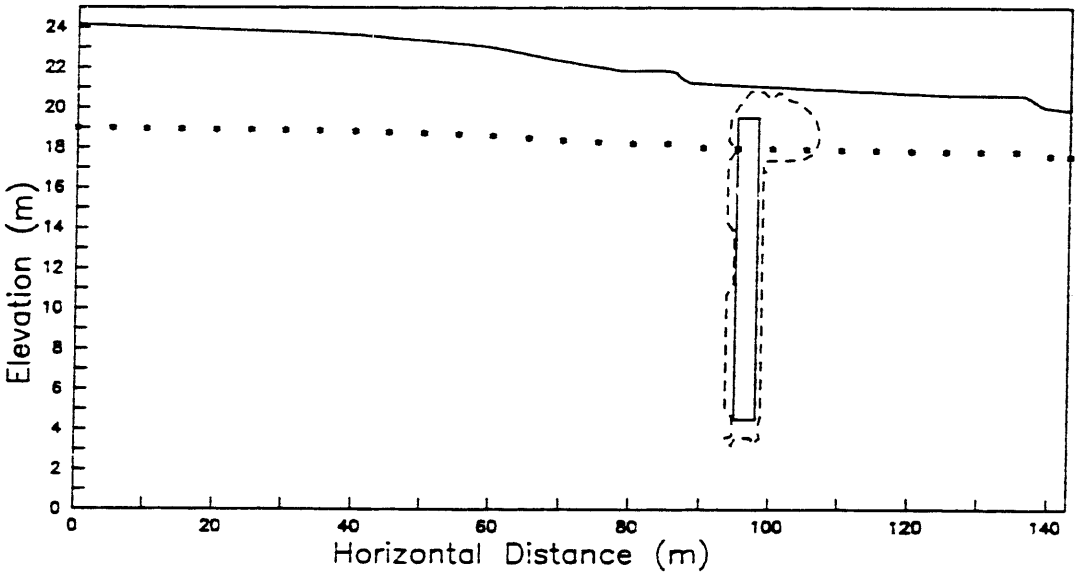

Figure 5.10 Sr-90 migration after 20 years for second transport scenario; concentration contour represents 10^{-3} μCi/L level.

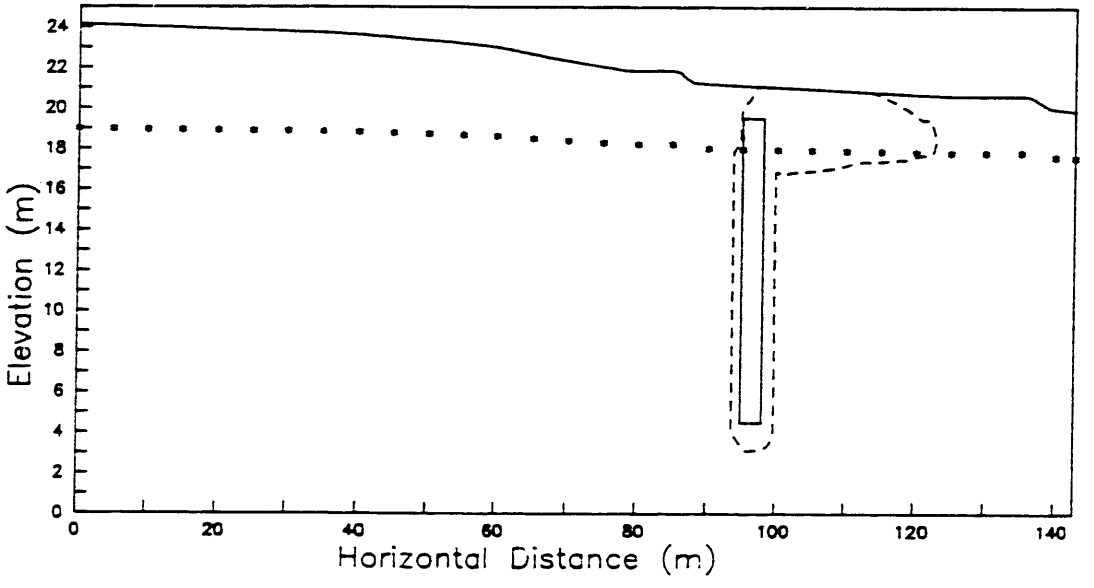

Figure 5.11 Sr-90 migration after 200 years for second transport scenario; concentration contour represents 10^{-3} μCi/L level.

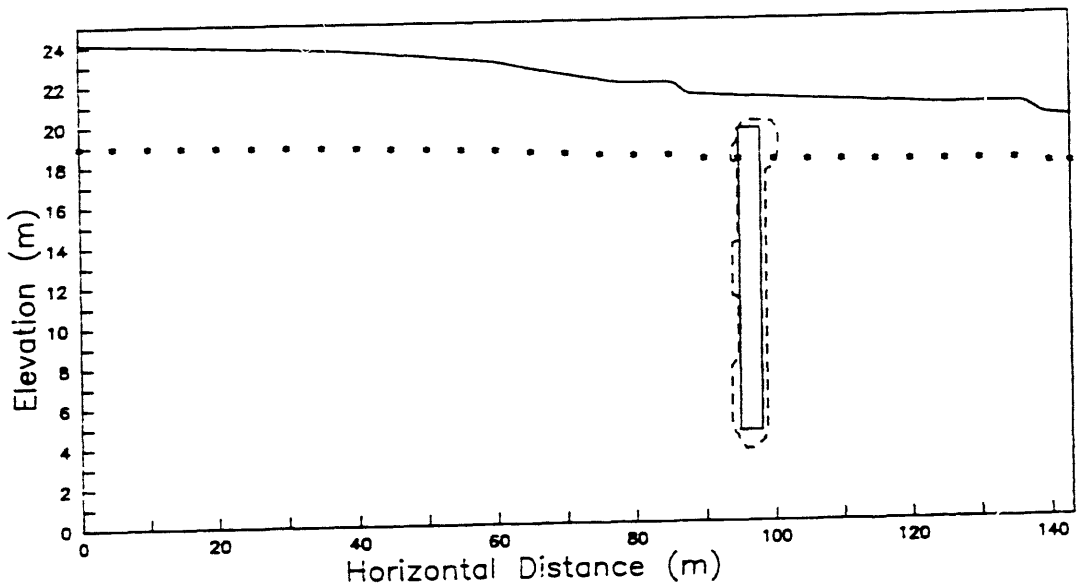

Figure 5.12 Cs-137 migration after 20 years for second transport scenario; concentration contour represents 10^{-3} μCi/L level.

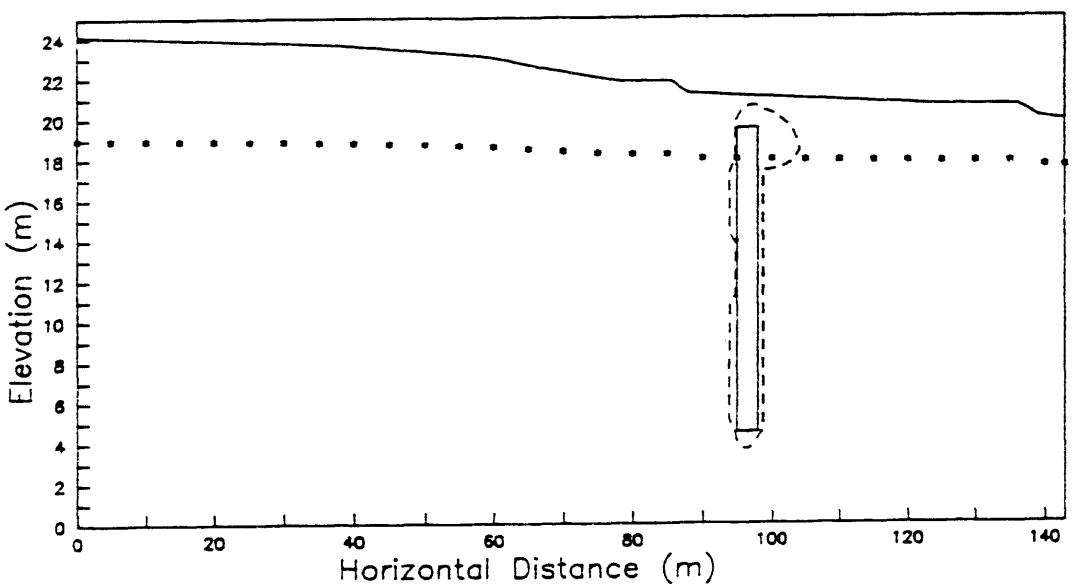

Figure 5.13 Cs-137 migration after 200 years for second transport scenario; concentration contour represents 10^{-3} μCi/L level.

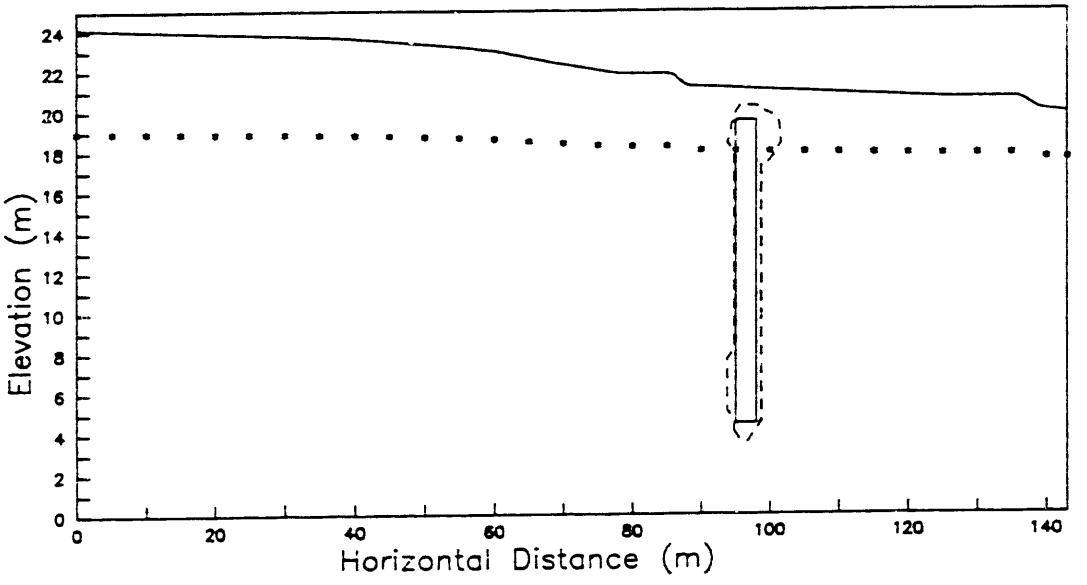

Figure 5.14 Pu-239 migration after 50 years for second transport scenario; concentration contour represents 10^{-3} μg/L level.

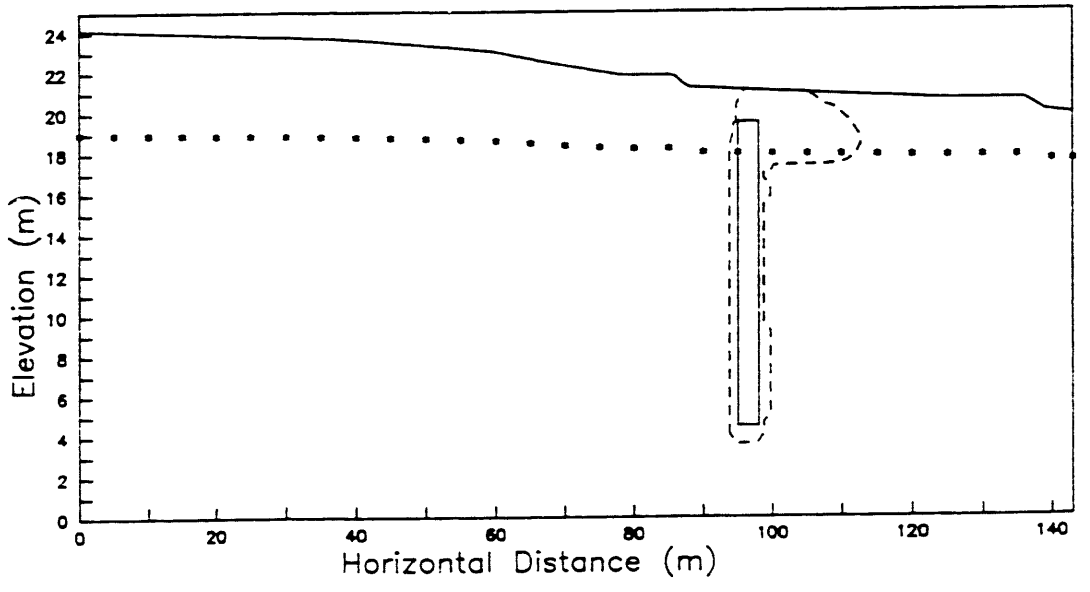

Figure 5.15 Pu-239 migration after 500 years for second transport scenario; concentration contour represents 10^{-3} μg/L level.

6 DISCUSSION

In the preceding sections the results of a transient groundwater flow and radionuclide transport modeling investigation were presented. The results of these simulations are discussed here. Model limitations and ways to improve them are identified. Flow modeling results are analyzed first, followed by transport modeling results.

6.1 FLOW MODELING

The emphasis in the flow modeling has been as modeling flow through the fractured till layer. Observed precipitation data for the 3-month period of March to May, 1990 provided the main inputs to the model. The flow model was calibrated by matching observed inflows into the interceptor trench located around the FDA, treating the saturated hydraulic conductivity of the upper, fractured layer as the main calibration parameter. The motivation for treating the saturated hydraulic conductivity of the till as the primary calibration parameter was that this hydraulic conductivity is poorly known and that predicted inflow into the interceptor trench is quite sensitive to this permeability value. The starting point in the calibration procedure has the steady state flow model of Bergeron and Bugliosi (1988). Use of permeability values from this steady state model resulted in a severe underprediction of inflow into the trench. Reasonably good agreement with observed trench inflow data was obtained in two simulations. In the first of these (see Section 4.2.3) the fractured till was assigned an effective permeability of 5×10^{-3} m/d, or 25 times greater than the initial value obtained from Bergeron and Bugliosi. In this simulation, the predicted trench inflow during the initial three weeks of the simulation period was significantly less than observed, but a much better agreement was obtained for the latter part of the simulation period. In this case, which will be referred to as case A, the model also predicted that the water table would be right at or near the soil surface throughout the entire simulation period. Shallow solvent plume monitoring wells indicate that actual water levels are several feet below the soil surface. Better agreement with the latter observations could be obtained by introducing a shallow lower permeability layer at the soil surface, overlying the higher permeability fractured till. In this simulation (Section 4.2.4) the predicted trench inflow was also increased, improving agreement with early trench inflow data although trench inflow at later times was over predicted. The trench inflow rate in the second case, which will be referred to as case B, was approximately twice as high as in the first case.

A number of factors have been identified which may affect the accuracy and validity of the transient flow model. These factors include:

1) Unknown influence of seepage through the trench cap during the early part of the simulation period

2) Unknown influence of evapotranspiration during the latter part of the simulation period

3) Short duration of the model calibration period, and

4) Limitations of 2D cross-sectional model

Observed trench inflow data show a sharp reduction in daily inflow rates between March and May, 1990. On the one hand, the large initial inflow may reflect direct seepage of surface run-off through the trench cap. Alternatively, the reduced measured inflow in the latter part of April and May, could reflect the influence of evapotranspiration. In the present VAM2D model neither of these processes is accounted for, implicitly it is assumed that all inflow into the trench originates from subsurface seepage. The results for simulation B showed that a reasonably good agreement with the early time inflow can be achieved, but that inflow at later times is then overpredicted. The latter discrepancy would, in this case, be attributed to evapotranspiration. Depending on the actual magnitude of inflow through the trench cap, this model scenario may overpredict actual flow through fractured till by attributing too much of the observed trench inflow to subsurface seepage.

While the transient flow model presented here may still have many limitations, the data are presently available to resolve some of the important questions. In particular, the availability of trench inflow data for 1991 should allow the questions of the importance of infiltration through the trench cap to be resolved. The present model was calibrated using data for a 3-month period only. This was done in part to reduce computational expense, but also because accurate trench inflow records for a longer period were not available. However, reliable trench inflow data have now been collected since early 1991 and use of this data should allow the transient flow model to be improve substantially. Simulations of flow over a longer time period are needed, not only to improve the flow model itself, but also to get a more useful basis for subsurface transport predictions. The timescale for radionuclide transport is on the order of hundreds of years. It is impractical to model flow in a transient way over such long periods. It is therefore likely that any future transport assessment will be based on steady state flow conditions as was done here. To determine these average conditions in a meaningful way, it may be necessary to conduct transient flow modeling for a period of at least a full year. In view of the importance of surface runoff and evapotranspiration, these processes should be included in a model. Since many subsurface flow codes have only limited capability to handle these processes, the most appropriate model may involve the use of a rainfall-runoff code (e.g. CREAMS or similar code) to provide infiltration inputs for a separate transient subsurface flow code.

Another limitation of the present model is that it is restricted to two-dimensions. Transient simulation of the first cross-section showed that the 2D assumption can introduce certain artifacts such as accumulation of water in areas of locally lower topography. The second cross-section allows water to move freely downhill, following the surface topography. A related assumption is that the observed total inflow to the trench can be divided by the length of the trench for comparison with the 2-D model. This is valid provided the inflow in indeed more or less uniform along the length of the trench. In reality, near surface groundwater flow is expected to be three-dimensional, in response to topographic differences and other factors. The presence of three-dimensional flow paths is likely to be even more important when radionuclide

transport is considered, because of the non-uniform distribution of disposal pits. Consequently, use of a three-dimensional model should be considered in future studies.

While the transient flow simulation cases A and B show significant differences in the predicted magnitude of flow through the fractured till zone, the groundwater velocity plots that were presented for case A and B (Figure 4.20/4.21 and 4.26/4.27) indicate that in both cases flow through the fractured till along the entire cross-section is in the lateral direction. This result from the transient simulations is fundamentally different from earlier steady state simulations which indicated that even in the near surface zone, flow in the lateral direction would occur only over short distances. Apart from the unresolved questions of the magnitude of this flow, the present simulations indicate that at least during the wet periods of the year (Spring, Fall), lateral flow through the fractured till can be significant. Also noteworthy is the fact that the flow simulations agreed quite well with trench inflow data in terms of the occurrence of inflow peaks. The simulations reproduced the observed response between rainfall and trench inflow, note for instance the occurrence of observed and simulated highs and lows in trench inflow in Figure 4.24 particularly during the first month of the simulation. This result shows that the observed quick response of the trench inflow to rainfall can be reproduced correctly by the model without involving short-circuiting of flow through surface run-off and direct infiltration through the trench cap.

6.2 RADIONUCLIDE TRANSPORT

The radionuclide transport analysis presented in this report was designed as a qualitative assessment of potential subsurface radionuclide migration pathways, particularly, the importance of the near surface pathway. The results of this analysis indicate that for wastes disposed below the depth of the fractured zone there is very little migration at all; radionuclide movement in the unweathered till is diffusion controlled as pointed out in earlier studies (e.g., Prudic, 1986) and therefore very slow. On the other hand, the simulations also show that the fractured till can be a significant pathway for radionuclides that are present within the zone of fracturing. For the three radionuclides considered here and under the assumed transport conditions, Sr-90 showed the greatest extent of migration. Of the three radionuclides considered, Sr-90 is the least strongly sorbed and thus moves the most rapidly. Note however that for times scales greater than the few hundred years considered here, Pu-239 will show the greatest migration. While it travels more slowly than Sr-90, it is also much more long-lived ($t_{1/2}$ = 24,400 years). In contrast Cs-137 is both strongly sorbed and has a relatively short half-life ($t_{1/2}$ = 30.2 years), two factors that combine to limit the migration of Cs-137.

Two mechanisms may introduce radionuclides into the fractured till zone. The first is burial of wastes at shallow depths; the other involves upward movement of radionuclides by transient groundwater flow. Particularly, rising water levels following extended dry periods may carry radionuclides upward into the fractured zone; a somewhat analogous mechanism to that hypothesized to have introduced solvents from buried tanks into the near-surface zone (Blickwedehl et al., 1989). This aspect of the transient flow behavior was not addressed in the flow model presented here, since a relatively short, wet period was modeled. Assessing the

importance of water table fluctuations for bringing radionuclides from the unweathered till into the fractured till provides another argument for longer term transient simulations, e.g. on the order of a year or more.

A tacit assumption in both the flow and transport simulations is that the fractured upper till zone can be adequately represented with a porous medium flow and transport model. The use of the porous medium VAM2D code for the simulation was motivated by the fact that it incorporates many other features that were required in modeling the site, including the ability to accommodate transient infiltration and seepage face boundaries and internal first-order decaying sources for describing radionuclide release from the waste. Another consideration is that there is not sufficient quantitative information on important fracture characteristics such as fracture aperture and connectivity to justify the use of a fracture flow and transport model. Nevertheless, it is useful to review the physical justification for using a porous medium transport model and identify the errors that may result from using an inappropriate model.

Studies on the applicability of porous media continuum models to describe fractured media are mostly based on theoretical and computer analyses; there are few if any examples of actual field verification and validation. The general conclusion from the literature is that, at least for fully saturated media, solute transport is much more affected by fractures than is groundwater flow (e.g., Long et al, 1982; Khaleel, 1989). The situation is more complex for variably saturated media since the exchange of fluid between fractures and matrix must be accounted for. In the present investigation, saturated-unsaturated conditions do indeed exists in the fracture zone. However, the capillary characteristics of the clay matrix are such that even though fractures may become desaturated, the matrix itself will still remain saturated, with the result that there will be little or no matrix - fracture interaction during flow. This favors the use of a porous medium flow model for the site. The sharp reduction in effective permeability as fractures are desaturated is accounted for by the use of a very steep permeability - saturation curve (Figure 3.6). The effective saturated conductivity of the fractured medium will be complex function of fracture aperture, spacing and connectivity; and is thus almost impossible to determine directly. This difficulty was circumvented by simply treating it as a calibration parameter in the flow simulations.

The applicability of a porous medium model to describe solute transport at a fractured site depends on the combination of several factors and fracture characteristics. Various published studies (e.g., Pankow et al, 1976, Bear and Berkowitz, 1988) indicate that the porous medium approximation will be more accurate if: (i) the fracture network is regular rather than irregular, (ii) the fracture density increases, (iii) matrix diffusion is significant. The latter process will tend to smooth out the concentration contrast between fractures and matrix and favor porous media-like behavior. Kool and Wu (1991) showed, for a hypothetical fractured site, that the VAM2D model could accurately predict plume migration behavior. There are relatively few published results on the actual application and validation of porous medium models for modeling actual fractured waste disposal sites similar to the West Valley site. However, a number of studies indicate that transport properties of glacial tills may favor the porous medium approximation. Grisak et al. (1980) noted the strong influence of matrix

diffusion in laboratory column tests. Transport studies have been conducted by the University of Waterloo in a fractured glacial till at a waste disposal site in southern Ontario (Cherry, 1989). Although no modeling results are reported, a strong effect of matrix diffusion was observed in field tracer tests (Cherry, 1989). Many reported characteristics of the till at this site are similar to the West Valley site, including the glacial origin and dominantly vertical fracturing of the upper part of the till. Considering these similarities and also the relative intense scale of fracturing (Figure 2.4) compared to the much larger transport scale of interest, there is good justification for the use of a porous medium transport model. Although this is a subjective evaluation, it is felt that any errors due to the inappropriate use of a porous medium model are not greater, and may well be less significant than other sources of uncertainty in the modeling analysis.

REFERENCES

Bergeron, M.P., J.L. Smoot, M.L. Kemner and W.E. Cronin. June, 1991. Hydrogeologic Performance Assessment Analysis of the Commercial Low-Level Radioactive Waste Disposal Facility near West Valley, New York. NUREG/CR-5737, U.S. Nuclear Regulatory Commission, Washington D.C.

Bergeron, M.P., M.L. Kemner, and J.L. Smoot. May 1989. Performance Assessment Analysis of the Commercial Low-Level Radioactive Waste Disposal Facility near West Valley, NY. Pacific Northwest Laboratory, Richland, WA, (unpublished report available through U.S. NRC, Office of Nuclear Material Safety & Safeguards, Division of Low-Level Waste Management & Decommissioning).

Bergeron, M.P. et al. 1984. Hydrogeology at a Nuclear Fuel Reprocessing Plant and Related Waste Facilities Near West Valley, New York. U.S. Geological Survey Open-File Report.

Bergeron, M.P., and E.F. Bugliosi. 1988. Ground-Water Flow Near Two Radioactive-Waste-Disposal Areas at the Western New York Nuclear Service Center, Cattaraugus County, New York--Results of Simulation. Water-Resources Investigations Report 86-4351, U.S. Geological Survey, Ithaca, N.Y.

Blickwedehl, R.R., B. Beyer, D. Aloysius, M.W. Grant, T. Weiss, and W. Bridenbaker. 1989. Characterization of Solvent Leakage and Migration NRC Licensed Disposal Area Western New York Nuclear Service Center, West Valley, New York. West Valley Nuclear Services Co., Inc., West Valley, N.Y.

Brooks, R.H. and A.T. Corey. 1964. Hydraulic Properties of Porous Media. Hydrology Paper No. 3, Colorado State University, Fort Collins, CO.

Dana, R.H., R.H. Fakundiny, Jr., R.G. Lafleur, S.A. Mollello, and P.R. Whitney. 1979. Geologic Study of the Burial Medium at a Low-Level Radioactive Waste Burial Site at West Valley, New York. NYSG/79-2411, New York State Geological Survey, Albany, N.Y.

Grisak, G.E. and J.F. Pickens. 1980. "Solute transport through fractured media 2. Column study of fractured till", Water Resources Research, 16(4):731-739.

Huyakorn, P.S., J.B. Kool and Y.S. Wu. October, 1991. VAM2D - Variably Saturated Analysis Model in Two Dimensions, Version 5.2 with Hysteresis and Chain Decay Transport. NUREG/CR-5352, Rev. 1. U.S. Nuclear Regulatory Commission, Washington, D.C.

Khaleel, R. 1989. "Scale dependence of continuum models for fractured basalts", Water Resources Research, 25(8):1847-1855, 1989.

Kool, J.B. and Y.S. Wu. October, 1991. Validation and Testing of the VAM2D Computer Code. NUREG/CR-5795, U.S. Nuclear Regulatory Commission.

Long, J.C.S., J.S. Remer, C.R. Wilson and P.A. Witherspoon. 1982. "Porous media equivalents for networks of discontinuous fractures", Water Resources Research, 18(3):645-658.

Mualem, Y. 1976. "A new model for predicting the hydraulic conductivity of unsaturated porous media." Water Resour. Res. 12(3):513-522.

Nicholson, T.J. and R.D. Hurt. August, 1985. Information on the Confinement Capability of the Facility Disposal Area at West Valley, New York. NUREG-1164, U.S. Nuclear Regulatory Commission, Washington, D.C.

Pankow, J.F., R.L. Johnson, J.P. Newetson and J.A. Cherry. 1986. "An evaluation of contaminant migration patterns at two waste disposal sites on fractured porous media in terms of the equivalent porous medium (EPM) model," Journal of Contaminant Hydrology, 1(1):65-70.

Prudic, D.E. 1982. "Hydraulic Conductivity of a Fine-Grained Till, Cattaraugus County, New York". Ground Water 20(2):194.

Prudic, D.E. 1986. Ground-Water Hydrology and Subsurface Migration of Radionuclides at a Commercial Radioactive-Waste Burial Site, West Valley, Cattaraugus County, New York U.S. Geological Survey Professional Paper 1325, U.S. Government Printing Office, Washington, D.C.

Saxton, K.E. and J.L. McGuinness. 1982. Evapotranspiration, in: C.T. Haam et al. (Eds) "Hydrologic modeling of small watersheds." ASAE Monograph, American Soc. Agric. Engineers, St. Joseph, MI.

Smoot, J.L. September, 1989. A Review of Geoscience Characteristics and Disposal Experience at the Commercial Low-Level Radioactive Waste Disposal Facility near West Valley, N.Y.. NUREG/CR-5431, U.S. Nuclear Regulatory Commission, Washington, D.C.

U.S. DOE. 1986. Environmental Assessment for Disposal of Project Low-Level Waste, Part I: Environmental Assessment. United States Department of Energy, West Valley Project Office, West Valley, N.Y.

U.S. DOE. 1985. Results of Tests from a Research Trench in the NDA. United States Department of Energy, West Valley Project Office, West Valley, N.Y.

van Genuchten, M.Th. 1980. "A closed-form equation for predicting the hydraulic conductivity of unsaturated soils." Soil Sci. Soc. Am. J. 44:892-898.

Yager, R.M. 1987. Simulation of Ground-Water Flow Near the Nuclear-Fuel Facility at the Western New York Nuclear Service Center, Cattaraugus County, New York. Water Resources Investigations Report 85-4308, U.S. Geological Survey, Ithaca, N.Y.

APPENDIX A

MEASURED RELATIVE PERMEABILITY AND SOIL MOISTURE TENSION DATA

Table A.1 Parameters of unsaturated flow constitutive relations used for fitting the functions of relative permeability and capillary pressure (U.S. DOE, 1988).

Soil Water Content	Relative Permeability	Soil Moisture Tension (m)
0.299	1.000E+00	0.43
0.288	2.255E-02	8.36
0.276	1.626E-02	48.12
0.265	1.293E-02	71.13
0.254	1.026E-02	82.52
0.242	8.050E-03	86.40
0.231	6.229E-03	90.66
0.220	4.745E-03	95.37
0.208	3.551E-03	100.59
0.197	2.603E-03	106.41
0.186	1.863E-03	112.95
0.174	1.295E-03	120.34
0.163	8.688E-04	128.75
0.152	5.575E-04	138.43
0.140	3.375E-04	149.68
0.129	1.886E-04	162.91
0.118	9.375E-05	178.70
0.106	3.849E-05	197.86
0.095	1.097E-05	221.61
0.084	1.605E-06	251.81

APPENDIX B

OBSERVED PRECIPITATION DATA

March - August, 1990

Table B.1 Precipitation data for West Valley FDA Site, March 1 to August 10, 1990.

Date (1990)	Day #	Precipitation (in/d)	Precipitation (m/d)	Cum. Precipitation (in)	Cum. Precipitation (m)
3/ 1	1	..	..	..	..
3/ 2	2	..	..	..	..
3/ 3	3	0.00	0.0000	0.00	0.0000
3/ 4	4	0.00	0.0000	0.00	0.0000
3/ 5	5	0.00	0.0000	0.00	0.0000
3/ 6	6	0.00	0.0000	0.00	0.0000
3/ 7	7	0.00	0.0000	0.00	0.0000
3/ 8	8	0.00	0.0000	0.00	0.0000
3/ 9	9	0.17	0.0043	0.17	0.0043
3/10	10	0.00	0.0000	0.17	0.0043
3/11	11	0.44	0.0112	0.61	0.0155
3/12	12	0.00	0.0000	0.61	0.0155
3/13	13	0.00	0.0000	0.61	0.0155
3/14	14	0.00	0.0000	0.61	0.0155
3/15	15	0.00	0.0000	0.61	0.0155
3/16	16	0.03	0.0008	0.64	0.0162
3/17	17	0.70	0.0178	1.34	0.0340
3/18	18	0.06	0.0015	1.40	0.0356
3/19	19	0.24	0.0061	1.64	0.0416
3/20	20	0.00	0.0000	1.64	0.0416
3/21	21	0.00	0.0000	1.64	0.0416
3/22	22	0.00	0.0000	1.64	0.0416
3/23	23	0.14	0.0036	1.78	0.0452
3/24	24	0.00	0.0000	1.78	0.0452
3/25	25	0.00	0.0000	1.78	0.0452
3/26	26	0.01	0.0003	1.79	0.0455
3/27	27	0.00	0.0000	1.79	0.0455
3/28	28	0.00	0.0000	1.79	0.0455
3/29	29	0.00	0.0000	1.79	0.0455
3/30	30	0.21	0.0053	2.00	0.0508
3/31	31	0.00	0.0000	2.00	0.0508
4/ 1	32	0.11	0.0028	2.11	0.0536
4/ 2	33	0.39	0.0099	2.50	0.0635
4/ 3	34	0.11	0.0028	2.61	0.0663
4/ 4	35	0.94	0.0239	3.55	0.0902
4/ 5	36	0.20	0.0051	3.75	0.0952
4/ 6	37	0.01	0.0003	3.76	0.0955
4/ 7	38	0.02	0.0005	3.78	0.0960
4/ 8	39	0.00	0.0000	3.78	0.0960
4/ 9	40	0.00	0.0000	3.78	0.0960
4/10	41	1.35	0.0343	5.13	0.1303
4/11	42	0.04	0.0010	5.17	0.1313

Date (1990)	Day #	Precipitation (in/d)	(m/d)	Cum. Precipitation (in)	(m)
4/12	43	0.00	0.0000	5.17	0.1313
4/13	44	0.00	0.0000	5.17	0.1313
4/14	45	0.48	0.0122	5.65	0.1435
4/15	46	0.00	0.0000	5.65	0.1435
4/16	47	0.00	0.0000	5.65	0.1435
4/17	48	0.16	0.0041	5.81	0.1475
4/18	49	0.00	0.0000	5.81	0.1475
4/19	50	0.00	0.0000	5.81	0.1475
4/20	51	0.39	0.0099	6.20	0.1575
4/21	52	0.18	0.0046	6.38	0.1620
4/22	53	0.00	0.0000	6.38	0.1620
4/23	54	0.00	0.0000	6.38	0.1620
4/24	55	0.08	0.0020	6.46	0.1641
4/25	56	0.00	0.0000	6.46	0.1641
4/26	57	0.00	0.0000	6.46	0.1641
4/27	58	0.00	0.0000	6.46	0.1641
4/28	59	0.00	0.0000	6.46	0.1641
4/29	60	0.00	0.0000	6.46	0.1641
4/30	61	0.00	0.0000	6.46	0.1641
5/ 1	62	0.00	0.0000	6.46	0.1641
5/ 2	63	0.00	0.0000	6.46	0.1641
5/ 3	64	0.00	0.0000	6.46	0.1641
5/ 4	65	1.02	0.0259	7.48	0.1900
5/ 5	66	0.53	0.0135	8.01	0.2034
5/ 6	67	0.00	0.0000	8.01	0.2034
5/ 7	68	0.00	0.0000	8.01	0.2034
5/ 8	69	0.00	0.0000	8.01	0.2034
5/ 9	70	0.00	0.0000	8.01	0.2034
5/10	71	0.89	0.0226	8.90	0.2260
5/11	72	0.07	0.0018	8.97	0.2278
5/12	73	0.14	0.0036	9.11	0.2314
5/13	74	1.09	0.0277	10.20	0.2590
5/14	75	0.00	0.0000	10.20	0.2590
5/15	76	0.25	0.0063	10.45	0.2654
5/16	77	0.65	0.0165	11.10	0.2819
5/17	78	0.69	0.0175	11.79	0.2994
5/18	79	0.30	0.0076	12.09	0.3070
5/19	80	0.00	0.0000	12.09	0.3070
5/20	81	0.32	0.0082	12.41	0.3152
5/21	82	0.01	0.0003	12.42	0.3155
5/22	83	0.00	0.0000	12.42	0.3155
5/23	84	0.00	0.0000	12.42	0.3155
5/24	85	0.00	0.0000	12.42	0.3155
5/25	86	0.00	0.0000	12.42	0.3155
5/26	87	0.00	0.0000	12.42	0.3155

Date (1990)	Day #	Precipitation (in/d)	Precipitation (m/d)	Cum. Precipitation (in)	Cum. Precipitation (m)
5/27	88	0.04	0.0010	12.46	0.3165
5/28	89	0.00	0.0000	12.46	0.3165
5/29	90	0.62	0.0157	13.08	0.3322
5/30	91	0.00	0.0000	13.08	0.3322
5/31	92	0.00	0.0000	13.08	0.3322
6/ 1	93	0.00	0.0000	13.08	0.3322
6/ 2	94	0.00	0.0000	13.08	0.3322
6/ 3	95	0.17	0.0043	13.25	0.3365
6/ 4	96	0.15	0.0038	13.40	0.3403
6/ 5	97	0.00	0.0000	13.40	0.3403
6/ 6	98	0.00	0.0000	13.40	0.3403
6/ 7	99	0.00	0.0000	13.40	0.3403
6/ 8	100	0.10	0.0025	13.50	0.3429
6/ 9	101	0.02	0.0005	13.52	0.3434
6/10	102	0.32	0.0081	13.84	0.3515
6/11	103	0.00	0.0000	13.84	0.3515
6/12	104	0.00	0.0000	13.84	0.3515
6/13	105	0.00	0.0000	13.84	0.3515
6/14	106	0.00	0.0000	13.84	0.3515
6/15	107	0.00	0.0000	13.84	0.3515
6/16	108	0.00	0.0000	13.84	0.3515
6/17	109	0.00	0.0000	13.84	0.3515
6/18	110	0.63	0.0160	14.47	0.3675
6/19	111	0.03	0.0008	14.50	0.3683
6/20	112	0.00	0.0000	14.50	0.3683
6/21	113	0.00	0.0000	14.50	0.3683
6/22	114	0.00	0.0000	14.50	0.3683
6/23	115	0.24	0.0061	14.74	0.3744
6/24	116	0.08	0.0020	14.82	0.3764
6/25	117	0.00	0.0000	14.82	0.3764
6/26	118	0.00	0.0000	14.82	0.3764
6/27	119	0.00	0.0000	14.82	0.3764
6/28	120	0.00	0.0000	14.82	0.3764
6/29	121	0.02	0.0005	14.84	0.3769
6/30	122	0.00	0.0000	14.84	0.3769
7/ 1	123	0.00	0.0000	14.84	0.3769
7/ 2	124	0.00	0.0000	14.84	0.3769
7/ 3	125	0.00	0.0000	14.84	0.3769
7/ 4	126	0.00	0.0000	14.84	0.3769
7/ 5	127	0.02	0.0005	14.86	0.3774
7/ 6	128	0.00	0.0000	14.86	0.3774
7/ 7	129	0.00	0.0000	14.86	0.3774
7/ 8	130	0.00	0.0000	14.86	0.3774
7/ 9	131	1.84	0.0467	16.70	0.4242
7/10	132	0.00	0.0000	16.70	0.4242

Date (1990)	Day #	Precipitation (in/d)	Precipitation (m/d)	Cum. Precipitation (in)	Cum. Precipitation (m)
7/11	133	0.00	0.0000	16.70	0.4242
7/12	134	0.36	0.0091	17.06	0.4333
7/13	135	0.00	0.0000	17.06	0.4333
7/14	136	0.01	0.0003	17.07	0.4336
7/15	137	0.59	0.0150	17.66	0.4485
7/16	138	0.00	0.0000	17.66	0.4485
7/17	139	0.00	0.0000	17.66	0.4485
7/18	140	0.00	0.0000	17.66	0.4485
7/19	141	0.00	0.0000	17.66	0.4485
7/20	142	0.08	0.0020	17.74	0.4506
7/21	143	0.00	0.0000	17.74	0.4506
7/22	144	0.26	0.0066	18.00	0.4572
7/23	145	0.73	0.0185	18.73	0.4757
7/24	146	0.00	0.0000	18.73	0.4757
7/25	147	0.00	0.0000	18.73	0.4757
7/26	148	0.00	0.0000	18.73	0.4757
7/27	149	0.00	0.0000	18.73	0.4757
7/28	150	0.00	0.0000	18.73	0.4757
7/29	151	0.00	0.0000	18.73	0.4757
7/30	152	0.00	0.0000	18.73	0.4757
7/31	153	0.01	0.0002	18.74	0.4759
8/ 1	154	0.00	0.0000	18.74	0.4759
8/ 2	155	0.00	0.0000	18.74	0.4759
8/ 3	156	0.00	0.0000	18.74	0.4759
8/ 4	157	0.01	0.0003	18.75	0.4762
8/ 5	158	0.48	0.0122	19.23	0.4884
8/ 6	159	0.03	0.0008	19.26	0.4891
8/ 7	160	0.00	0.0000	19.26	0.4891
8/ 8	161	0.00	0.0000	19.26	0.4891
8/ 9	162	0.00	0.0000	19.26	0.4891
8/10	163	0.00	0.0000	19.26	0.4891

APPENDIX C

OBSERVED TRENCH INFLOW DATA

Table C.1 Observed daily inflow rate and cumulative inflow into interceptor trench from March 1 to August 10, 1990

Date (1990)	Day #	Daily Rate (GPM)	(m**3/d)	Cumulative Inflow (G)	(m**3)
3/ 1	1	..	..	..	..
3/ 2	2	..	..	..	..
3/ 3	3	..	..	..	..
3/ 4	4	0.07	0.3815	97.9	0.3704
3/ 5	5	0.05	0.2725	171.4	0.6488
3/ 6	6	0.05	0.2725	245.0	0.9274
3/ 7	7	0.03	0.1635	294.0	1.1129
3/ 8	8	0.06	0.3270	379.7	1.4373
3/ 9	9	0.03	0.1635	428.6	1.6224
3/10	10	0.08	0.4360	538.8	2.0395
3/11	11	0.26	1.4171	905.9	3.4290
3/12	12	0.73	3.9781	1959.2	7.4156
3/13	13	0.21	1.1445	2265.6	8.5754
3/14	14	0.23	1.2435	2596.2	9.8265
3/15	15	0.15	0.8175	2806.5	10.6225
3/16	16	0.14	0.7630	3002.4	11.3641
3/17	17	0.35	1.9076	3512.6	13.2951
3/18	18	0.28	1.5261	3916.8	14.8251
3/19	19	0.14	0.7631	4112.6	15.5663
3/20	20	0.31	1.6896	4553.1	17.2334
3/21	21	0.13	0.7085	4740.5	17.9427
3/22	22	0.09	0.4905	4862.9	18.4061
3/23	23	0.26	1.4171	5241.6	19.8396
3/24	24	0.13	0.7085	5424.4	20.5316
3/25	25	0.03	0.1635	5497.9	20.8095
3/26	26	0.04	0.2180	5559.1	21.0411
3/27	27	0.06	0.3270	5644.8	21.3655
3/28	28	0.05	0.2725	5718.2	21.6434
3/29	29	0.04	0.2180	5777.0	21.8659
3/30	30	0.06	0.3270	5865.1	22.1994
3/31	31	0.11	0.5995	6024.3	22.8021
4/ 1	32	0.08	0.4360	6134.4	23.2188
4/ 2	33	0.16	0.8720	6367.1	24.0994
4/ 3	34	0.14	0.7630	6574.7	24.8852
4/ 4	35	0.10	0.5450	6721.9	25.4424
4/ 5	36	0.03	0.1526	7125.8	26.9713
4/ 6	37	0.32	1.7441	7591.3	28.7331
4/ 7	38	0.14	0.7631	7799.0	29.5193
4/ 8	39	0.06	0.3270	7884.2	29.8416
4/ 9	40	0.11	0.5995	8043.2	30.4437
4/10	41	0.09	0.4905	8177.8	30.9532
4/11	42	0.25	1.3626	8533.2	32.2981

Date (1990)	Day #	Daily Rate (GPM)	(m**3/d)	Cumulative (G)	Inflow (m**3)
4/12	43	0.08	0.4360	8648.4	32.7342
4/13	44	0.08	0.4360	8770.6	33.1968
4/14	45	0.02	0.1090	8795.1	33.2895
4/15	46	0.10	0.5450	8944.6	33.8554
4/16	47	0.03	0.1635	8981.3	33.9944
4/17	48	0.18	0.9811	9240.3	34.9748
4/18	49	0.05	0.2725	9319.3	35.2737
4/19	50	0.03	0.1635	9368.0	35.4578
4/20	51	0.03	0.1635	9416.9	35.6429
4/21	52	0.11	0.5995	9576.1	36.2455
4/22	53	0.11	0.5995	9731.2	36.8327
4/23	54	0.05	0.2725	9804.7	37.1109
4/24	55	0.04	0.2180	9865.9	37.3426
4/25	56	0.03	0.1635	9914.8	37.5276
4/26	57	0.04	0.2180	9976.1	37.7597
4/27	58	0.03	0.1635	10025.0	37.9448
4/28	59	0.04	0.2180	10081.8	38.1598
4/29	60	0.04	0.2180	10143.0	38.3915
4/30	61	0.03	0.1635	10191.9	38.5766
5/ 1	62	0.03	0.1635	10240.9	38.7621
5/ 2	63	0.03	0.1635	10277.6	38.9010
5/ 3	64	0.04	0.2180	10338.9	39.1327
5/ 4	65	0.03	0.1635	10387.9	39.3182
5/ 5	66	0.04	0.2180	10448.6	39.5479
5/ 6	67	0.04	0.2180	10509.8	39.7796
5/ 7	68	0.04	0.2180	10571.0	40.0112
5/ 8	69	0.02	0.1090	10595.5	40.1040
5/ 9	70	0.04	0.2180	10656.7	40.3357
5/10	71	0.03	0.1635	10705.6	40.5208
5/11	72	0.07	0.3815	10809.1	40.9126
5/12	73	0.01	0.0545	10821.3	40.9587
5/13	74	0.01	0.0545	10833.6	41.0053
5/14	75	0.01	0.0545	10845.8	41.0515
5/15	76	0.08	0.4360	10965.7	41.5053
5/16	77	0.04	0.2180	11026.9	41.7370
5/17	78	0.03	0.1635	11075.9	41.9225
5/18	79	0.06	0.3270	11161.6	42.2469
5/19	80	0.04	0.2180	11218.0	42.4604
5/20	81	0.03	0.1635	11266.9	42.6455
5/21	82	0.03	0.1635	11316.0	42.8310
5/22	83	0.03	0.1635	11352.6	42.9699
5/23	84	0.04	0.2180	11413.9	43.2016
5/24	85	0.03	0.1635	11450.6	43.3405
5/25	86	0.02	0.1090	11475.1	43.4333
5/26	87	0.01	0.0545	11492.0	43.4972

Date (1990)	Day #	Daily Rate (GPM)	(m**3/d)	Cumulative (G)	Inflow (m**3)
5/27	88	0.03	0.1635	11533.3	43.6536
5/28	89	0.03	0.1635	11574.6	43.8099
5/29	90	0.03	0.1635	11615.9	43.9663
5/30	91	0.04	0.2180	11677.2	44.1983
5/31	92	0.03	0.1635	11713.9	44.3372
6/ 1	93	0.06	0.3270	11795.3	44.6453
6/ 2	94	0.02	0.1090	11822.7	44.7490
6/ 3	95	0.02	0.1090	11851.2	44.8569
6/ 4	96	0.02	0.1090	11879.8	44.9652
6/ 5	97	0.02	0.1090	11904.3	45.0579
6/ 6	98	0.03	0.1635	11953.2	45.2429
6/ 7	99	0.03	0.1635	12002.2	45.4284
6/ 8	100	0.02	0.1090	12026.7	45.5212
6/ 9	101	0.03	0.1635	12067.5	45.6756
6/10	102	0.03	0.1635	12108.3	45.8300
6/11	103	0.03	0.1635	12149.1	45.9844
6/12	104	0.02	0.1090	12182.4	46.1105
6/13	105	0.04	0.2180	12243.6	46.3421
6/14	106	0.10	0.5450	12255.8	46.3883
6/15	107	0.03	0.1635	12292.6	46.5276
6/16	108	0.02	0.1090	12325.2	46.6510
6/17	109	0.02	0.1090	12357.8	46.7744
6/18	110	0.02	0.1090	12390.5	46.8982
6/19	111	0.02	0.1090	12415.0	46.9909
6/20	112	0.03	0.1635	12451.7	47.1298
6/21	113	0.02	0.1090	12476.2	47.2225
6/22	114	0.03	0.1635	12512.9	47.3614
6/23	115	0.02	0.1090	12545.5	47.4848
6/24	116	0.02	0.1090	12578.1	47.6082
6/25	117	0.02	0.1090	12610.7	47.7316
6/26	118	0.01	0.0545	12623.0	47.7782
6/27	119	0.02	0.1090	12623.7	47.7809
6/28	120	0.02	0.1090	12671.9	47.9632
6/29	121	0.04	0.2180	12733.1	48.1949
6/30	122	0.01	0.0545	12753.5	48.2721
7/ 1	123	0.01	0.0545	12773.9	48.3493
7/ 2	124	0.01	0.0545	12794.3	48.4265
7/ 3	125	0.02	0.1090	12818.8	48.5193
7/ 4	126	0.02	0.1090	12849.4	48.6351
7/ 5	127	0.02	0.1090	12880.0	48.7509
7/ 6	128	0.01	0.0545	12892.3	48.7975
7/ 7	129	0.06	0.3270	12974.4	49.1082
7/ 8	130	0.06	0.3270	13056.0	49.4171
7/ 9	131	0.06	0.3270	13137.6	49.7259
7/10	132	0.03	0.1635	13186.6	49.9114

Date (1990)	Day #	Daily Rate (GPM)	(m**3/d)	Cumulative (G)	Inflow (m**3)
7/11	133	0.02	0.1090	13211.1	50.0041
7/12	134	0.03	0.1635	13260.0	50.1892
7/13	135	0.03	0.1635	13309.0	50.3747
7/14	136	0.03	0.1635	13345.7	50.5136
7/15	137	0.03	0.1635	13382.4	50.6525
7/16	138	0.03	0.1635	13419.1	50.7914
7/17	139	0.10	0.5450	13437.5	50.8611
7/18	140	0.03	0.1635	13474.2	51.0000
7/19	141	0.01	0.0545	13486.4	51.0461
7/20	142	0.02	0.1090	13510.9	51.1389
7/21	143	0.02	0.1090	13539.1	51.2456
7/22	144	0.02	0.1090	13568.0	51.3550
7/23	145	0.02	0.1090	13596.6	51.4632
7/24	146	0.02	0.1090	13621.1	51.5560
7/25	147	0.01	0.0545	13633.3	51.6021
7/26	148	0.03	0.1635	13670.1	51.7414
7/27	149	0.01	0.0545	13682.3	51.7876
7/28	150	0.02	0.1090	13710.9	51.8959
7/29	151	0.02	0.1090	13739.4	52.0037
7/30	152	0.02	0.1090	13768.0	52.1120
7/31	153	0.00	0.0000	13770.6	52.1218
8/ 1	154	0.02	0.1090	13795.0	52.2142
8/ 2	155	0.02	0.1090	13819.5	52.3069
8/ 3	156	0.03	0.1635	13856.2	52.4458
8/ 4	157	0.02	0.1090	13880.7	52.5386
8/ 5	158	0.02	0.1090	13905.2	52.6313
8/ 6	159	0.02	0.1090	13929.7	52.7240
8/ 7	160	0.01	0.0545	13941.9	52.7702
8/ 8	161	0.02	0.1090	13966.4	52.8629
8/ 9	162	0.03	0.1635	14015.4	53.0484
8/10	163	0.02	0.1090	14039.8	53.1408

APPENDIX D

DIGITIZED WATER TABLE LEVELS IN SELECTED WELLS

Table D.1 Observed Water levels in Well 89-13-W

Time (d) from 3/1/90	Water Level below Soil Surface (m)	Time (d) from 3/1/90	Water Level below Soil Surface (m)
-200.23	0.66	-144.97	0.60
-199.04	0.64	-143.60	0.60
-198.31	0.62	-141.45	0.60
-197.57	0.60	-140.96	0.62
-197.11	0.60	-139.25	0.63
-196.05	0.59	-138.79	0.63
-193.64	0.56	-138.02	0.63
-193.04	0.55	-136.00	0.65
-192.31	0.53	-135.23	0.65
-191.57	0.51	-133.54	0.65
-188.69	0.50	-131.21	0.67
-186.24	0.49	-129.82	0.68
-182.26	0.49	-129.07	0.67
-181.34	0.49	-126.91	0.68
-179.21	0.48	-126.28	0.69
-178.12	0.49	-123.98	0.69
-174.41	0.51	-121.47	0.73
-171.96	0.51	-120.47	0.77
-170.28	0.50	-120.27	0.80
-168.87	0.52	-119.81	0.81
-167.81	0.51	-119.34	0.81
-166.59	0.51	-117.49	0.82
-164.44	0.51	-113.83	0.81
-163.18	0.53	-112.77	0.80
-162.41	0.53	-109.87	0.79
-161.65	0.53	-106.66	0.78
-159.96	0.53	-104.23	0.77
-158.42	0.53	-101.47	0.76
-157.33	0.55	- 96.25	0.77
-157.06	0.52	- 93.31	0.79
-156.31	0.51	- 89.16	0.79
-153.97	0.54	- 87.32	0.80
-153.17	0.56	- 85.02	0.79
-152.39	0.57	- 83.03	0.79
-151.52	0.54	- 79.81	0.79
-149.65	0.55	- 77.66	0.79
-149.33	0.56	- 74.91	0.79
-147.47	0.58	- 72.10	0.82
-146.85	0.58	- 71.61	0.84
-145.42	0.61	- 71.23	0.88
-144.97	0.60	- 71.04	0.91

Time (d) from 3/1/90	Water Level from Soil Surface (m)
-71.29	0.84
-71.35	0.81
-70.91	0.80
-69.86	0.78
-67.57	0.78
-65.43	0.77
-63.41	0.79
-58.85	0.77
-54.88	0.75
-53.96	0.76
-52.12	0.75
-49.07	0.74
-46.63	0.74
-43.43	0.73
-43.12	0.73
-35.98	0.68
-30.82	0.65
-29.31	0.64
-26.28	0.62
-24.16	0.60
-22.63	0.60
-18.51	0.58
-15.61	0.58
-12.38	0.58
-10.40	0.58
-8.74	0.56
-7.71	0.53
-6.07	0.50
-4.27	0.48
-3.25	0.45
-3.40	0.45
-1.38	0.46
2.78	0.48
6.46	0.48
10.92	0.49
16.11	0.47
20.53	0.46
24.33	0.44
28.00	0.43
31.33	0.40
36.95	0.37
40.59	0.35
42.11	0.33
44.06	0.31

Time (d) from 3/1/90	Water Level below Soil Surface (m)
45.26	0.30
47.29	0.32
50.08	0.33
52.23	0.34
53.93	0.34
55.29	0.33
59.18	0.27
61.43	0.24
63.26	0.23
64.94	0.23
67.52	0.21
71.79	0.20
77.13	0.19
81.87	0.18
84.15	0.17
86.29	0.16
89.80	0.15
95.00	0.14
98.68	0.14
104.65	0.13
107.86	0.13
109.10	0.14
112.45	0.13
116.41	0.11
121.57	0.07
123.73	0.09
125.45	0.10
130.95	0.09
134.86	0.14
135.32	0.14
137.35	0.16
138.42	0.16
140.14	0.18
141.97	0.18
143.34	0.17
144.72	0.17
145.64	0.17
147.76	0.15
150.94	0.13

Table D.2 Observed Water levels in Well 85-I-11

Time (d) from 3/1/90	Water Level below Soil Surface (m)	Time (d) from 3/1/90	Water Level below Soil Surface (m)
-200.19	-2.51	-153.90	-1.76
-199.20	-2.51	-152.53	-1.79
-198.68	-2.55	-150.87	-1.86
-198.68	-2.50	-149.35	-1.88
-198.69	-2.58	-147.56	-1.77
-197.99	-2.56	-146.66	-1.83
-196.38	-2.55	-145.91	-1.87
-193.31	-2.52	-145.55	-1.93
-192.48	-2.54	-144.65	-1.99
-191.64	-2.56	-144.28	-2.02
-190.34	-2.56	-144.28	-2.03
-188.67	-2.59	-143.59	-2.01
-186.28	-2.52	-143.56	-1.92
-185.77	-2.61	-142.92	-1.85
-184.18	-2.65	-141.78	-1.86
-182.79	-2.62	-139.83	-1.98
-180.80	-2.60	-137.79	-2.06
-178.65	-2.57	-136.36	-2.11
-177.59	-2.61	-134.59	-2.09
-176.74	-2.59	-134.28	-2.07
-174.15	-2.61	-132.75	-2.06
-171.94	-2.64	-127.52	-1.99
-171.57	-2.66	-127.47	-2.06
-171.78	-2.62	-123.99	-2.16
-171.23	-2.58	-122.09	-2.19
-171.07	-2.54	-119.94	-2.18
-169.82	-2.47	-115.81	-2.17
-168.58	-2.42	-110.90	-2.12
-168.86	-2.36	-107.06	-2.09
-170.14	-2.29	-103.22	-2.02
-170.57	-2.20	- 97.35	-1.88
-170.31	-2.12	- 95.44	-1.87
-168.13	-2.01	- 93.98	-1.84
-168.24	-1.88	- 91.35	-1.76
-169.12	-1.76	- 89.92	-1.82
-164.96	-1.68	- 88.02	-1.86
-163.76	-1.75	- 85.51	-1.90
-162.92	-1.77	- 83.29	-1.90
-160.57	-1.82	- 81.14	-1.88
-158.86	-1.74	- 77.62	-1.86
-157.24	-1.70	- 78.47	-1.89
-154.73	-1.74	- 75.87	-1.89

Time (d) from 3/1/90	Water Level below Soil Surface (m)
-72.67	1.92
-71.90	1.91
-68.95	1.78
-63.38	1.80
-61.76	1.78
-61.77	1.58
-62.24	1.39
-61.67	1.07
-58.72	0.70
-57.89	0.31
-54.97	0.48
-52.25	0.56
-49.23	0.68
-44.84	0.81
-43.87	0.89
-42.92	0.80
-42.51	0.71
-40.48	0.58
-36.88	0.56
-27.11	0.39
-22.50	0.34
-16.94	0.40
-11.61	0.46
-5.36	0.52
-2.46	0.54
0.56	0.66
5.03	0.78
5.26	0.78
5.96	0.76
5.74	0.70
6.46	0.62
6.80	0.53
7.36	0.45
9.00	0.34
9.94	0.29
11.50	0.19
14.68	0.29
16.48	0.38
21.04	0.46
24.05	0.60
26.63	0.66
29.67	0.72
31.56	0.78
33.84	0.83
34.14	0.84
34.69	0.80
36.02	0.72
37.20	0.63
38.08	0.51
38.48	0.45
42.17	0.39
47.36	0.42
53.91	0.50
56.49	0.57
59.35	0.68
60.93	0.76
63.27	0.84
63.27	0.86
64.37	0.77
64.39	0.71
64.12	0.60
66.08	0.46
72.85	0.35
73.92	0.35
77.59	0.36
80.91	0.49
82.58	0.51
84.56	0.54
84.78	0.56
85.53	0.60
85.68	0.61
86.28	0.65
86.50	0.69
88.69	0.77
90.64	0.86
95.20	0.94
95.89	0.95
99.39	0.99
100.98	1.03
102.65	1.07
107.29	1.15
108.96	1.19
112.15	1.26
114.50	1.30
117.23	1.36
120.12	1.43
122.17	1.46
123.00	1.49

Time (d) from 3/1/90	Water Level below Soil Surface (m)
127.65	1.54
130.00	1.58
131.68	1.60
133.81	1.64
134.64	1.66
136.39	1.70
136.99	1.73
138.06	1.71
139.91	1.67
140.15	1.65
146.44	1.81
148.79	1.87
151.30	1.92
154.79	1.98
157.52	2.05
158.80	2.10
161.77	2.15
163.67	2.18
165.65	2.20
168.47	2.23
170.90	2.27
171.96	2.30
173.40	2.34
175.07	2.38

NRC FORM 335 (2-89) NRCM 1102, 3201, 3202

U.S. NUCLEAR REGULATORY COMMISSION

BIBLIOGRAPHIC DATA SHEET

(See instructions on the reverse)

1 REPORT NUMBER (Assigned by NRC, Add Vol., Supp., Rev., and Addendum Numbers, If any.)

NUREG/CR-5794

2. TITLE AND SUBTITLE

Ground-Water Flow and Transport Modeling of the NRC-Licensed Waste Disposal Facility, West Valley, New York

3 DATE REPORT PUBLISHED

MONTH: October YEAR: 1991

4. FIN OR GRANT NUMBER

L1273

5. AUTHOR(S)

J.B. Kool, Y.S. Wu

6. TYPE OF REPORT

Technical

7. PERIOD COVERED *(Inclusive Dates)*

9/29/89 - 7/31/91

8. PERFORMING ORGANIZATION – NAME AND ADDRESS *(If NRC, provide Division, Office or Region, U.S. Nuclear Regulatory Commission, and mailing address; if contractor, provide name and mailing address.)*

HydroGeoLogic, Inc.
1165 Herndon Parkway
Suite 900
Herndon, VA 22070

9. SPONSORING ORGANIZATION – NAME AND ADDRESS *(If NRC, type "Same as above"; if contractor, provide NRC Division, Office or Region, U.S. Nuclear Regulatory Commission, and mailing address.)*

Division of Regulatory Applications
Office of Nuclear Regulatory Research
U.S. Nuclear Regulatory Commission
Washington, DC 20555

10. SUPPLEMENTARY NOTES

11. ABSTRACT *(200 words or less)*

This report describes a simulation study of groundwater flow and radionuclide transport from disposal pits at the NRC licensed waste disposal facility in West Valley, New York. A transient, precipitation driven, flow model of the near-surface fractured till layer and underlying unweathered till was developed and calibrated against observed inflow data into a recently constructed interceptor trench for the period March - May, 1990. The results suggest that lateral flow through the upper, fractured till layer may be more significant than indicated by previous, steady state flow modeling studies. A conclusive assessment of the actual magnitude of lateral flow through the fractured till could however not be made. A primary factor contributing to this uncertainty is the unknown contribution of vertical infiltration through the interceptor trench cap to the total trench inflow. The second part of the investigation involved simulation of the migration of Sr-90, Cs-137 and Pu-239 from the one of the fuel hull disposal pits. A first-order radionuclide leach rate with rate coefficient of 10^{-6}/day was assumed to describe radionuclide release into the disposal pit. The simulations indicated that for wastes buried below the fractured till zone, no significant migration would occur. However, under the assumed conditions, significant lateral migration could occur for radionuclides present in the upper, fractured till zone.

12. KEY WORDS/DESCRIPTORS *(List words or phrases that will assist researchers in locating the report.)*

waste disposal facility
groundwater flow model
radionuclide transport model
disposal pits
West Valley, NY

13. AVAILABILITY STATEMENT

unlimited

14. SECURITY CLASSIFICATION

(This Page) unclassified

(This Report) unclassified

15. NUMBER OF PAGES

16. PRICE

END

DATE FILMED

01/07/92